

令和元年 修士論文



# Hybrid Port–Hamiltonian Systems and their Application to Robotics

ハイブリッド・ポート・ハミルトン系のロボット応用

Supervisor: Professor Hajime Asama  
浅間一教授

Department of Precision Engineering, Graduate School of Engineering  
The University of Tokyo

Student ID 37-175037

Stefano Massaroli  
マッサロリ ステファノ



# Abstract

Accurate and robust control of robots in highly dynamic tasks is arguably one of the hardest open problems in robotics. The incapability of robots to safely and reliably interact with their environment is what still refrain them from becoming ubiquitous in our society. The main challenge is due to the *nonsmooth* nature of such dynamic tasks, as they often involve impacts between parts of the robot and its environment. Examples are *legged locomotion*, *non-prehensile* manipulation or aerial robot landing.

This issue in robotics is a fundamental control challenge, extremely appealing for the research community, which is trying to fulfill the needs of industries who are seeking more autonomy for commercial robots. This interest expands swiftly to a theoretical level once the problem is formalized. Discontinuities of any sort used to be sworn enemies of most control theorists. However, in recent years, a new emerging field of control theory: the *hybrid dynamical systems*, promises a complete set of mathematical tools to deal with tasks characterized by interacting continuous and discrete time dynamics. Besides, this framework is by no means close to solve the robotics problem. Control theorists often spend too much time on over-complicated math without foresight of its applications.

Nevertheless, the work presented in this thesis hinges on the most fundamental concept of classical and modern physics: *energy*. Energy is the key to understand, and thus control, the behavior of dynamical system by physical insights. The most relevant mathematical tool in this context is the one of *port-Hamiltonian systems*. The aim of this thesis is to provide a unified modeling framework merging the ones of port-Hamiltonian and hybrid systems through consistent and practically useful results.

The research work embraces four different objectives: characterize a new unified modeling strategy to tackle highly dynamic robotic tasks; apply the theory to cope with the challenging *ball-dribbling robot* problem; show the broad applications' spectrum of the developed framework by adopting it into to bear pure control theory problem; perform a first step towards real implementation of such control systems through system identification task.

The contribution of this thesis is primarily theoretical, however, all chapters are application-oriented displaying real examples with simulations.



---

# Contents

<b>Chapter 1 Introduction .....</b>	<b>1</b>
1.1 Background.....	2
1.1.1 Energy as Common Factor Among Interactions .....	2
1.1.2 Research Problem: Control Highly Dynamic Robotic Tasks .....	3
1.1.3 Beyond Robot Control .....	4
1.1.4 The Identification Problem .....	5
1.2 Aims and Objectives .....	7
1.3 Thesis Content and Structure.....	8
1.3.1 Thesis Outline.....	8
1.3.2 Thesis Content .....	9
<b>Chapter 2 Preliminaries .....</b>	<b>13</b>
2.1 Introduction .....	14
2.2 Stability and Passivity.....	15
2.2.1 Stability of Autonomous Systems .....	15
2.2.2 Passivity: Basic Definitions .....	16
2.2.3 Output Feedback Stabilization of Passive Systems .....	17
2.3 Port–Hamiltonian Systems.....	19
2.3.1 Input–State–Output Model.....	19
2.3.2 Passivity–Based Control .....	25
2.4 Hybrid Dynamical Systems.....	29
2.4.1 Hybrid Inclusions.....	29
2.4.2 Stability.....	31
2.5 Summary .....	33
<b>Chapter 3 Hybrid Port–Hamiltonian Systems.....</b>	<b>35</b>
3.1 Introduction .....	36
3.2 Definitions and Basic Assumptions .....	37
3.2.1 Impulsive Port–Hamiltonian Systems.....	37
3.2.2 Hybrid port–Hamiltonian Systems.....	38
3.3 Passivity .....	42
3.4 Lyapunov Stability of Autonomous Systems.....	44
3.5 Summary .....	46
<b>Chapter 4 Iterative Energy Shaping of a Ball–Dribbling Robot .....</b>	<b>47</b>
4.1 Introduction .....	48

4.2	Model of the Ball–Dribbling Robot.....	49
4.2.1	Port-Hamiltonian Model of Flows.....	49
4.2.2	Model of the Impacts .....	49
4.3	Analysis of the Autonomous Model .....	52
4.3.1	Passivity and Autonomous Stability .....	52
4.3.2	Chaotic Trajectories .....	52
4.4	Dribbling Control .....	57
4.5	Numerical Simulations.....	60
4.5.1	Autonomous System .....	60
4.5.2	Controlled System .....	60
4.5.3	Numerical Stability and Robustnes Analysis .....	62
4.6	Summary .....	76
<b>Chapter 5</b>	<b>Multistable Energy Shaping of Linear-Time-Invariant Systems...</b>	<b>77</b>
5.1	Introduction .....	78
5.2	Multistable Energy Shaping of LTI Systems .....	80
5.2.1	Passivity of LTI Systems .....	80
5.2.2	Multistable Passivity-Based Control of LTI Systems .....	81
5.2.3	Application Example .....	83
5.2.4	Choice of the Dissipation Rate: Shaping the Basins of Attraction ....	84
5.3	Hybrid Mode Selector.....	88
5.3.1	Impulse generation .....	88
5.3.2	Overall Hybrid System .....	89
5.4	Hybrid Port–Hamiltonian Model and Stability .....	90
5.5	Numerical Simulation.....	92
5.6	Summary .....	95
<b>Chapter 6</b>	<b>Identification of a Class of Hybrid Dynamical Systems.....</b>	<b>97</b>
6.1	Introduction .....	98
6.2	Problem Setting .....	99
6.3	Jump Detection.....	101
6.4	Identification Procedure .....	104
6.4.1	Approximation of the Smoothness Bound .....	104
6.4.2	Parameters Estimation .....	105
6.4.3	Reduced Order Identification .....	106
6.4.4	Flow and Jump Sets Approximation .....	108
6.5	Simulation Experiments .....	110
6.5.1	Case of Study: Impact Mass-Spring-Damper System .....	110
6.5.2	Numerical Simulation .....	112
6.6	Summary .....	118
<b>Chapter 7</b>	<b>Conclusion and Future Work .....</b>	<b>119</b>
7.1	Conclusion.....	120
7.2	Future Work .....	121

---

Acknowledgements.....	123
Research Publications.....	131



---

# List of Figures

1.1	One-dimensional ball-dribbling and ball-juggling robotic systems. ....	4
1.2	Thesis outline.....	10
1.3	Venn diagram of the contents presented in this thesis.....	11
2.1	Block diagram of the port-Hamiltonian model of a fully-actuated $n$ -degrees of freedom mechanical systems.....	21
2.2	Mass-spring-damper system. ....	21
2.3	State-space trajectory of the mass-spring damper system for different values of the damping coefficient.....	22
2.4	Time evolution of the Energy of the mass-spring damper system. ....	23
2.5	Block diagram representation of the Lotka-Volterra equations in port-Hamiltonian form. ....	24
2.6	Phase-space trajectory of the mass-spring-damper system control via EB-PBC.....	28
2.7	Ball bouncing on an actuated surface .....	30
2.8	Time evolution of the ball bouncing on the actuated platform (autonomous case) .....	31
2.9	Energy descent during a trajectory of the autonomous system.....	32
3.1	Impact pendulum .....	38
3.2	Hopping robot on elastic ground.....	40
4.1	One-dimensional ball-dribbling robotic system.....	48
4.2	Hybrid automata of the autonomous system .....	51
4.3	Time evolution of the autonomous system' state in the Monte Carlo simulation .....	53
4.4	Phase-space trajectory of the autonomous system in the Monte Carlo simulation .....	54
4.5	Time evolution of the energy in the Monte Carlo simulation .....	54
4.6	Histograms and reconstructed spatial (probability) density functions of the state.....	55
4.7	Phase-gram of the state spatial density function .....	56
4.8	Finite state machine of the controller .....	59

4.9	Hybrid automata representing the controlled system .....	60
4.10	Uncontrolled system: time evolution of the robot and ball position states.	61
4.11	Uncontrolled system: Phase–space trajectory over the energy function....	61
4.12	Uncontrolled system: time evolution of the Hamiltonian function.....	62
4.13	Uncontrolled system: Energy distribution within the system.....	63
4.14	Iterative energy shaping control: time evolution of the robot and ball states .....	64
4.15	Iterative energy shaping control: detailed view of the time evolution of the ball and robot positions at steady state .....	65
4.16	Iterative energy shaping control: the time evolution of the Hamiltonian function.....	65
4.17	Iterative energy shaping control: detailed view of the the Hamiltonian at steady-state.....	66
4.18	Iterative energy shaping control: Distribution of the energy across the system’s components and time .....	67
4.19	Iterative energy shaping control: detailed view of the energy distribution across the system’s components and time.....	68
4.20	Iterative energy shaping control: (discrete) time evolution of the tracking error $e$ and of the energy shaping gain $\varphi_\xi(e)$ .....	69
4.21	Iterative energy shaping control: phase–space trajectories.....	69
4.22	Time evolution of the controlled system’ state in the Monte Carlo simulation .....	70
4.23	Phase–space trajectory of the controlled system in the Monte Carlo simulation .....	71
4.24	Time evolution of the energy in the Monte Carlo simulation .....	71
4.25	Convergence of the tracking error and controller gain in the Monte Carlo simulation .....	72
4.26	Robustness to parameters variations: reference position.....	73
4.27	Robustness to parameters variations: ball’s mass.....	74
4.28	Robustness to parameters variations: restitution coefficients .....	75
5.1	A block representation of a classic feedback control system .....	78
5.2	Graphical representation of a state-space trajectory of the controlled system .....	79
5.3	A block representation of the controlled system. Here, the energy shap- ing and damping injection control actions asymptotically stabilize all the desired working modes of the system, i.e. the minima of the new energy function. ....	82
5.4	Desired shaped energy function.....	83
5.5	Phase–space portraits of the autonomous and the multistable EB–PBC controlled system .....	84

---

5.6	Basins of attraction of the fixed points of the system for different values of $k_d$ .....	85
5.7	Graphical representation of the necessary condition given by Theorem 5.2.6.....	87
5.8	Hybrid automata representing the overall controlled system with the hybrid mode selector.....	89
5.9	A block representation of interconnection of the hybrid systems.....	90
5.10	Simulation experiment of the overall hybrid system with $\gamma = 10^{-3}$ .....	93
5.11	Simulation experiment of the overall hybrid system with $\gamma = 2$ .....	94
6.1	Hybrid automata representation of the system.....	99
6.2	Example 6.3.4: Time evolution of the state, Euler derivative norm and smoothness bound.....	103
6.3	Impact mass–spring–damper system.....	110
6.4	Time evolution of the position and velocity of the system.....	112
6.5	Nominal experiment: norm of the Euler derivative and estimated smoothness bound.....	114
6.6	Nominal experiment: parameters estimation results.....	115
6.7	Noisy experiment: norm of the Euler derivative and estimated smoothness bound.....	116
6.8	Noisy experiment: parameters estimation results.....	117



---

# List of Tables

1.1	Efforts and flows variables for various physical domains.....	3
5.1	Hybrid controller optimization results. ....	92



---

# Notations, Symbols and Acronyms

Matrices are capitalized and in bold font, vectors are in bold font and scalars are in italic font; unless specifically noted.

Notations	Meaning
$x$	scalar
$\mathbf{x}$	vector
$\mathbf{X}$	matrix
$\mathcal{X}$	set
$\mathbf{x}_i$	$i$ -th element of $\mathbf{x}$
$\mathbf{X}_{ij}$	entry of $\mathbf{X}$ corresponding to the $i$ -th row and $j$ -th column
$>, <, \geq, \leq$	symbols used in matrix inequalities
$(\mathbf{v}, \mathbf{w})$	given two vectors $\mathbf{v}$ and $\mathbf{w}$ , $(\mathbf{v}, \mathbf{w}) \triangleq [\mathbf{v}^\top, \mathbf{w}^\top]^\top$
$\dot{x}$	time derivative of the variable $x$ , $\dot{x} \triangleq \frac{dx}{dt}$
$x^+$	next value of the quantity $x$ after a discrete-time event

---

Symbols	Meaning
$\mathbb{R}$	Set of Reals
$\mathbb{N}$	Set of Naturals
$\mathbb{R}^+$	Nonnegative reals
$\mathbb{N}_{\leq s}$	Naturals less than $s$
$\mathbb{N}^*$	Naturals without the zero element
$\mathbb{I}_n$	$n$ by $n$ identity matrix
$\mathbb{O}_n$	$n$ by $n$ zero matrix
$\mathbb{O}_{n \times m}$	$n$ by $m$ zero matrix
$\mathbf{0}_n$	origin of $\mathbb{R}^n$
$\mathbf{1}_n$	unitary vector of $\mathbb{R}^n$
$\mathcal{L}_2^m$	set of square-integrable functions $z : \mathbb{R} \rightarrow \mathbb{R}^m$
$\mathcal{C}^n$	set of $n$ times continuously differentiable functions in their domain.
$\langle \cdot, \cdot \rangle$	inner product of $\mathbb{R}^n$ . $\langle \cdot, \cdot \rangle : \mathbb{R}^n \times \mathbb{R}^n \rightarrow \mathbb{R}$ . Let $\mathbf{v}, \mathbf{w} \in \mathbb{R}^n$ , $\langle \mathbf{v}, \mathbf{w} \rangle = \mathbf{v}^\top \mathbf{w}$
$\ \cdot\ _2$	induced norm of $\mathbb{R}^n$ . Let $\mathbf{v} \in \mathbb{R}^n$ , $\ \cdot\ _2 \triangleq \sqrt{\langle \mathbf{v}, \mathbf{v} \rangle}$
$\ \cdot\ _\infty$	infinity norm
$\nabla \mathcal{H}(\mathbf{x})$	Given a scalar-valued function $\mathcal{H} : \mathbb{R}^n \supseteq \mathcal{X} \rightarrow \mathbb{R}$ , $\nabla \mathcal{H}(\mathbf{x})$ denotes its transposed gradient, i.e. $\nabla \mathcal{H}(\mathbf{x}) : \mathcal{X} \rightarrow \mathbb{R}^n$ such that $\nabla \mathcal{H}(\mathbf{x}) \triangleq \left( \frac{\partial \mathcal{H}}{\partial \mathbf{x}} \right)^\top$
$\nabla^2 \mathcal{H}(\mathbf{x})$	Hessian matrix of $\mathcal{H}$ , i.e. $\nabla^2 \mathcal{H}(\mathbf{x}) : \mathcal{X} \rightarrow \mathbb{R}^{n \times n}$ such that $\nabla^2 \mathcal{H}(\mathbf{x}) \triangleq \frac{\partial}{\partial \mathbf{x}} \frac{\partial \mathcal{H}}{\partial \mathbf{x}}$
$\text{conv}(\Lambda)$	convex hull of a finite subset $\Lambda \subset \mathbb{R}^n$ defined by the convex combinations of its elements.

Acronyms	Meaning
PH	Port-Hamiltonian
HDS	Hybrid Dynamical System



# Chapter 1

## Introduction

---

1.1	Background.....	2
1.1.1	Energy as Common Factor Among Interactions .....	2
1.1.2	Research Problem: Control Highly Dynamic Robotic Tasks .....	3
1.1.3	Beyond Robot Control .....	4
1.1.4	The Identification Problem .....	5
1.2	Aims and Objectives .....	7
1.3	Thesis Content and Structure.....	8
1.3.1	Thesis Outline.....	8
1.3.2	Thesis Content .....	9

---

## 1.1 Background

**M**ODELLING, analysis and control of *nonsmooth* systems is an interesting and open problem which attracts the attention of a wide range of researchers, from physicists and mechanical engineers to specialists in control and automation (Brogliato, 1999; Stronge, 2018). The interaction between continuous and discrete-time dynamics arises, for instance, while considering the behavior of a mechanical system in presence of impacts: its dynamics cannot be represented only by means of differential equations. The theory of *hybrid dynamical systems* (HDS) is the formalism in which this type of models can be described. Overviews of this framework are given in (Van Der Schaft and Schumacher, 2000; Haddad et al. , 2006). In particular, the most general and recent modeling approach is the one of *hybrid inclusions* developed in recent years (Goebel et al. , 2009b). This field of Automatic Controls generally investigates systems characterized by the interaction of continuous and discrete time dynamics as well as by multimodality (Goebel et al. , 2012).

In the last three decades, the fundamental concept of *energy* experienced an impressive growth process in engineering practice and in particular in system theory. The framework of *passivity-based control* (PBC) is now a well-established branch of nonlinear control theory and aims at treating dynamical systems as devices able to exchange energy, rather than to process signals (Ortega et al. , 2001). This is possible by equipping dynamical systems with additional structure (e.g. storage functions, supply rates, etc.) by means of which the concepts of energy and input/output characterization of the system are connected in a unique framework (Sontag, 2008).

In this context, another fundamental paradigm regards the *interconnection* of systems by means of *power ports* (Duindam et al. , 2009), which led to the definition of *port-Hamiltonian systems* (Maschke and Schaft, 1992; Ortega et al. , 2001; Van Der Schaft et al. , 2014), the mathematical framework in which PBC developed naturally, merging geometry and network theory. Hence, the control problem reduces to the design of a dynamical system (the controller) and an interconnection structure that “shapes”, in a desired way, the energy of the original system (Ortega et al. , 2001, 2008). This approach allows control engineers to pay particular attention to the performance of the control system and not only to stabilizability (as common in nonlinear control). In classic robot control, the theory of passivity lead to several successful approaches, such as the *gravity-compensation* (Arimoto, 1984) and *impedance* controller (Secchi et al. , 2007). Other interesting application are robots with flexible links (Macchelli et al. , 2009) and elastic joints (Zhang and Liu, 2016).

### 1.1.1 Energy as Common Factor Among Interactions

Driven by a physical intuition, it is rather straightforward to recognize energy as the *lingua franca* between different physical domains. This idea lead, in the early sixties, H. Paynter to establish the field of *port-based modeling* (Paynter, 1961).

Table 1.1: Efforts and flows variables for various physical domains.

Domain	Effort	Flow
Mechanics (translational)	Force $F$	Velocity $v$
Mechanics (rotational)	Torque $\tau$	Angular Velocity $\omega$
Electric	Voltage $v$	Current $i$
Hydraulic	Pressure $p$	Volume Flow $Q$
Thermodynamic	Temperature $T$	Entropy Flow $\dot{E}$

A physical system, in fact, may exhibit a *dynamical behavior* if and only if some energy exchange happen within its *internal structure* (components) or with the external world. In any physical domain there exists pair of dual variables (see Appendix A) often called *flows* and *efforts* which intrinsically form *power ports*, interfaces through which energy flows (Secchi et al. , 2007). Table 1.1 lists the effort and flow variables for several physical domains.

In robot manipulation, this description of dynamical phenomena may result particularly useful to model the interaction between the robot end–effector and the object, which indeed exchange energy with each other in a continuous fashion. In fact, the port–Hamiltonian framework allows to explicitly capture the physical phenomena behind this continuous interaction. Furthermore, in this perspective, the robot controller can also be thought as an other dynamical system interconnected with the robot and exchanging energy with it. This approach results to be both, general and versatile. The theory of passivity–based control of port–Hamiltonian system has been already successfully applied in a variety of manipulation tasks: from grasping (Stramigioli et al. , 1999) and soft–finger manipulation (Ficuciello et al. , 2010) to non–prehensile tasks, e.g. object rolling (Donaire et al. , 2017; Serra et al. , 2019).

Besides, when the robot tasks involve *nonsmooth* phenomena such as mechanical impacts or dynamic friction (Brogliato, 1999), the classical passivity–based techniques cease to work due to the discontinuities in system’s state along trajectories.

However it can be noticed that energy is the undisputed protagonist also of this type on discrete (instantaneous) interactions. Thus, an energy–based reasoning might be carried out to overcome the challenges given by the hybrid nature of these robot tasks.

From now on, we will refer to any robotic tasks which is hybrid in nature, i.e. it includes interacting continuous and discrete phenomena, as *highly dynamic tasks*.

### 1.1.2 Research Problem: Control Highly Dynamic Robotic Tasks

The extension of passivity–based control of port–Hamiltonian systems to the hybrid case is highly desirable. In fact, this will allow to establish a new general and unified

framework to model and control robots performing highly dynamic tasks.

Examples of these tasks in the manipulation context are: ball-juggling (Sanfelice et al. , 2007; Tian et al. , 2013), ball-dribbling (Bätz et al. , 2010; Haddadin et al. , 2018) or even tossing/catching of a deformable object (Ruggiero et al. , 2018). Other hybrid tasks may be related to *self-manipulation*, e.g. dynamic walking (Spong et al. , 2007; Westervelt et al. , 2018), hopping robots (Ishikawa et al. , 2003) and control of powered exoskeletons (Harib et al. , 2018; Lv et al. , 2018). The one-dimensional version of the ball-juggling and ball-dribbling systems are represented in Fig. 1.1.

One of the most clear proofs of the necessity of an novel unified framework merging energy-based approaches to hybrid systems is given by all the research work present in literature: although they belong to the same class of robot control problems, each tasks is solved with *ad-hoc* solutions, without any analysis of a bigger picture.

Furthermore, as underlined in Subsection 1.1.1, the span of validity of this new general framework could indeed be extended to any physical domain, and thus employed to find potential solutions in different branches of engineering.

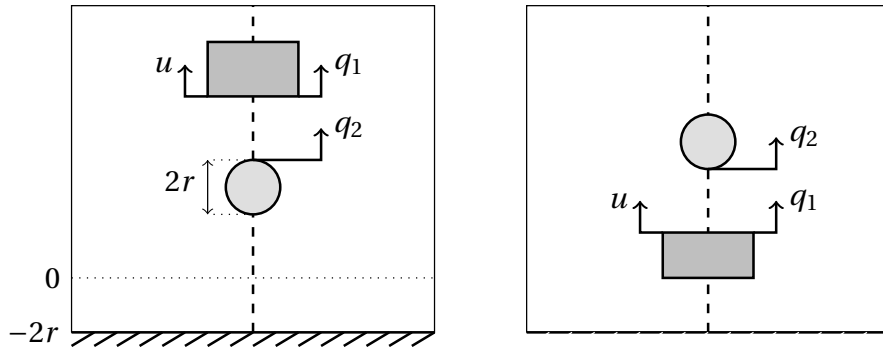


Fig. 1.1: One-dimensional ball-dribbling (left) and ball-juggling (right) robotic systems. The position of the robot (rectangle), is represented by the variable  $q_1$  while  $u$  is an input force applied to it. The position of the ball (circle), of radius  $r$ , is represented by  $q_2$ . The ball-juggling system presents a single impact, i.e. the one between the robot and the ball. The ball-dribbling system, instead, is characterized by two impacts: ball-robot and ball-ground.

### 1.1.3 Beyond Robot Control

It has been proven that a novel unified framework for controlling highly dynamic robotic tasks is needed but cannot be approached in a systematic general way due to the *nonsmooth* nature of the robotic tasks.

However, many control systems presents discontinuities and multimodality due to the control algorithm itself rather then physics. For example, a system subjected to a *sliding-mode controller* (Pisano and Usai, 2011) is, technically speaking, an hybrid

system. Moreover, the whole framework of *switching control* belongs to field of hybrid dynamical systems.

Very simple practical example of how a controller give an hybrid nature to dynamical systems, are the temperature regulator of a room or the water-level control in tanks.

In the light of this considerations, it is legitimate pose the following questions:  
*Can hybrid control systems be modeled from an energetic point of view in port-Hamiltonian fashion?*

*If yes, which theoretical advantages would this formulation give?*

#### 1.1.4 The Identification Problem

As common in Automatic Controls, controller design, simulations and diagnostics of hybrid dynamical systems require an accurate knowledge of the model. However, these processes are always characterized by sets of parameters which are typically not available.

System identification techniques are the interface between real world application and mathematical world of control theory and mathematical abstraction (Ljung, 2010). These methods aim to obtain estimates of the parameters and update the model from direct measurements collected during the time evolution of the system (Söderström, 2018, 2019).

It is well known that, when dealing with robotic systems, the inertial parameters must often be thoroughly estimated with well designed identification experiments. Moreover, if the robot experiences impacts or unexpected state changes, it is intuitive to understand that further parameters given by the hybrid part of the system must also be estimated. Thus, in order to implement any robot controllers for highly dynamic tasks, it is necessary to solve the identification problem first.

The majority of the literature on identification of hybrid systems is related to classes of (discrete-time) Piece Wise Affine systems (PWA), i.e. systems which are defined by subdividing the space into polyhedral regions which have associated an affine state update equation (Bemporad et al. , 2001; Ferrari-Trecate et al. , 2001; Juloski et al. , 2005a,b; Paoletti et al. , 2007).

Besides, the identification of hybrid dynamical system in the form of *hybrid inclusions* has to be explored yet. In fact, a systematic identification procedure for this class of systems is currently still missing. Note that, many of the robotics tasks discussed above can be modeled within this framework.

Real implementation of those tasks would undoubtedly require the knowledge of some parameters of the plant. Thus, if a novel unified modeling framework merging

port-Hamiltonian and hybrid systems is proposed alongside new control techniques, the systematic estimation of physical parameters of both continuous (e.g. mass, inertia, friction) and discrete (e.g. impact restitution coefficient) parts of models will be needed.

## 1.2 Aims and Objectives

The aim of this thesis is to present a novel control theoretical framework for physical systems with nonsmooth and multimodal behaviors, with a special insight toward robot control tasks where the current-state-of-the-art approaches fail.

The main objectives are:

- 1. To develop a novel control theoretical framework by merging the theories of port–Hamiltonian systems and hybrid systems.**

With the aim of solving a robot control problem, the theory of *hybrid port–Hamiltonian systems* is developed combining the theories of port–Hamiltonian systems and *hybrid inclusions*, one of the most general representations of hybrid dynamical systems.

- 2. To apply the developed theory to a robot control task and prove its effective within the robotics framework.**

Considering the ball–dribbling robot problem, a novel controller, the *iterative energy shaping* is systematically synthesized, proving the capabilities of the proposed framework.

- 3. To demonstrate how the developed theory goes beyond robotics and can be used to model a broad variety of control systems.**

A novel nonlinear hybrid controller for linear time–invariant system is derived from passivity–based techniques, and then this purely control theoretical problem is expressed via hybrid port–Hamiltonian systems.

- 4. To derive a new systematic identification procedure for a class of hybrid systems.**

As most of hybrid control systems (including the proposed ones) require some knowledge of the physical parameters of the controlled plant, a new systematic procedure is presented to solve the estimation problem. This method can be applied to a variety of hybrid port–Hamiltonian systems

## 1.3 Thesis Content and Structure

### 1.3.1 Thesis Outline

This thesis is structured in seven chapters which implement the aim described in Section 1.2. These seven chapter can be logically clustered in four main parts: Introduction and background, theoretical results, applications and conclusions. In line with the objectives, a detailed structure of this thesis is shown in Figure 1.2.

**Chapter 1** describes the main motivations, purpose and approach of this study.

**Chapter 2** briefly introduces the fields of port–Hamiltonian systems and hybrid dynamical systems. Throughout the chapter, several illustrative examples related to robotics, mathematical biology and physics are provided to highlight the practical importance of the presented theoretical concepts. Firstly, general notions of stability and passivity of dynamical systems are provided. Then, the input–state–output model of a port–Hamiltonian system is derived and its most relevant properties are described. Moreover, the basic theory of the energy–balancing passivity–based control is also presented. In the latter part of the chapter, the basic results on hybrid systems are introduced. In particular, it focuses on the class of *hybrid inclusions* and its stability/passivity theory.

**Chapter 3** deals with the definition and characterization of hybrid-port Hamiltonian systems. Starting from the concepts revised in the previous chapter, the new framework is here consistently developed. First, the basic assumptions are stated and the hybrid port–Hamiltonian model is derived. The concept of passivity is subsequently extended to the new model. Necessary and sufficient conditions for passivity are also reported and proved. Then, Lyapunov stability is extended from the one for hybrid inclusions. As for Chapter 2, application examples will be provided throughout the chapter.

**Chapter 4** introduces the first real application of the developed theory. In particular, the problem of modeling and control a ball–dribbling robot is considered. The main challenges offered by this systems are: under-actuation, dynamic decoupling between the robot and the ball and impacting interactions. First, the system is consistently modeled in hybrid port–Hamiltonian form. Then, a novel energy–based controller is derived from physical intuitions on the system. This controller enhance the classic energy shaping with the iterative learning, allowing the robot to rhythmically bounce the ball at a desired height. Simulations are performed to prove the effectiveness and robustness of the controller.

**Chapter 5** considers the problem of controlling a linear time–invariant system with a finite number of set points. At first, a nonlinear passive controller is used to stabilize simultaneously all the desired set points. Then, a hybrid optimal impulse controller is

designed to switch between the set points. Numerical simulations are carried out for a mechanical system, proving the results. Alongside the theoretical relevance of the developed control technique, it is finally shown how the controlled system can be modeled as hybrid port–Hamiltonian system, implicitly inheriting some useful properties to analyze its behavior.

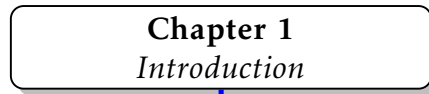
**Chapter 6** proposes a new systematic approach for the identification of a class of hybrid dynamical systems. The main challenge offered by the considered class of systems is the detection of state discontinuities from a time series of state measurements. The proposed solution is based on the analytical computation of an upper bound on the numerically computed time–derivative of the state, above which the system is considered to be “jumping”. After implementing the jump detection function, the parameters of the system are estimated recursively. Simulations are performed on a mechanical systems to show the effectiveness of the proposed method.

**Chapter 7** presents the conclusions of this study and future work.

### 1.3.2 Thesis Content

This thesis is developed across three main broad fundamental fields: control theory, robotics and statistics. The Venn diagram in Fig. 1.3 clarifies how the contents are interconnected within the main research fields. In particular, the first three chapters are related to pure control as port–Hamiltonian systems and hybrid dynamical systems are firstly introduced in Chapter 2 and then merged in Chapter 3. Chapter 5 is also mostly related to theoretical aspects. However, the concepts of Chapter 4, which introduces the ball–dribbling robot encompasses the intersection of control theory and robotics with . Chapter 6 treats the parameters estimation problem for a class of hybrid dynamical systems, spanning in the intersection of control theory and statistics.

Preliminaries & Background



Chapter 2  
*Preliminaries*

Port–Hamiltonian Systems      Hybrid Dynamical Systems

Theoretical Results

Chapter 3  
*Hybrid Port–Hamiltonian Systems*

Applications

Chapter 4  
*Iterative Energy shaping of a Ball–dribbling Robot*

Chapter 5  
*Multistable Energy Shaping with Hybrid Mode Selector*

Chapter 6  
*Identification of a Class of Hybrid Systems*

Conclusion

Chapter 7  
*Discussion and conclusions*

Fig. 1.2: Thesis outline. The colored arrows indicate the logical flows of the contents throughout the thesis, highlighting how the theory presented in the first chapters is employed in the various applications. Chapters in gray blocks contain exclusively original content developed by the author.

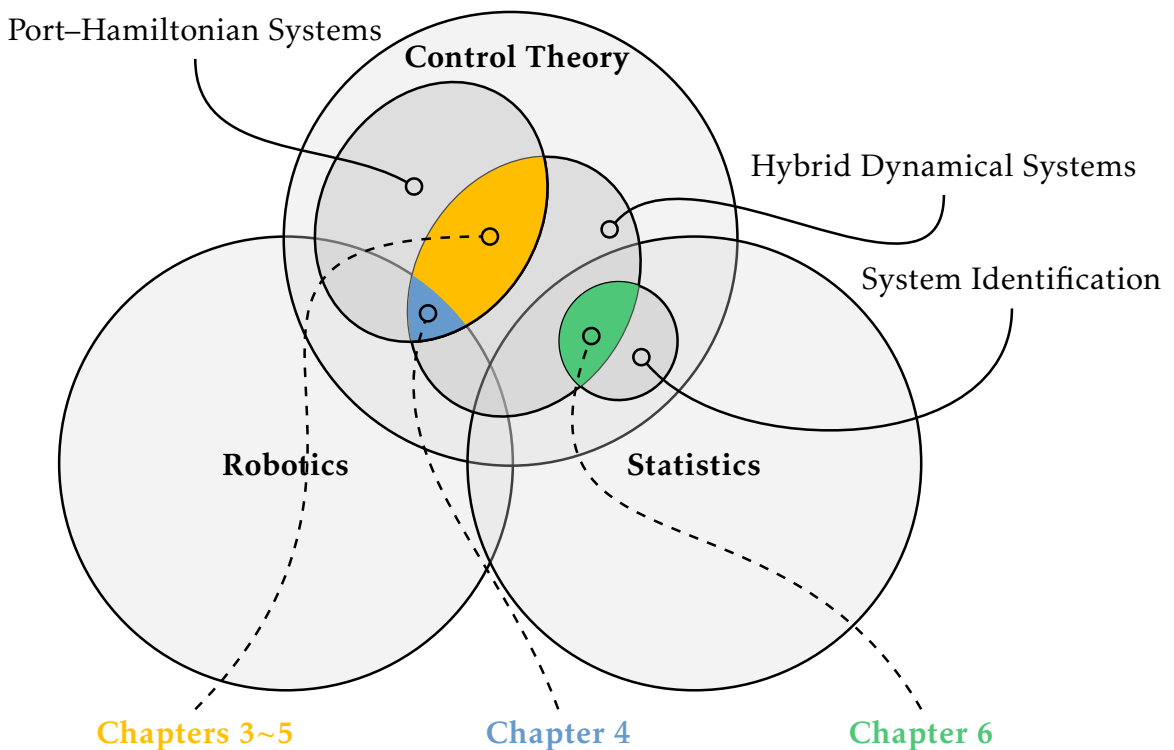


Fig. 1.3: Venn diagram of the contents presented in this thesis. In particular, Chapters 3 and 5 are related to theoretical aspects of hybrid port–Hamiltonian systems. Chapter 4 presents the application of hybrid port–Hamiltonian systems to robotics. Finally, Chapter 6 deals with the identification of hybrid systems, located in the meeting point of control theory and statistics.



# Chapter 2

## Preliminaries

---

2.1	Introduction .....	14
2.2	Stability and Passivity.....	15
2.2.1	Stability of Autonomous Systems .....	15
2.2.2	Passivity: Basic Definitions .....	16
2.2.3	Output Feedback Stabilization of Passive Systems .....	17
2.3	Port–Hamiltonian Systems.....	19
2.3.1	Input–State–Output Model.....	19
2.3.2	Passivity–Based Control .....	25
2.4	Hybrid Dynamical Systems.....	29
2.4.1	Hybrid Inclusions.....	29
2.4.2	Stability.....	31
2.5	Summary .....	33

---

## 2.1 Introduction

THIS chapter briefly introduces the fundamental theories which are employed in the development of this thesis, i.e. the ones of *port-Hamiltonian systems* and *hybrid dynamical systems*. The inclusion of this Chapter in this thesis is justified by the need of smoothly introducing the reader – which might not be an expert on control theory – to the very basic concepts which will be used intensively in the rest of the manuscript. Firstly, the concept of Lyapunov stability and passivity are recalled together with some of the properties of passive system, e.g. output feedback stabilization.

Secondly, the input–state–output model of a port–Hamiltonian (PH) system is defined. Then, it is shown how the power balance equation, derived from the model, highlights the most important properties of this framework. Three modeling examples are provided to give a physical and practical meaning to the theory. The first two examples are related to the dynamics of mechanical systems while the third one is taken from mathematical biology, proving the generality of the PH framework. The passivity–based control of port–Hamiltonian system is then briefly treated, showcasing the popular *energy–balancing* technique. Both theoretical and numerical examples are given.

The latter part of the Chapter deals with hybrid dynamical systems, their *hybrid inclusions* specialization and the basic stability properties of this type of systems. The definition of hybrid inclusion is provided alongside the concept and parametrization of the solutions of this type of models in time domain. Then, an example is provided to consolidate the theory. Finally, the Lyapunov stability theorem for hybrid inclusions is enunciated and applied to the previous examples.

## 2.2 Stability and Passivity

### 2.2.1 Stability of Autonomous Systems

Consider an autonomous time-invariant nonlinear dynamical system

$$\dot{\mathbf{x}} = \mathbf{f}(\mathbf{x}), \quad (2.1)$$

where  $\mathbf{f}: \mathbb{R}^n \supseteq \mathcal{X} \rightarrow \mathbb{R}^n$  is assumed smooth enough such that solutions are forward complete for all initial conditions  $\mathbf{x}_0 \in \mathcal{X}$ . Let  $\mathbf{x}^*$  be a fixed point of (2.1).

**Definition 2.2.1** (Lyapunov Stability (Khalil and Grizzle, 2002)). *The equilibrium point  $\mathbf{x}^*$  of (2.1) is*

- *stable if*

$$\forall \varepsilon > 0 \ \exists \delta_\varepsilon > 0 : \|\mathbf{x}_0 - \mathbf{x}^*\|_2 < \delta_\varepsilon \Rightarrow \|\mathbf{x}(t) - \mathbf{x}^*\|_2 < \varepsilon. \quad (2.2)$$

- *asymptotically stable if*

$$\exists \delta > 0 : \|\mathbf{x}_0 - \mathbf{x}^*\|_2 < \delta \Rightarrow \lim_{t \rightarrow \infty} \mathbf{x}(t) = \mathbf{x}^*. \quad (2.3)$$

- *unstable if it is not stable.*

Stability in the sense of Lyapunov of a system in the form (2.1) can be addressed using Lyapunov's Second theorem.

**Theorem 2.2.2** (Lyapunov's Second Theorem (Khalil and Grizzle, 2002)). *Let  $\mathbf{x}^*$  be a fixed point for (2.1) and  $\mathbf{x}^* \in \mathcal{A} \subset \mathbb{R}^n$ . Let  $V: \mathcal{A} \rightarrow \mathbb{R}$ ,  $V \in \mathcal{C}_1^n$  such that*

$$\forall \mathbf{x} \in \mathcal{A} \setminus \mathbf{x}^* \quad V(\mathbf{x}) > 0 \text{ and } V(\mathbf{x}^*) = 0, \quad (2.4)$$

$$\forall \mathbf{x} \in \mathcal{A} \quad \dot{V}(\mathbf{x}) \leq 0, \quad (2.5)$$

*then  $\mathbf{x}^*$  is stable. Furthermore, if*

$$\forall \mathbf{x} \in \mathcal{A} \setminus \mathbf{x}^* \quad \dot{V}(\mathbf{x}) < 0, \quad (2.6)$$

*then  $\mathbf{x}^*$  is asymptotically stable.*

### 2.2.2 Passivity: Basic Definitions

Let us consider a controlled affine system:

$$\begin{cases} \dot{\mathbf{x}} = \mathbf{f}(\mathbf{x}) + \mathbf{g}(\mathbf{x})\mathbf{u} \\ \mathbf{y} = \mathbf{h}(\mathbf{x}) \end{cases}, \quad (2.7)$$

where  $\mathbf{x} \in \mathcal{X} \subset \mathbb{R}^n$ ,  $\mathbf{u} \in \mathcal{U} \subset \mathbb{R}^m$ ,  $\mathbf{y} \in \mathcal{Y} \subset \mathbb{R}^m$ .  $\mathbf{f}: \mathcal{X} \rightarrow \mathbb{R}^n$ ,  $\mathbf{g}: \mathcal{X} \rightarrow \mathbb{R}^{m \times n}$  ( $\text{rank}(\mathbf{g}) = m \leq n$ ) and  $\mathbf{h}: \mathcal{X} \rightarrow \mathbb{R}^m$  are assumed smooth enough such that the solutions are forward-complete for all initial conditions  $\mathbf{x}_0 \in \mathcal{X}$  and all inputs  $\mathbf{u}(t) \in \mathcal{L}_2^m$ . Let  $\phi(t, \mathbf{x}_0, \mathbf{u})$  denote the state trajectory at time  $t \geq 0$ . A *supply rate* is a real valued function  $w$  defined on  $\mathcal{Y} \times \mathcal{U}$ . The system (2.7) is said to be *dissipative* with respect to the supply rate  $w$  if there exists a continuous function  $\mathcal{H}: \mathcal{X} \rightarrow \mathbb{R}^+$ , called *storage function* such that, for all  $\mathbf{u} \in \mathcal{U}$ ,  $\mathbf{x} \in \mathcal{X}$  and  $t \geq 0$ , it holds

$$\mathcal{H}(\mathbf{x}(t)) - \mathcal{H}(\mathbf{x}(0)) \leq \int_0^t w(s) ds. \quad (2.8)$$

Furthermore, the system is said to be *passive* if it is dissipative with respect to the supply rate  $w = \langle \mathbf{y}, \mathbf{u} \rangle$ . The supply rate  $w$  and the storage function  $\mathcal{H}(\mathbf{x})$  can be thought as the generalized power and the generalized energy<sup>\*1</sup>, respectively. In fact, the pair  $(\mathbf{u}, \mathbf{y})$  represents the medium by which the system can exchange generalized energy through  $w$  (Secchi et al. , 2007).

**Definition 2.2.3.** (Kalman-Yakubovich-Popov (KYP) Property). System (2.7) is said to enjoy the KYP property if there exists a storage function  $\mathcal{H}: \mathcal{X} \rightarrow \mathbb{R}^+$ ,  $\mathcal{H}(\mathbf{x}) \in \mathcal{C}^1$ ,  $\mathcal{H}(\mathbf{0}_n) = 0$  such that:

$$\begin{cases} \nabla \mathcal{H}(\mathbf{x}) \mathbf{f}(\mathbf{x}) \leq 0 \\ \nabla \mathcal{H}(\mathbf{x}) \mathbf{g}(\mathbf{x}) = \mathbf{h}^\top(\mathbf{x}) \end{cases}, \quad (2.9)$$

for all  $\mathbf{x} \in \mathcal{X}$ .

It is worth to notice that  $\nabla \mathcal{H}(\mathbf{x}) \mathbf{f}(\mathbf{x})$  is the natural dissipation of the system while  $\nabla \mathcal{H}(\mathbf{x}) \mathbf{g}(\mathbf{x}) \mathbf{u}(t) = \mathbf{y}^\top(t) \mathbf{u}(t)$  is the instant power flow at time  $t$ .

**Proposition 2.2.4** (Byrnes et al. , 1991a). System (2.7) is passive with storage function  $\mathcal{H}(\mathbf{x}) \in \mathcal{C}^1$  if and only if it enjoys the KYP property.

**Remark 2.2.5.**

- i) Dissipative (and thus passive) systems have no internal production of generalized energy, only its dissipation is possible;
- ii) The total amount of generalized energy that can be extracted from a dissipative system is bounded from above by the amount that is initially stored;
- iii) Strict minima of  $\mathcal{H}$  corresponding to fixed points of (2.7) are Lyapunov stable, as it can be deduced comparing the KYP Property with Theorem 2.2.2.

<sup>\*1</sup> Without any loss of generality,  $\mathcal{H}(\mathbf{x})$  can be taken bounded from below rather than nonnegative, since the properties of storage functions hold regardless of an additive constant.

### 2.2.3 Output Feedback Stabilization of Passive Systems

**Definition 2.2.6** (Observability). A system (2.7) is locally zero state observable if there exists a neighborhood  $\mathcal{B} \subset \mathcal{X}$  such that

$$\forall \mathbf{x} \in \mathcal{B}, \forall t \geq 0 \quad \mathbf{h}(\boldsymbol{\phi}(t, \mathbf{x}, \mathbf{0}_m)) = \mathbf{0}_n \Rightarrow \mathbf{x} = \mathbf{0}_n. \quad (2.10)$$

If  $\mathcal{B} \equiv \mathcal{X}$  the system is said zero state observable.

**Definition 2.2.7** (Detectability). A system (2.1) is locally zero state detectable if there exists a neighborhood  $\mathcal{B} \subset \mathcal{X}$  of  $\mathbf{0}_n$  such that,

$$\forall \mathbf{x} \in \mathcal{B}, \forall t \geq 0 \quad \mathbf{h}(\boldsymbol{\phi}(t, \mathbf{x}, \mathbf{0}_m)) = \mathbf{0}_n \Rightarrow \lim_{t \rightarrow \infty} \boldsymbol{\phi}(t, \mathbf{x}, \mathbf{0}_m) = \mathbf{0}_n. \quad (2.11)$$

If  $\mathcal{B} \equiv \mathcal{X}$  the system is said zero state detectable.

**Definition 2.2.8** (Radially Unbounded (Proper) Function). A nonnegative function  $\mathcal{H}: \mathcal{X} \rightarrow \mathbb{R}^+$  is a radially unbounded (proper) function if

$$\forall r \in \mathbb{R}^{*,+} \quad \{\mathbf{x} \in \mathcal{X} : 0 \leq \mathcal{H}(\mathbf{x}) \leq r\}, \quad (2.12)$$

is compact.

A basic stabilization property of passive system is given by the following theorem, whose proof is closely related to the La Salle's invariance principle (LaSalle, 1960).

**Theorem 2.2.9** (Output Feedback Asymptotic Stabilization (Byrnes et al. , 1991b)). Consider a passive system (2.7):

- i) with a fixed point  $\mathbf{x}^* = \mathbf{0}_n$ ;
- ii) with positive definite storage function  $\mathcal{H}$ ;
- iii) locally zero state detectable.

Let  $\boldsymbol{\alpha}: \mathcal{Y} \rightarrow \mathcal{U}$  be a smooth function such that

$$\boldsymbol{\alpha}(\mathbf{0}_m) = \mathbf{0}_m \quad \wedge \quad \forall \mathbf{y} \in \mathcal{Y} \setminus \{\mathbf{0}_m\} \quad \mathbf{y}^\top \boldsymbol{\alpha}(\mathbf{y}) > 0. \quad (2.13)$$

The control law:

$$\mathbf{u} = -\boldsymbol{\alpha}(\mathbf{y}), \quad (2.14)$$

asymptotically stabilizes the equilibrium point.

**Corollary 2.2.10.** If the system is zero state detectable and  $\mathcal{H}$  is radially unbounded, then the control law (2.14) globally asymptotically stabilizes the system.

Applying a change of coordinates, it can be shown that any strict minimum of the storage function can be (locally) asymptotically stabilized by the output feedback (2.14).

It is also possible to show that an analogous result holds without explicitly assuming the zero-state detectability of the nonlinear system.

**Proposition 2.2.11** (Macchelli, 2003). *If (2.7) is passive with positive definite storage function  $\mathcal{H}$ , the control law 2.14 (locally) asymptotically stabilizes  $\mathbf{x} = \mathbb{0}_n$ , if given a neighborhood  $\mathcal{B}_0$  of  $\mathbf{x} = \mathbb{0}_n$ , the largest invariant set contained in*

$$\{\mathbf{x} \in \mathcal{X} \cap \mathcal{B}_0 : \mathbf{y}(\mathbf{x}) = \mathbb{0}_m\}, \quad (2.15)$$

is  $\{\mathbb{0}_n\}$ .

The final consideration recalled in this section will be one of the most useful in the sect Sections and Chapters.

**Corollary 2.2.12.** *Suppose that a system (2.7) with  $\mathbf{x} = \mathbb{0}_n$  as fixed point, is passive with a  $\mathcal{C}^1$  proper positive definite storage function  $\mathcal{H}$ . If the system is zero-state observable then,  $\forall \mathbf{K} > 0$ , the control law*

$$\mathbf{u} = -\mathbf{K}\mathbf{y}, \quad (2.16)$$

*globally asymptotically stabilizes the equilibrium point.*

## 2.3 Port–Hamiltonian Systems

### 2.3.1 Input–State–Output Model

The input–state–output representation of a port–Hamiltonian system is

$$\begin{cases} \dot{\mathbf{x}} = [\mathbf{J}(\mathbf{x}) - \mathbf{R}(\mathbf{x})] \nabla \mathcal{H}(\mathbf{x}) + \mathbf{G}(\mathbf{x}) \mathbf{u} \\ \mathbf{y} = \mathbf{G}^\top(\mathbf{x}) \nabla \mathcal{H}(\mathbf{x}) \end{cases}, \quad (2.17)$$

where  $\mathbf{x} \in \mathbb{R}^n$  is the state of the system,  $\mathbf{u} \in \mathcal{U} \subset \mathbb{R}^m$  is the input and  $\mathbf{y} \in \mathcal{Y} \subset \mathbb{R}^m$  is the output. Furthermore, the scalar function  $\mathcal{H} : \mathbb{R}^n \rightarrow \mathbb{R}$  is the Hamiltonian of the system (i.e. its energy), the skew symmetric matrix  $\mathbf{J}(\mathbf{x}) = -\mathbf{J}^\top(\mathbf{x})$ ,  $\mathbf{J} \in \mathbb{R}^{n \times n}$  is the interconnection matrix representing power–preserving interconnections related to a Dirac structure. The positive semidefinite matrix  $\mathbf{R}(\mathbf{x}) = \mathbf{R}^\top(\mathbf{x}) \succeq 0$ ,  $\mathbf{R} \in \mathbb{R}^{n \times n}$  represents dissipative effects in the system while the matrix  $\mathbf{G} \in \mathbb{R}^{n \times m}$  ( $\text{rank } \mathbf{G}(\mathbf{x}) = m$ ) represents the power ports.

Note that, in general,  $\mathbf{x} \in \mathcal{X} \subset \mathbb{R}^n$  with  $\mathcal{X}$  being a  $n$ –dimensional manifold,  $\mathcal{U}$  a  $m$ –dimensional vector space and  $\mathcal{Y} = \mathcal{U}^*$  its *dual space*. Consequently the natural pairing  $\langle \mathbf{u}, \mathbf{y} \rangle = \mathbf{y}^\top \mathbf{u}$  can be defined, which carries the unit measure of power.

It is immediate to show that Port–Hamiltonian systems are *passive* by inspecting their power–balance equation. In fact,

$$\dot{\mathcal{H}} = \nabla^\top \mathcal{H}(\mathbf{x}) \dot{\mathbf{x}} \quad (2.18)$$

$$= \nabla^\top \mathcal{H}(\mathbf{x}) [\mathbf{J}(\mathbf{x}) - \mathbf{R}(\mathbf{x})] \nabla \mathcal{H}(\mathbf{x}) + \nabla^\top \mathcal{H}(\mathbf{x}) \mathbf{G}(\mathbf{x}) \mathbf{u} \quad (2.19)$$

$$= -\nabla^\top \mathcal{H}(\mathbf{x}) \mathbf{R}(\mathbf{x}) \nabla \mathcal{H}(\mathbf{x}) + \mathbf{y}^\top \mathbf{u} \quad (2.20)$$

$$\leq \mathbf{y}^\top \mathbf{u}. \quad (2.21)$$

Note that the term  $\nabla^\top \mathcal{H}(\mathbf{x}) \mathbf{R}(\mathbf{x}) \nabla \mathcal{H}(\mathbf{x})$  is given by the natural (internal) dissipation effects of the system as, for instance, friction in mechanical systems, or electrical resistance. and it is often denoted as  $d(t)$ .

The first direct consequence is that any local minimum  $\mathbf{x}^*$  of  $\mathcal{H}(\mathbf{x})$ , i.e.

$$\mathbf{x}^* : \nabla \mathcal{H}(\mathbf{x}^*) = \mathbf{0}_n \wedge \nabla^2 \mathcal{H}(\mathbf{x}^*) \succeq 0, \quad (2.22)$$

is a Lyapunov stable equilibrium point of the system. Furthermore,  $\mathbf{x}^*$  can be asymptotically stabilized with a proper output feedback law (see Subsection 2.2.3).

#### Remark 2.3.1.

1. The PH description of a physical system underlines the energetic properties of the system: the amount of energy stored, (state energy variables), the energy dissipation (dissipative elements), the interfaces with the external world (power ports) and the interconnection structure through which the parts of the system exchange energy.

2. The concepts of port-based modeling have also been extended to distributed parameters systems by Maschke and der Schaft (2000); Maschke and van der Schaft (2001) Rodríguez et al. (2001); Macchelli (2003); Macchelli and Melchiorri (2004); Macchelli et al. (2004a,b).

Three examples of port-Hamiltonian modeling are hereafter reported.

**Example 2.3.2** (Fully-actuated mechanical system). Consider an  $n$ -degrees-of-freedom fully-actuated mechanical system with Lagrange generalized coordinates  $\mathbf{q} \in \mathcal{Q} \subset \mathbb{R}^n$ , inertia matrix  $\mathbf{M}(\mathbf{q})$ , kinetic energy  $\mathcal{K}(\dot{\mathbf{q}}) \triangleq \frac{1}{2}\dot{\mathbf{q}}^\top \mathbf{M}(\mathbf{q})\dot{\mathbf{q}}$  and potential  $\mathcal{V}(\mathbf{q})$ . The Lagrangian of the system  $\mathcal{L}: \mathbb{R}^n \times \mathbb{R}^n \rightarrow \mathbb{R}$  is

$$\mathcal{L}(\mathbf{q}, \dot{\mathbf{q}}) \triangleq \mathcal{K}(\dot{\mathbf{q}}) - \mathcal{V}(\mathbf{q}). \quad (2.23)$$

By defining the generalized momenta conjugated to  $\mathbf{q}$  as

$$\mathbf{p} \triangleq \frac{\partial \mathcal{L}}{\partial \dot{\mathbf{q}}} = \mathbf{M}(\mathbf{q})\dot{\mathbf{q}}, \quad (2.24)$$

an explicit port-Hamiltonian representation of the system can be obtained by defining:

$$\mathbf{x} \triangleq (\mathbf{q}, \mathbf{p}) \in \mathbb{R}^{2n}, \quad (2.25)$$

$$\mathcal{H}(\mathbf{q}, \mathbf{p}) \triangleq \frac{1}{2}\mathbf{p}^\top \mathbf{M}^{-1}(\mathbf{q})\mathbf{p} + \mathcal{V}(\mathbf{q}), \quad (2.26)$$

and, at last,

$$\mathbf{J} = \begin{bmatrix} \mathbb{O}_n & \mathbb{I}_n \\ -\mathbb{I}_n & \mathbb{O}_n \end{bmatrix} \in \mathbb{R}^{2n \times 2n}, \quad \mathbf{R}(\mathbf{q}, \mathbf{p}) = \begin{bmatrix} \mathbb{O}_n & \mathbb{O}_n \\ \mathbb{O}_n & \mathbf{D}(\mathbf{q}, \mathbf{p}) \end{bmatrix} \in \mathbb{R}^{2n \times 2n}, \quad \mathbf{G}(\mathbf{q}) = \begin{bmatrix} \mathbb{O}_n \\ \mathbf{B}(\mathbf{q}) \end{bmatrix} \in \mathbb{R}^{2n \times n},$$

with  $\mathbf{D}(\mathbf{q}, \mathbf{p}) = \mathbf{D}^\top(\mathbf{q}, \mathbf{p}) \succeq 0$ , which takes into account the dissipation effects (friction). Moreover, since the system is fully actuated,  $\mathbf{u} \in \mathbb{R}^n$ ,  $\mathbf{G} \in \mathbb{R}^{2n \times n}$  and  $\text{rank}(\mathbf{G}) = n$ .

Physically, inputs represent external forces (torques) and the outputs are joint velocities. The resulting model is the following:

$$\begin{cases} \begin{bmatrix} \dot{\mathbf{q}} \\ \dot{\mathbf{p}} \end{bmatrix} = \begin{bmatrix} \mathbb{O}_n & \mathbb{I}_n \\ -\mathbb{I}_n & -\mathbf{D}(\mathbf{q}, \mathbf{p}) \end{bmatrix} \begin{bmatrix} \nabla_{\mathbf{q}} \mathcal{H} \\ \nabla_{\mathbf{p}} \mathcal{H} \end{bmatrix} + \begin{bmatrix} \mathbb{O}_n \\ \mathbf{B}(\mathbf{q}) \end{bmatrix} \mathbf{u} \\ \mathbf{y} = [\mathbb{O}_n \quad \mathbf{B}^\top(\mathbf{q})] \begin{bmatrix} \nabla_{\mathbf{q}} \mathcal{H} \\ \nabla_{\mathbf{p}} \mathcal{H} \end{bmatrix} \end{cases}. \quad (2.27)$$

Note that, as expected the natural dissipation of the system (given by friction) becomes

$$d(t) = -\nabla_{\mathbf{p}}^\top \mathcal{H} \mathbf{D}(\mathbf{q}, \mathbf{p}) \nabla_{\mathbf{p}}^\top \mathcal{H} = \quad (2.28)$$

$$= \mathbf{p}^\top \mathbf{M}^{-1}(\mathbf{q}) \mathbf{D}(\mathbf{q}, \mathbf{p}) \mathbf{M}^{-1}(\mathbf{q}) \mathbf{p} = \quad (2.29)$$

$$= \dot{\mathbf{q}}^\top \mathbf{D}(\mathbf{q}, \mathbf{p}) \dot{\mathbf{q}}. \quad (2.30)$$

A graphical representation of the model is provided in Fig. 2.1.

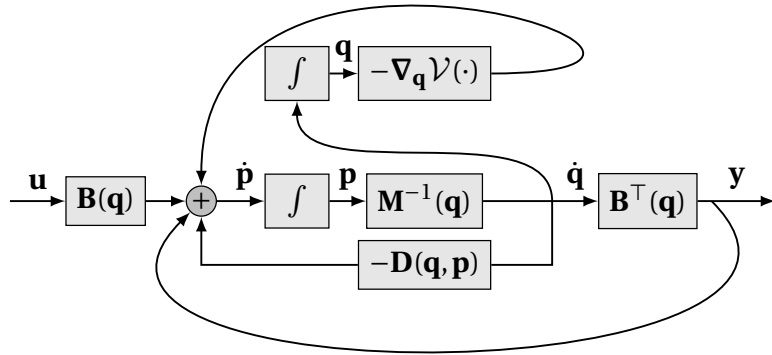


Fig. 2.1: Block diagram of the port-Hamiltonian model of a fully-actuated  $n$ -degrees of freedom mechanical systems. The diagram can be easily obtained from equation (2.27) recognizing that  $\nabla_q \mathcal{H} = \nabla_q \mathcal{V}(q)$  and  $\nabla_p \mathcal{H} = M^{-1}(q)p$ .

With the aim of showing numerical simulations, the linear specialization of the previous example will be now introduced.

**Example 2.3.3** (Mass–spring–damper system). Consider the mass–spring–damper system represented by Fig. 2.2 where  $q$  indicates the absolute position of the mass,  $k$  is the stiffness of the spring and  $b$  is the damping coefficient of the dashpot. Moreover, let  $m$  be the mass of the cart and  $p = m\dot{q}$  its momentum. Indeed, the model is included in the class of systems

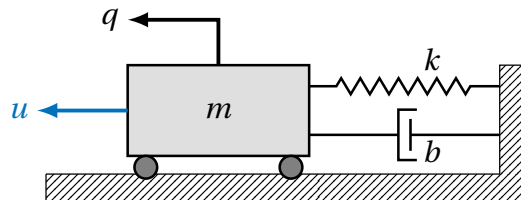


Fig. 2.2: Mass–spring–damper system:  $q$  indicates the absolute position of the mass,  $k$  is the stiffness of the spring and  $b$  is the damping coefficient of the dashpot;  $u$  is an external forcing term , i.e. the control input.

treated in Example 2.3.2 and, thus, admits a port–Hamiltonian representation in the form (2.27):

$$\begin{cases} \begin{bmatrix} \dot{q} \\ \dot{p} \end{bmatrix} = \begin{bmatrix} 0 & 1 \\ -1 & -b \end{bmatrix} \begin{bmatrix} \nabla_q \mathcal{H} \\ \nabla_p \mathcal{H} \end{bmatrix} + \begin{bmatrix} 0 \\ 1 \end{bmatrix} u \\ y = \dot{q} \end{cases}, \quad (2.31)$$

having  $\mathcal{H}$  the following expression

$$\mathcal{H}(q, p) \triangleq \frac{1}{2} \left( \frac{1}{m} p^2 + k q^2 \right). \quad (2.32)$$

The natural dissipation of the system results to be

$$d(t) = \frac{b}{m} p^2(t), \quad (2.33)$$

which means that, if no external inputs are applied ( $u = 0$ ), the energy dissipated in a time interval  $\Delta t$  is

$$\mathcal{H}(t + \Delta t) - \mathcal{H}(t) = - \int_t^{t + \Delta t} d(s) ds = - \frac{b}{m} \int_t^{t + \Delta t} p^2(s) ds. \quad (2.34)$$

A numerical simulation of the autonomous system ( $u = 0$ ) has been performed with  $m = 1\text{Kg}$ ,  $k = 1\text{N}\cdot\text{m}^{-1}$ ,  $[q_0, p_0] = [-0.9, 0]$  and increasing values of  $b$  ( $b = \{0, 0.5, 4\}$ ). The state-space trajectories are shown in Fig. 2.3 while the trend of the energy function  $\mathcal{H}$  and its derivative are plotted in Fig. 2.4. It can be noticed that when there is no dissipation, the state moves on a closed trajectory coinciding to the level set of  $\mathcal{H}$  corresponding to the initial condition. On the other hand, when  $b > 0$ , the trajectory moves on continuously decreasing isolines of  $\mathcal{H}$ , converging to the minimum of  $\mathcal{H}$ .

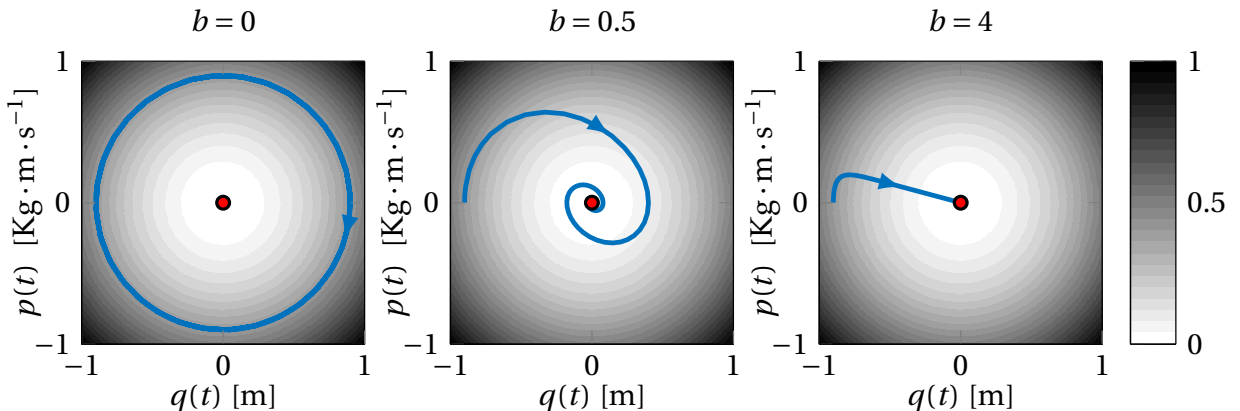


Fig. 2.3: State–space trajectory of the mass–spring damper system for different values of the damping coefficient. The background is the filled contour of the energy function  $\mathcal{H}$ . When  $b = 0$ , there is no energy dissipation and the motion consists in a periodic trajectory (closed curve), i.e. the level set of  $\mathcal{H}$  corresponding to the initial conditions. When  $b = 0.5, 4$ , the state converges toward the minimum of the energy with or without oscillations. The convergence happens by converting elastic potential energy into kinetic energy which is partially dissipated by the dashpot before being reconverted to elastic potential. Higher values of the damping coefficient implies greater dissipation.

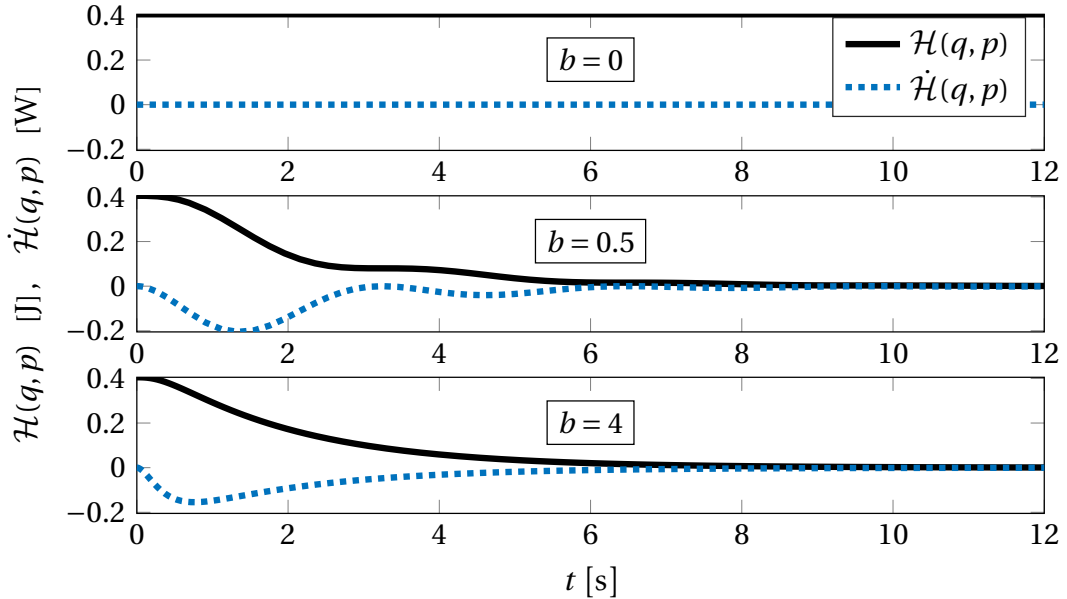


Fig. 2.4: Time evolution of the Energy and its time derivative for the mass–spring damper system. When  $b = 0$ , the energy is conserved. When  $b \neq 0$ , the energy is dissipated as the system’s state reaches its minimum. By increasing the value of the damping coefficient, the energy dissipation rate becomes more uniform as  $\dot{\mathcal{H}}$  has a less oscillations. Note that the convergence time in the cases  $b = 0.5$  and  $b = 4$  is comparable.

**Example 2.3.4** (Lotka–Volterra equations). *This example is inspired by the content of [j2]. The classical formulation of the LV model is the following autonomous dynamical system:*

$$\begin{cases} \dot{\xi} = a\xi - b\xi\eta \\ \dot{\eta} = -c\eta + d\xi\eta \end{cases}, \quad (2.35)$$

where  $\xi(t), \eta(t) \in \mathbb{R}$  represent the time evolution of the populations of prey and predators, respectively. The positive parameters  $a, b, c$ , and  $d$  have the following meaning:

- a: Natural growth rate of the prey in absence of predators;
- b: effect of predation on the prey;
- c: natural death rate of the predators in absence of prey;
- d: efficiency and propagation rate of the predators in the presence of prey.

The Lotka–Volterra model has the structure of a canonical Hamiltonian system (Vulpiani, 2010). Let us divide the two equations in (2.35) by  $\xi$  and  $\eta$ , respectively, and  $(q, p) \triangleq (\ln(\xi), \ln(\eta))$ . This leads to

$$\begin{cases} \frac{\dot{\xi}}{\xi} = a - b\eta \\ \frac{\dot{\eta}}{\eta} = -c + d\xi \end{cases} \Leftrightarrow \begin{cases} \dot{q} = -c + de^p = \frac{\partial}{\partial p}(-cp + de^p + \gamma(q)) \\ \dot{p} = a - be^q = -\frac{\partial}{\partial q}(-aq + be^q + \mu(p)) \end{cases},$$

for any scalar functions  $\gamma(q)$  and  $\mu(p)$ . Selecting

$$\gamma(q) = aq - be^q, \quad \mu(p) = -cp + de^p, \quad (2.36)$$

yields

$$\begin{cases} \dot{q} = \frac{\partial}{\partial p}(-cp + de^p - aq + be^q) = \nabla_p \mathcal{H} \\ \dot{p} = -\frac{\partial}{\partial q}(-cp + de^p - aq + be^q) = -\nabla_q \mathcal{H} \end{cases},$$

and, consequently, the Hamiltonian function results in

$$\mathcal{H}(q, p) = -aq + be^q - cp + de^p. \quad (2.37)$$

The final port-Hamiltonian model is

$$\begin{cases} \begin{bmatrix} \dot{q} \\ \dot{p} \end{bmatrix} = \begin{bmatrix} 0 & 1 \\ -1 & 0 \end{bmatrix} \begin{bmatrix} \nabla_q \mathcal{H} \\ \nabla_p \mathcal{H} \end{bmatrix} + \mathbf{G}(q, p)\mathbf{u} \\ \mathbf{y} = \mathbf{G}^\top(q, p) \begin{bmatrix} \nabla_q \mathcal{H} \\ \nabla_p \mathcal{H} \end{bmatrix} \end{cases}. \quad (2.38)$$

Note that the Lotka–Volterra system is lossless, i.e. the variation of  $\mathcal{H}$  is solely due to the injected (extracted) power:

$$\dot{\mathcal{H}}(\mathbf{x}) = \mathbf{y}^\top \mathbf{u}. \quad (2.39)$$

In the case of classical mechanics, the Hamiltonian function physically represents the total energy of the system. In this case, it simply reflects the “conserved quantity”. Moreover, it is not clear by first principles what inputs and outputs should be. In practice, they would depend on how it is possible to influence the biological system;

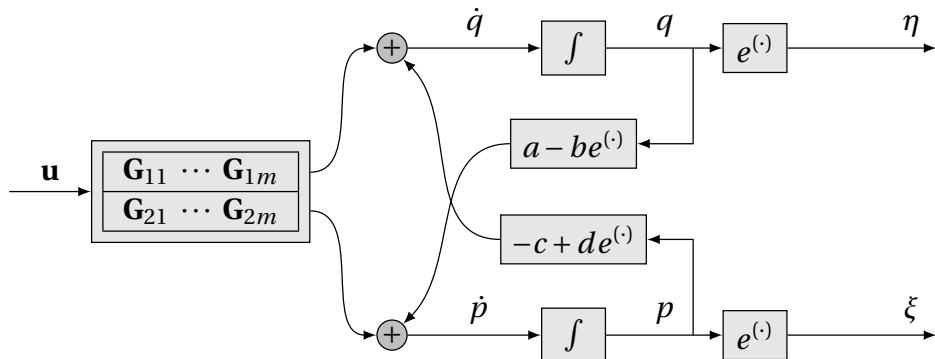


Fig. 2.5: Block diagram representation of the Lotka–Volterra equations in port–Hamiltonian form. The diagram is obtained from equation (2.38).

Up to this point, it has been showed the generality of port–Hamiltonian systems, underlying their use in modeling both physical systems (from first principles) and purely mathematical dynamics. In the following, the basic notions of passivity-based–control (PBC) and the *energy–balancing* PBC technique will be discussed.

### 2.3.2 Passivity-Based Control

As pointed out in the previous Section, any local minimum of the energy is a (locally) stable equilibrium point of the system. Thus, it is intuitive to understand how the *shape* of the energy function is always related to stability properties. In the framework of passivity-based control of port–Hamiltonian systems, controllers are aimed at modify the closed-loop energy function of the plant by changing its *shape* to obtain the desired stability property, e.g. shift the minimum of the energy into a desired set point. This approach is referred to as “energy shaping control”. The energy shaping control problem is hereafter formally introduced.

**Problem 2.3.5** (Passivity-based control). *Consider a PH system (2.17). A control action  $\mathbf{u} = \boldsymbol{\beta}(\mathbf{x}) + \mathbf{v}$  solves the PBC problem if the closed-loop system satisfies a desired power-balance equation*

$$\dot{\mathcal{H}}^*(\mathbf{x}) = \mathbf{z}^\top \mathbf{v} - d^*,$$

where  $\mathcal{H}^*(\mathbf{x})$  is the desired energy function,  $d^*$  the desired dissipation function and  $\mathbf{z} \in \mathbb{R}^m$  the new power conjugated (passive) output.

The most common solution to the PBC problem is the *energy-balancing PBC* (EB-PBC) proposed by Ortega and Mareels (2000). Roughly speaking, the controller is obtained directly from the power balance equation by setting the desired dissipation  $d^*$  equal to the natural dissipation of the system, i.e,

$$d^* \triangleq \nabla^\top \mathcal{H}(\mathbf{x}) \mathbf{R}(\mathbf{x}) \nabla \mathcal{H}(\mathbf{x}) \quad (2.40)$$

and keeping the same output

$$\mathbf{z} \triangleq \mathbf{y}. \quad (2.41)$$

The following proposition gives an operative insight of how to accomplish the EB-PBC control task

**Proposition 2.3.6** (Secchi et al. , 2007). *If it is possible to find a function  $\boldsymbol{\beta}(\mathbf{x})$  such that*

$$\dot{\mathcal{H}}_a(\mathbf{x}) = -\mathbf{y}^\top \boldsymbol{\beta}(\mathbf{x}), \quad (2.42)$$

*then the control law  $\mathbf{u} = \boldsymbol{\beta}(\mathbf{x}) + \mathbf{v}$  is such that*

$$\dot{\mathcal{H}}^*(\mathbf{x}) = \mathbf{y}^\top \mathbf{v} - d^*, \quad (2.43)$$

*is satisfied for  $\mathcal{H}^*(\mathbf{x}) \triangleq \mathcal{H}(\mathbf{x}) + \mathcal{H}_a(\mathbf{x})$ .*

This implies that the state feedback  $\boldsymbol{\beta}(\mathbf{x})$  is such that the *added energy*  $\mathcal{H}_a$  equals the energy supplied to the system and, consequently,  $\mathcal{H}^*$  is the difference between the stored and supplied energy.

In (Ortega et al. , 2008) the closed-form solution of the EB-PBC controller is given by

$$\boldsymbol{\beta}(\mathbf{x}) = -(\mathbf{G}^\top(\mathbf{x}) \mathbf{G}(\mathbf{x}))^{-1} \mathbf{G}^\top(\mathbf{x}) [\mathbf{J}(\mathbf{x}) - \mathbf{R}(\mathbf{x})]^\top \nabla \mathcal{H}_a(\mathbf{x}), \quad (2.44)$$

where  $\mathcal{H}_a$  satisfies the following matching equations

$$\begin{bmatrix} \mathbf{G}^\perp [\mathbf{J} - \mathbf{R}]^\top \\ \mathbf{G}^\top \end{bmatrix} \nabla \mathcal{H}_a(\mathbf{x}) = \mathbb{0}_{n+m}, \quad (2.45)$$

being  $\mathbf{G}^\perp$  a left full-rank annihilator of  $\mathbf{G}$ .

The idea behind this state-feedback control is to “shape” the energy function so that its minima translates towards a new minimum, representing the desired working condition of the controlled system (e.g. *PD + gravity compensation* in robot regulation, Arimoto (1984); Secchi et al. (2007)).

The closed-loop system might still be rewritten in port-Hamiltonian form as

$$\begin{cases} \dot{\mathbf{x}} = [\mathbf{J}(\mathbf{x}) - \mathbf{R}(\mathbf{x})] \nabla \mathcal{H}^*(\mathbf{x}) + \mathbf{G}(\mathbf{x}) \mathbf{v} \\ \mathbf{y} = \mathbf{G}^\top(\mathbf{x}) \nabla \mathcal{H}^*(\mathbf{x}) \end{cases}. \quad (2.46)$$

Furthermore, it is worth to note that the control law

$$\mathbf{v} \triangleq -\mathbf{K}_d \mathbf{y}, \quad (\mathbf{K}_d = \mathbf{K}_d^\top > 0), \quad (2.47)$$

asymptotically stabilizes the minima of  $\mathcal{H}^*(\mathbf{x})$ . This negative output feedback law is usually referred to as *damping injection*. Reasoning in a physical manner, the control law (2.47) behaves as an *dissipative element*, contributing to the energy dissipation together to matrix  $\mathbf{R}(\mathbf{x})$ . In fact,

$$\dot{\mathbf{x}} = [\mathbf{J}(\mathbf{x}) - \mathbf{R}(\mathbf{x})] \nabla \mathcal{H}^*(\mathbf{x}) + \mathbf{G}(\mathbf{x}) \mathbf{v} \quad (2.48)$$

$$= [\mathbf{J}(\mathbf{x}) - \mathbf{R}(\mathbf{x})] \nabla \mathcal{H}^*(\mathbf{x}) - \mathbf{G}(\mathbf{x}) \mathbf{K}_d \mathbf{y} \quad (2.49)$$

$$= [\mathbf{J}(\mathbf{x}) - \mathbf{R}(\mathbf{x})] \nabla \mathcal{H}^*(\mathbf{x}) - \mathbf{G}(\mathbf{x}) \mathbf{K}_d \mathbf{G}^\top(\mathbf{x}) \nabla \mathcal{H}^*(\mathbf{x}) \quad (2.50)$$

$$= [\mathbf{J}(\mathbf{x}) - (\mathbf{R}(\mathbf{x}) + \mathbf{G}(\mathbf{x}) \mathbf{K}_d \mathbf{G}^\top(\mathbf{x}))] \nabla \mathcal{H}^*(\mathbf{x}) \quad (2.51)$$

and  $\mathbf{G}(\mathbf{x}) \mathbf{K}_d \mathbf{G}^\top(\mathbf{x}) \succeq 0$ .

**Remark 2.3.7.** Generally speaking, the design of an EB-PBC might be nontrivial. In fact, it is needed to find such a  $\beta(\mathbf{x})$  which guarantees the solvability of the following partial differential equation

$$\nabla^\top \mathcal{H}_a(\mathbf{x}) [(\mathbf{J}(\mathbf{x}) - \mathbf{R}(\mathbf{x})) \nabla \mathcal{H}(\mathbf{x}) + \mathbf{G}(\mathbf{x}) \beta(\mathbf{x})] = -\mathbf{G}^\top(\mathbf{x}) \nabla \mathcal{H}_a(\mathbf{x}) \beta(\mathbf{x}). \quad (2.52)$$

Few practical examples of the EB-PBC will be given hereafter.

**Example 2.3.8** (Fully-actuated mechanical system). Consider the model (2.27) discussed in Example 2.3.2 and let  $\mathbf{q}^*$  be a desired configuration of the system. A possible choice of  $\beta(\mathbf{q})$  which satisfies the conditions given by Proposition 2.3.6 is

$$\beta(\mathbf{x}) = \mathbf{B}^{-1}(\mathbf{q}) [\nabla_{\mathbf{q}} \mathcal{V}(\mathbf{q}) - \nabla_{\mathbf{q}} \mathcal{H}_a(\mathbf{q}, \mathbf{p})], \quad (2.53)$$

with  $\mathcal{H}_a(\mathbf{q}, \mathbf{p})$  having a minimum is  $\mathbf{q}^*$ . This control action “cancels” the potential  $\mathcal{V}(\mathbf{q})$  and introduces a new potential  $\mathcal{H}_a(\mathbf{q}, \mathbf{p})$ . A simple choice is a spring-like potential, i.e.

$$\mathcal{H}_a(\mathbf{q}, \mathbf{p}) = (\mathbf{q} - \mathbf{q}^*)^\top \mathbf{K}_p (\mathbf{q} - \mathbf{q}^*), \quad \mathbf{K}_p = \mathbf{K}_p^\top > 0. \quad (2.54)$$

Thus, including the damping injection action  $\mathbf{v} = -\mathbf{K}_d \mathbf{y} = -\mathbf{K}_d \mathbf{B}^\top \dot{\mathbf{q}}$ , the control law becomes:

$$\boldsymbol{\beta}(\mathbf{x}) = \mathbf{B}^{-1}(\mathbf{q}) [\nabla_{\mathbf{q}} \mathcal{V}(\mathbf{q}) - \mathbf{K}_p (\mathbf{q} - \mathbf{q}^*)] - \mathbf{K}_d \mathbf{B}^\top \dot{\mathbf{q}}. \quad (2.55)$$

The EB-PBC will then be applied to the mass–spring–damper of Example 2.3.3 to show some numerical insights.

**Example 2.3.9** (Mass–spring–damper system). Consider the mass–spring–damper model (2.31) of Example 2.3.3. We want to apply the control law (2.44). Let us set the desired energy function to

$$\mathcal{H}^*(q, p) \triangleq \frac{1}{2} \left( \frac{1}{m} p + k_p (q - q^*)^2 \right), \quad (2.56)$$

where  $q^*$  is a desired set point. It holds,

$$\mathcal{H}_a = \mathcal{H}^* - \mathcal{H} = \frac{1}{2} k_p (q - q^*)^2 - k q^2 \Rightarrow \nabla \mathcal{H}_a = \left[ k_p (q - q^*) - k q, \frac{p}{m} \right]^\top \quad (2.57)$$

and, therefore,

$$\boldsymbol{\beta}(q) = -[0, 1] \begin{bmatrix} 0 & -1 \\ 1 & -b \end{bmatrix} \begin{bmatrix} k_p (q - q^*) - k q \\ \frac{p}{m} \end{bmatrix} \quad (2.58)$$

$$= -k_p (q - q^*) + k q. \quad (2.59)$$

By adding the damping injection term, the total control input becomes

$$u = -k_p (q - q^*) + k q - k_d \dot{q}. \quad (2.60)$$

A numerical simulation has been performed with  $m = 1\text{Kg}$ ,  $k = 1\text{N}\cdot\text{m}^{-1}$ ,  $b = 0.5\text{N}\cdot(\text{m}\cdot\text{s})^{-1}$ ,  $k_p = 1$ ,  $q^* = 0.5$ ,  $k_d = 4$  and  $[q_0, p_0] = [-0.9, 0]$ . The state–space trajectory is reported in Fig. 2.6. It can be noticed how the minimum of the energy function is shifted to  $[q^*, 0]^\top$  and how the damping injection allow a more “direct” convergence toward the minimum.

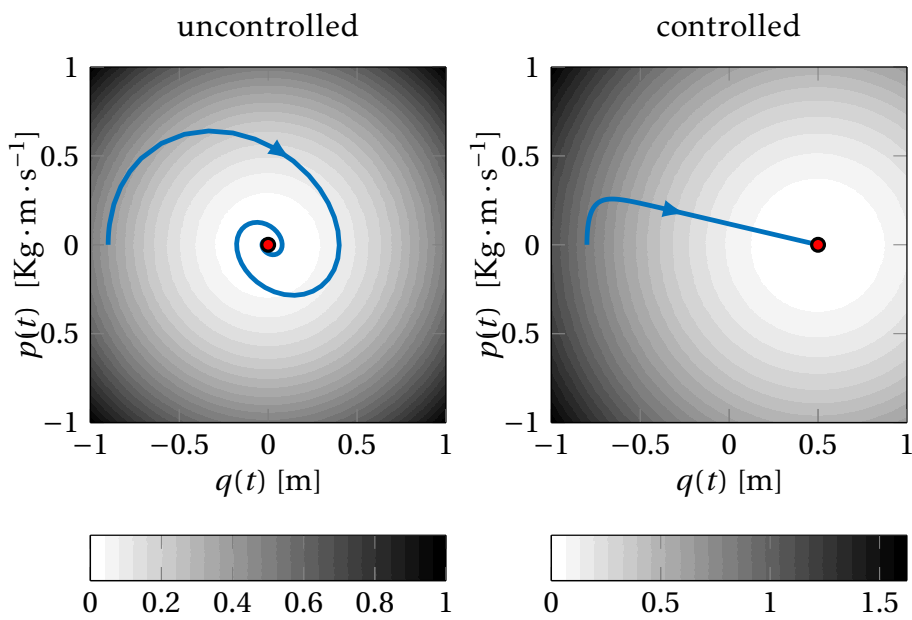


Fig. 2.6: Phase-space trajectory of the mass–spring–damper system control via EB-PBC. When the EB-PBC control input is applied, the location of the minimum of  $\mathcal{H}$  is shifted to the desired set point which, in turns, becomes a Lyapunov stable equilibrium of the closed-loop system. Moreover, the dissipation properties are changed via *damping injection*, removing the oscillations during the motion of the system.

## 2.4 Hybrid Dynamical Systems

The basic notions of hybrid dynamical system and their hybrid inclusions formulation will be now defined. Part of the content of this Section is inspired by the work of Goebel et al. (2009b, 2012).

Hybrid dynamical systems represent a wide class of systems in which continuous time and discrete time dynamics interacts. In recent years, there has been a growing interest in this field. One of the main reason is that these kind of systems provide a new and promising modeling perspective for systems presenting discontinuous behaviors as well as multimodality. The presence of both discrete and continuous dynamics makes this formalism appealing also for modeling physical phenomena in many different areas, from biology and medical applications to robotics, manufacturing, traffic management and bio-molecular networks (Aihara and Suzuki, 2010; Bortolussi and Policriti, 2008). Overviews of this framework are given in (Van Der Schaft and Schumacher, 2000; Haddad et al. , 2006; Goebel et al. , 2009b, 2012).

### 2.4.1 Hybrid Inclusions

Hybrid Inclusions are the most general formulation within hybrid systems framework. They are compound with a constrained differential inclusion and a constrained difference inclusion in the form:

$$\begin{cases} \dot{\mathbf{x}} \in \mathcal{F}(\mathbf{x}, \mathbf{u}_c) & (\mathbf{x}, \mathbf{u}_c) \in \mathcal{C} \times \mathcal{U}_c \\ \mathbf{x}^+ \in \mathcal{G}(\mathbf{x}, \mathbf{u}_d) & (\mathbf{x}, \mathbf{u}_d) \in \mathcal{D} \times \mathcal{U}_d \end{cases}, \quad (2.61)$$

with state  $\mathbf{x} \subseteq \mathbb{R}^n$ , inputs  $\mathbf{u}_c \in \mathcal{U}_c \subseteq \mathbb{R}^{m_c}$ ,  $\mathbf{u}_d \in \mathcal{U}_d \subseteq \mathbb{R}^{m_d}$  acting during *flows* and *jumps* respectively.  $\mathcal{F}: \mathbb{R}^n \times \mathbb{R}^{m_c} \rightrightarrows \mathbb{R}^n$ ,  $\mathcal{G}: \mathbb{R}^n \times \mathbb{R}^{m_d} \rightrightarrows \mathbb{R}^n$  are set-valued mappings and  $\mathcal{C}$ ,  $\mathcal{D}$  are subsets of  $\mathbb{R}^n$  with. Let us call  $\mathcal{C}$  the *flow set*,  $\mathcal{F}$  the *flow map*,  $\mathcal{D}$  the *jump set* and  $\mathcal{G}$  the *jump map*.

The trajectories resulting from this kind of systems are defined on a *hybrid time domain*. In fact, given the dual nature of hybrid systems (continuous and discrete), to parametrize its solutions both a continuous time  $t$  and an discrete time  $k$  are needed.

**Definition 2.4.1** (Hybrid time domain). *Let  $\mathcal{E}$  be a subset of  $\mathbb{R}^+ \times \mathbb{N}$ , i.e.  $\mathcal{E} \subset \mathbb{R}^+ \times \mathbb{N}$ .  $\mathcal{E}$  is a compact hybrid time domain if*

$$\mathcal{E} \triangleq \bigcup_{k=0}^{j-1} [t_k, t_{k+1}] \times k, \quad (2.62)$$

such that

$$t_0 = 0 \wedge \forall k \leq j \quad t_k \leq t_{k+1}, \quad (2.63)$$

and one of the following hold:

- i) there are infinite intervals, i.e.  $j = \infty$ ;

ii)  $j < \infty$  and the last interval is of the form

$$[t_{j-1}, t_f) \times \{j\} \text{ with } t_f < \infty \vee t_f = \infty. \quad (2.64)$$

The solutions of (2.61) are definite on *hybrid arcs* and parametrized by an hybrid time domain  $\mathcal{E}$ . The technical details of this formulation are discussed in (Goebel et al., 2012).

**Example 2.4.2** (ball bouncing on actuated surface). Consider a ball bouncing on an mechanically actuated surface which controls the speed of the ball after impacts. This example is inspired by (Naldi and Sanfelice, 2013). A graphical representation of the system is show in Fig. 2.7. Let  $q$  be the height of the ball from the ground,  $v \triangleq \dot{q}$  be its velocity and let

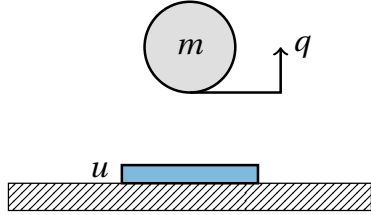


Fig. 2.7: Ball bouncing on an actuated surface.

$\mathbf{x} \triangleq (q, v)$ . While the ball is “flying”, the dynamic of the systems are just the one of a falling rigid body in a fluid of viscosity  $\beta > 0$  due to gravity ( $\gamma = 9.81$ ):

$$\begin{cases} \dot{q} = v \\ \dot{v} = -\gamma - \frac{\beta}{m} v \end{cases} \quad (2.65)$$

and, thus

$$\dot{\mathbf{x}} = \mathcal{F}(\mathbf{x}) \triangleq \begin{bmatrix} 0 & 1 \\ 0 & -\beta/m \end{bmatrix} \mathbf{x} + \begin{bmatrix} 0 \\ -\gamma \end{bmatrix} \quad \text{if } \mathbf{x} \in \mathcal{C} \triangleq \{\mathbf{x}: q \geq 0\} \setminus \{\mathbf{x}: q = 0 \wedge v \leq 0\}. \quad (2.66)$$

When the ball hits the actuated surface, the impact is modeled as

$$\begin{cases} q^+ = q \\ v^+ = (u - c)v \end{cases} \quad c \in (0, 1) \quad (2.67)$$

and, thus

$$\mathbf{x}^+ = \mathcal{G}(\mathbf{x}, u) \triangleq \begin{bmatrix} 1 & 0 \\ 0 & u - c \end{bmatrix} \mathbf{x} \quad \text{if } (\mathbf{x}, u) \in \mathcal{D} \times \mathcal{U}_d \triangleq \{\mathbf{x}: q = 0 \wedge v \leq 0\} \times \mathbb{R}. \quad (2.68)$$

The final hybrid system is

$$\begin{cases} \dot{\mathbf{x}} = \mathcal{F}(\mathbf{x}) & \mathbf{x} \in \mathcal{C} \\ \mathbf{x}^+ = \mathcal{G}(\mathbf{x}, u) & \mathbf{x} \in \mathcal{C} \times \mathcal{U}_d \end{cases}. \quad (2.69)$$

Note that the energy of the system is  $\mathcal{H}(\mathbf{x}) = \frac{m}{2} v^2 + myq$ . A numerical simulation of the autonomous system  $u = 0$  is given with  $m = 1$ ,  $\beta = 0.1$ ,  $c = 0.9$  and  $\mathbf{x} = (1, 0)$ . The resulting trajectory is shown in Fig. 2.8

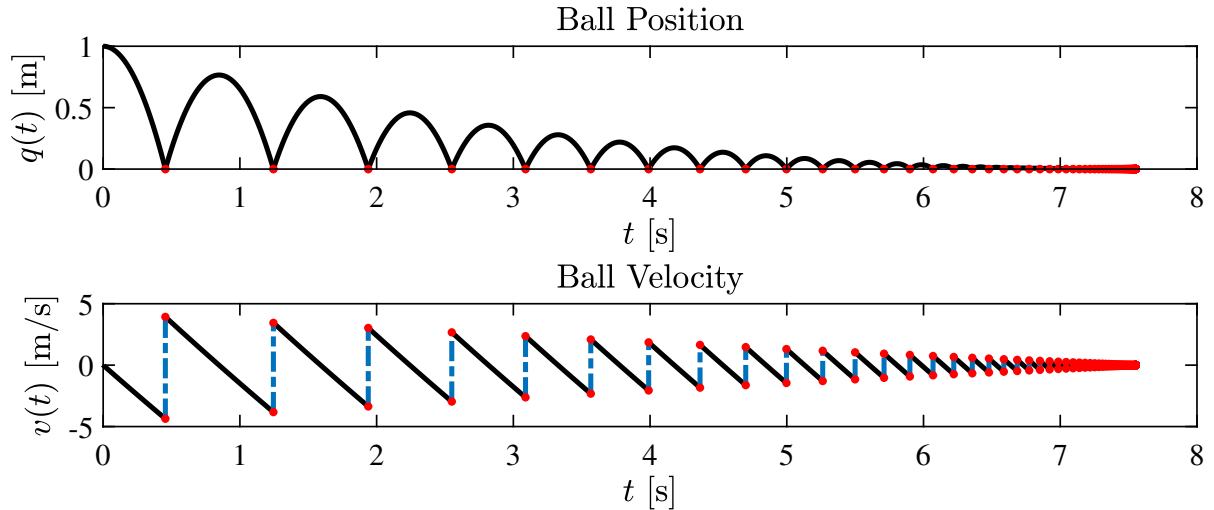


Fig. 2.8: Time evolution of the ball bouncing on the actuated platform (autonomous case).

### 2.4.2 Stability

Lyapunov stability theorems have been indeed extended to the hybrid case. In the case of continuous-time dynamical systems, the stability of equilibrium points is commonly discussed. However, in case of hybrid systems, it is rather convenient to analyze the stability of a set. Hereafter the very basic results on Lyapunov stability of hybrid systems will be introduced.

**Theorem 2.4.3** (Lyapunov Stability for Hybrid Systems (Goebel et al. , 2009b)). *Let us consider an autonomous hybrid system  $(\mathcal{C}, \mathcal{F}, \mathcal{D}, \mathcal{G})$  and a compact set  $\mathcal{A} \subset \mathbb{R}^n$  satisfying  $\mathcal{G}(\mathcal{D} \cap \mathcal{A}) \subset \mathcal{A}$ . If there exists a Lyapunov function candidate  $V : \mathcal{C} \cup \mathcal{D} \rightarrow \mathbb{R}$  such that:*

$$V(\mathbf{x}) > 0 \quad \forall \mathbf{x} \in (\mathcal{C} \cup \mathcal{D}) \setminus \mathcal{A} \quad (2.70a)$$

$$\langle \frac{\partial V}{\partial \mathbf{x}}, \mathbf{f}(\mathbf{x}) \rangle \leq 0 \quad \forall \mathbf{x} \in \mathcal{C} \setminus \mathcal{A}, \mathbf{f} \in \mathcal{F} \quad , \quad (2.70b)$$

$$V(\mathbf{g}(\mathbf{x})) - V(\mathbf{x}) \leq 0 \quad \forall \mathbf{x} \in \mathcal{D} \setminus \mathcal{A}, \mathbf{g} \in \mathcal{G} \quad (2.70c)$$

then the set  $\mathcal{A}$  is stable.

**Corollary 2.4.4** (Goebel et al. (2009b)).

*Let  $\Gamma_\mu := \{x \in \mathcal{C} \cup \mathcal{D} : V(x) = \mu\}$ . If there exists a compact neighborhood  $\mathcal{K}$  of  $\mathcal{A}$  such that, for all  $\mu > 0$ , no solution of the system remains in  $\Gamma_\mu \cap \mathcal{K}$ , then the set  $\mathcal{A}$  is pre-asymptotically stable. In this case the basin of pre-attraction contains every compact set contained in  $\mathcal{K}$  that is forward invariant.*

**Example 2.4.5** (Ball bouncing on actuated platform). *Let consider the autonomous case*

$(u=0)$  and let

$$\mathcal{A} \triangleq \{(q, v) : q \leq \delta q \in \mathbb{R}^+ \wedge |v| \leq \delta v \in \mathbb{R}^+\}. \quad (2.71)$$

Indeed it holds

$$\mathcal{A} \cap \mathcal{D} = \{(0, v) : v \leq 0 \wedge |v| \leq \delta v \in \mathbb{R}^+\} \quad (2.72)$$

and

$$\mathcal{G}(\mathcal{A} \cap \mathcal{D}) = \{(0, -cv) : v \leq 0 \wedge |v| \leq \delta v \in \mathbb{R}^+\} \subset \mathcal{A}. \quad (2.73)$$

Let's examine the stability of  $\mathcal{A}$ . By choosing as Lyapunov function the energy of the system:  $V(\mathbf{x}) = \mathcal{H}(\mathbf{x})$ . It holds,  $\mathcal{H}(\mathbf{x}) > 0 \quad \forall \mathbf{x} \in (\mathcal{C} \cup \mathcal{D}) \setminus \mathcal{A}$  and

$$\langle \frac{\partial \mathcal{H}}{\partial \mathbf{x}}, \mathcal{F}(\mathbf{x}) \rangle = [m\gamma, mv] \begin{bmatrix} 0 & 1 \\ 0 & -\beta/m \end{bmatrix} \begin{bmatrix} q \\ v \end{bmatrix} + [m\gamma, mv] \begin{bmatrix} 0 \\ -\gamma \end{bmatrix} \quad (2.74)$$

$$= -\beta v^2 \leq 0 \quad \forall v \in \mathbb{R}, \quad (2.75)$$

which indeed holds for all  $\mathbf{x} \in \mathcal{C} \setminus \mathcal{A}$ . Finally, stability of  $\mathcal{A}$  is proving noticing that

$$\mathcal{H}(\mathbf{x}^+) - \mathcal{H}(\mathbf{x}) = \frac{m}{2}(v^+)^2 + m\gamma q^+ - \frac{m}{2}v^2 + m\gamma q \quad (2.76)$$

$$= \frac{m}{2}(c-1)v^2 \leq 0 \quad \forall v \in \mathbb{R}, \quad \forall c \in (0, 1), \quad (2.77)$$

which holds also for any  $\mathbf{x} \in \mathcal{D} \setminus \mathcal{A}$ . Note that in the case of the controlled system,  $\mathcal{A}$  remains Lyapunov stable if and only if for all  $t \geq 0$ ,  $u(t) \leq c$ . The descent of the energy during a trajectory of the system is represented in Fig. 2.9.

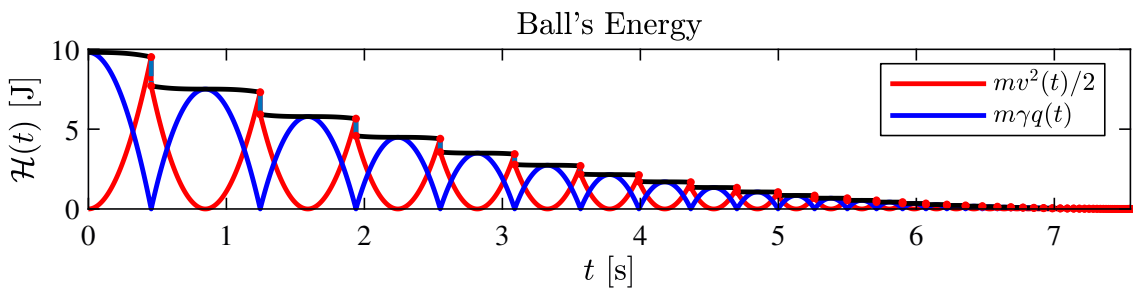


Fig. 2.9: Energy descent during a trajectory of the autonomous system.

## 2.5 Summary

In this chapter, the fundamental mathematical tools needed to develop both the theories and applications in the rest of the thesis, have been provided. In particular, stability and passivity of dynamical systems, port-Hamiltonian systems and hybrid systems

The next chapter will introduce the theory of hybrid port-Hamiltonian system, a major contribution of this thesis.



# Chapter 3

## Hybrid Port–Hamiltonian Systems

---

3.1	Introduction .....	36
3.2	Definitions and Basic Assumptions .....	37
3.2.1	Impulsive Port–Hamiltonian Systems.....	37
3.2.2	Hybrid port–Hamiltonian Systems.....	38
3.3	Passivity .....	42
3.4	Lyapunov Stability of Autonomous Systems.....	44
3.5	Summary .....	46

---

### 3.1 Introduction

**H**EREAFTER, the framework of hybrid port–Hamiltonian systems will be introduced. Starting from the results discussed in Chapter 2, the theories of port–Hamiltonian systems and hybrid inclusions will be merged. Previous attempts of modeling *nonsmooth* system in a port–Hamiltonian fashion exist.

In particular, (Valentin et al. , 2006, 2007) proposed a model for physical switching systems in an *implicit* port–Hamiltonian fashion using *network graph theory* and geometric considerations on the interconnection structure with main practical application to switching electrical circuits. An energy–based method for a class of (mechanical) impulsive port–Hamiltonian systems was also proposed in Haddad et al. (2003). Finally, Ishikawa et al. (2003) described a hopping robot by employing a port–Hamiltonian formulation.

Besides, the above mentioned works are mostly *ad hoc* solutions and do not provide a *big picture* of the framework. Indeed, a unified framework capable of capturing the intrinsic properties of a broad range hybrid dynamic phenomena from an energetic point of view, is still missing.

Firstly, the *impulsive port–Hamiltonian systems* will be characterized. It is a generalization of single–flowed hybrid inclusions in a port–Hamiltonian fashion. This class of system is relevant to this study as most mechanical systems exhibiting (partially) elastic impacts, including robotics applications, belong to this framework.

Afterwards, the general *hybrid port–Hamiltonian system* will be defined. Examples for both classes of the proposed models will be provided.

Then, the concept of passivity will be extended to the hybrid case in the port–Hamiltonian context. Finally Lyapunov stability theorem is also extended from the one of hybrid inclusions.

## 3.2 Definitions and Basic Assumptions

### 3.2.1 Impulsive Port–Hamiltonian Systems

Consider the single–flow specialization of the hybrid inclusion (2.61):

$$\begin{cases} \dot{\mathbf{x}} = \mathbf{f}(\mathbf{x}, \mathbf{u}) & (\mathbf{x}, \mathbf{u}) \in \mathcal{C} \times \mathcal{U} \\ \mathbf{x}^+ \in \mathcal{G}(\mathbf{x}) & \mathbf{x} \in \mathcal{D} \\ \mathbf{y} = \mathbf{h}(\mathbf{x}) \end{cases}, \quad (3.1)$$

with  $\mathbf{f}: \mathbb{R}^n \times \mathbb{R}^m \rightarrow \mathbb{R}^n$ . Here it is assumed that inputs enter into the dynamics only during flows and not during jumps. Therefore,

$$\mathbf{u} \triangleq \mathbf{u}_c, \quad \mathcal{U} \triangleq \mathcal{U}_c. \quad (3.2)$$

This assumption has been made to simplify the model since in most physical systems, no impulsive forcing terms can be practically applied.

**Definition 3.2.1** (Impulsive port–Hamiltonian Systems). *An impulsive port–Hamiltonian system is a system in the form (3.1) with port–Hamiltonian flows and output, i.e.*

$$\begin{cases} \dot{\mathbf{x}} = [\mathbf{J}(\mathbf{x}) - \mathbf{R}(\mathbf{x})] \nabla \mathcal{H}(\mathbf{x}) + \mathbf{G}(\mathbf{x}) \mathbf{u} & (\mathbf{x}, \mathbf{u}) \in \mathcal{C} \times \mathcal{U} \\ \mathbf{x}^+ \in \mathcal{G}(\mathbf{x}) & \mathbf{x} \in \mathcal{D} \\ \mathbf{y} = \mathbf{G}^\top(\mathbf{x}) \nabla \mathcal{H}(\mathbf{x}) \end{cases}. \quad (3.3)$$

The state–space of the system is  $\mathcal{X} \triangleq \mathcal{C} \cup \mathcal{D}$  and  $\mathcal{H}: \mathcal{X} \rightarrow \mathbb{R}$ .

An example of this type of systems is the *ball–dribbling* and *ball–juggling* robots of Fig. 1.1. Note that most mechanical systems exhibiting impacts admit a representation in the form (3.3).

**Example 3.2.2** (Impact Pendulum). *Consider an impact pendulum of mass  $m$  and length  $\ell$  as in Fig. 3.1. Let  $q$  be the pendulum angle and  $p \triangleq m\ell^2 \dot{q}$  its angular momentum. The flows of the system are:*

$$\dot{q} = \frac{1}{m\ell^2} p, \quad \dot{p} = -m\gamma\ell \sin(q) - \frac{\beta}{m\ell^2} p + u, \quad (3.4)$$

where  $u$  is the input torque applied at the joint,  $\gamma$  is the gravitational constant and  $\beta$  is the viscous friction coefficient in the joint. The system admits an impulsive port–Hamiltonian form (3.3) with state  $\mathbf{x} \triangleq (q, p)$ . In particular, the flows are described by the system matrices:

$$\mathbf{J} \triangleq \begin{bmatrix} 0 & 1 \\ -1 & 0 \end{bmatrix}, \quad \mathbf{R} \triangleq \begin{bmatrix} 0 & 0 \\ 0 & \beta \end{bmatrix}, \quad \mathbf{G} \triangleq \begin{bmatrix} 0 \\ 1 \end{bmatrix}. \quad (3.5)$$

The Hamiltonian function is

$$\mathcal{H}(q, p) \triangleq \frac{1}{2m\ell^2} p^2 + mg\ell(1 - \cos(q)). \quad (3.6)$$

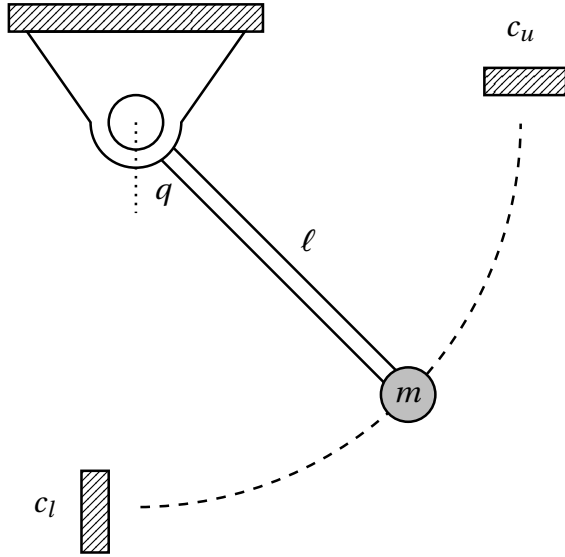


Fig. 3.1: Impact pendulum of mass  $m$  and length  $\ell$ . The system has two impacts, one when the pendulum is at the resting position ( $q = 0$ ) and at  $q = \pi/2$ .

The system has two impacts, one when the pendulum is at the resting position ( $q = 0$ ) and at  $q = \pi/2$ . Thus,

$$\mathbf{x}^+ = \mathbf{g}_1(\mathbf{x}) \triangleq \underbrace{\begin{bmatrix} 1 & 0 \\ 0 & -c_l \end{bmatrix}}_{\mathbf{M}_1} \mathbf{x} \quad \text{if } \mathbf{x} \in \mathcal{D}_1 \triangleq \{\mathbf{x}: q = 0 \wedge p \leq 0\} \quad (3.7)$$

$$\mathbf{x}^+ = \mathbf{g}_2(\mathbf{x}) \triangleq \underbrace{\begin{bmatrix} 1 & 0 \\ 0 & -c_u \end{bmatrix}}_{\mathbf{M}_2} \mathbf{x} \quad \text{if } \mathbf{x} \in \mathcal{D}_2 \triangleq \{\mathbf{x}: q = \pi/2 \wedge p \geq 0\} \quad (3.8)$$

and, therefore,

$$\mathcal{G} \triangleq \{\mathbf{g}_i : \mathbf{x} \in \mathcal{D}_i \Rightarrow \mathbf{x}^+ = \mathbf{g}_i(\mathbf{x}), i = 1, 2\}. \quad (3.9)$$

### 3.2.2 Hybrid port–Hamiltonian Systems

This thesis deals with systems which present a finite number of modes and thus, can be described through an *hybrid automata* (see Van Der Schaft and Schumacher (2000)). However, it is convenient to describe them as hybrid inclusions in the form (2.61). In (Goebel et al. , 2009b) an hybrid inclusion formulation of hybrid automata is given. However, the formulation of hybrid port–Hamiltonian systems will be derived starting from the notion of impulsive port–Hamiltonian system.

Let us consider a dynamical system whose behavior is the collection of  $r$  “modes”

in the form (3.3), i.e.

$$\begin{cases} \dot{\mathbf{x}} = [\mathbf{J}_s(\mathbf{x}) - \mathbf{R}_s(\mathbf{x})] \nabla \mathcal{H}_s(\mathbf{x}) + \mathbf{G}_s(\mathbf{x}) \mathbf{u} & (\mathbf{x}, \mathbf{u}) \in \mathcal{C}_s \times \mathcal{U} \\ \mathbf{x}^+ \in \mathcal{G}_s(\mathbf{x}) & \mathbf{x} \in \mathcal{D}_s \\ \mathbf{y} = \mathbf{G}_s^\top(\mathbf{x}) \nabla \mathcal{H}_s(\mathbf{x}) & s \in \mathcal{M} \end{cases} , \quad (3.10)$$

where  $\mathcal{M} \triangleq \mathbb{N}_{\leq r}^*$ . The transition between one mode and another may happen only during jumps. Therefore, a state extension might be performed to include the mode index in the state:

$$\mathbf{z} \triangleq (\mathbf{x}, s). \quad (3.11)$$

Let us now define the port–Hamiltonian flow set–valued mapping as

$$\mathcal{F}_{\text{PH}}(\mathbf{x}, \mathbf{u}) \triangleq \mathcal{F}(\mathbf{x}, \mathbf{u}) \times \{0\}, \quad (3.12)$$

where

$$\mathcal{F} \triangleq \{\mathbf{f}_i(\mathbf{x}, \mathbf{u}) = [\mathbf{J}_i(\mathbf{x}) - \mathbf{R}_i(\mathbf{x})] \nabla \mathcal{H}_i(\mathbf{x}) + \mathbf{G}_i(\mathbf{x}) \mathbf{u} : (\mathbf{x}, s) \in \mathcal{C}_i \times \{i\} \Rightarrow \dot{\mathbf{x}} = \mathbf{f}_i(\mathbf{x}, \mathbf{u})\}. \quad (3.13)$$

The flow set can be then defined as

$$\mathcal{C} \triangleq \bigcup_{s \in \mathcal{M}} (\mathcal{C}_s \times \{s\}). \quad (3.14)$$

Note that the jump set  $\mathcal{D}_s$  and the jump map  $\mathcal{G}_s(\mathbf{x})$  of each mode enjoy the following:

$$\mathcal{D}_s \triangleq \bigcup_{i \in \mathcal{M}} \mathcal{D}_{s \rightarrow i} \quad \text{and} \quad \mathcal{G}_s(\mathbf{x}) \triangleq \bigcup_{i \in \mathcal{M}} \mathcal{G}_{s \rightarrow i}(\mathbf{x}), \quad (3.15)$$

such that

$$\begin{bmatrix} \mathbf{x}^+ \\ s^+ \end{bmatrix} \in \mathcal{G}_{s \rightarrow i}(\mathbf{x}) \times \{i\} \quad (\mathbf{x}, s) \in \mathcal{D}_{s \rightarrow i} \times \{s\}. \quad (3.16)$$

The port–Hamiltonian jump set–valued mapping is then defined as

$$\mathcal{G}_{\text{PH}}(\mathbf{x}) \triangleq \bigcup_{s \in \mathcal{M}, i \in \mathcal{M}} (\mathcal{G}_{s \rightarrow i}(\mathbf{x}), i), \quad (3.17)$$

while the jump set as

$$\mathcal{D} \triangleq \bigcup_{s \in \mathcal{M}} (\mathcal{D}_s \times \{s\}). \quad (3.18)$$

If the output set valued mapping is also defined as

$$\mathcal{O}_{\text{PH}} \triangleq \{\mathbf{h}_i(\mathbf{x}) = \mathbf{G}_i^\top(\mathbf{x}) \nabla \mathcal{H}_i(\mathbf{x}) : (\mathbf{x}, s) \in \mathcal{C}_s \times \{i\} \Rightarrow y = \mathbf{h}_i(\mathbf{x})\}, \quad (3.19)$$

the formulation of *hybrid port–Hamiltonian system* is the following:

$$\begin{cases} (\dot{\mathbf{x}}, \dot{s}) \in \mathcal{F}_{\text{PH}} & (\mathbf{x}, s) \in \mathcal{C} \\ (\mathbf{x}^+, s^+) \in \mathcal{G}_{\text{PH}} & (\mathbf{x}, s) \in \mathcal{D} \\ y \in \mathcal{O}_{\text{PH}} & \end{cases} . \quad (3.20)$$

**Remark 3.2.3.** The output of both impulsive and hybrid port–Hamiltonian system is defined only during flows for two main reasons. Firstly, jumps occurrences are assumed to happen in zero-measure time intervals. Moreover, it is also assumed that no inputs are applied during jumps and, hence, undefined outputs cannot broke duality.

**Example 3.2.4** (Hopping Robot on elastic ground.). Consider the hopping robot on elastic ground represented in Fig. 3.2 and inspired by Ishikawa et al. (2003). The robot is made

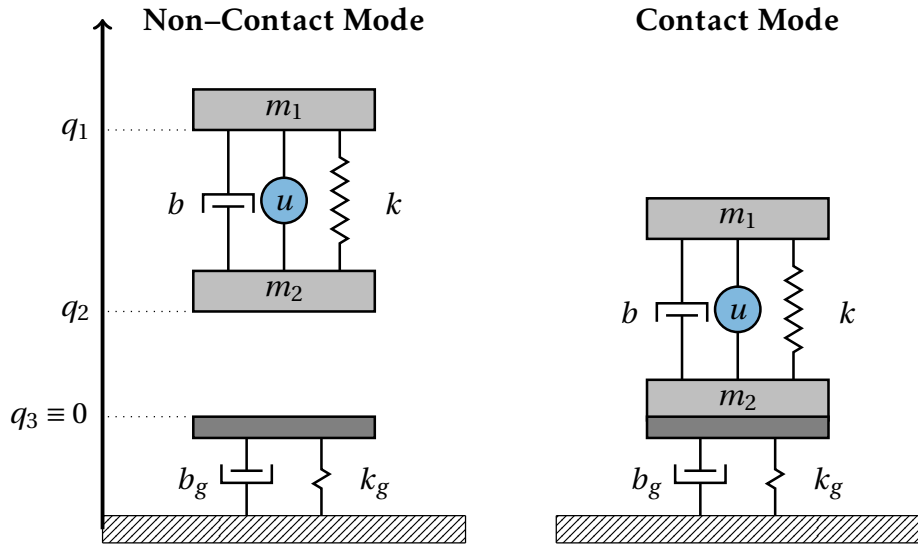


Fig. 3.2: Hopping robot on elastic ground.

up of two masses interconnected with a spring of stiffness  $k$  and resting length  $\ell$ , a dashpot with damping coefficient  $b$  and a linear actuator which exerts an axial force  $u$  (input to the system).  $q_1$ ,  $q_2$  are the absolute height of the masses.

The plate where the robots “hops” is assumed to be massless and connected to the ground with a spring of stiffness  $k_g$  and a dashpot of damping coefficient  $b_g$ .  $q_3$  is the position of the plate and assumed to be zero at rest.

Finally, impacts are considered completely inelastic and that takeoff from ground always happens at  $q_2 = q_3 = 0$ .

The system has two modes “Contact” and “Non-contact”. The flows in contact/non-contact modes are, respectively:

$$\text{non-contact} \quad \begin{cases} m_1 \ddot{q}_1 = -m_1 \gamma - k(q_1 - q_2 - \ell) - b(\dot{q}_1 - \dot{q}_2) + u \\ m_2 \ddot{q}_2 = -m_2 \gamma + k(q_1 - q_2 - \ell) + b(\dot{q}_1 - \dot{q}_2) - u \\ \ddot{q}_3 = 0 \end{cases}, \quad (3.21)$$

$$\text{contact} \quad \begin{cases} m_1 \ddot{q}_1 = -m_1 \gamma - k(q_1 - q_2 - \ell) - b(\dot{q}_1 - \dot{q}_2) + u \\ m_2 \ddot{q}_2 = -m_2 \gamma + k(q_1 - q_2 - \ell) + b(\dot{q}_1 - \dot{q}_2) - k_g q_3 - b_g \dot{q}_3 - u \\ \ddot{q}_3 = \dot{q}_2 \end{cases}. \quad (3.22)$$

Let  $s$  be the mode index and let  $s = 1$  in “non-contact” while  $s = 2$  in contact modes. Moreover, let  $\mathbf{q} \triangleq (q_1, q_2, q_3)$ ,  $\mathbf{p} \triangleq (m_1 q_1, m_2 q_2)$  and  $\mathbf{x} \triangleq (\mathbf{q}, \mathbf{p})$ . The flows of the two system modes

can be then transformed in port-Hamiltonian form with the following system matrices:

$$\mathbf{J}_1 \triangleq \begin{bmatrix} 0 & 0 & 0 & 1 & 0 \\ 0 & 0 & 0 & 0 & 1 \\ 0 & 0 & 0 & 0 & 0 \\ -1 & 0 & 0 & 0 & 0 \\ 0 & -1 & 0 & 0 & 0 \end{bmatrix}, \quad \mathbf{R}_1 \triangleq \begin{bmatrix} 0 & 0 & 0 & 0 & 0 \\ 0 & 0 & 0 & 0 & 0 \\ 0 & 0 & 0 & 0 & 0 \\ 0 & 0 & 0 & b & -b \\ 0 & 0 & 0 & -b & b \end{bmatrix}, \quad \mathbf{G}_1 \triangleq \begin{bmatrix} 0 \\ 0 \\ 0 \\ 1 \\ -1 \end{bmatrix}, \quad (3.23)$$

$$\mathbf{J}_2 \triangleq \begin{bmatrix} 0 & 0 & 0 & 1 & 0 \\ 0 & 0 & 0 & 0 & 1 \\ 0 & 0 & 0 & 0 & 1 \\ -1 & 0 & 0 & 0 & 0 \\ 0 & -1 & -1 & 0 & 0 \end{bmatrix}, \quad \mathbf{R}_2 \triangleq \begin{bmatrix} 0 & 0 & 0 & 0 & 0 \\ 0 & 0 & 0 & 0 & 0 \\ 0 & 0 & 0 & 0 & 0 \\ 0 & 0 & 0 & b & -b \\ 0 & 0 & 0 & -b & b+b_g \end{bmatrix}, \quad \mathbf{G}_2 \triangleq \begin{bmatrix} 0 \\ 0 \\ 0 \\ 1 \\ -1 \end{bmatrix}, \quad (3.24)$$

and Hamiltonian functions

$$\mathcal{H}_1(\mathbf{x}) \frac{1}{2} \triangleq \mathbf{p}^\top \begin{bmatrix} m_1 & 0 \\ 0 & m_2 \end{bmatrix}^{-1} \mathbf{p} + \frac{1}{2} k(q_1 - q_2 - \ell)^2 + \gamma[m_1, m_2] \mathbf{q}, \quad (3.25)$$

$$\mathcal{H}_2(\mathbf{x}) \frac{1}{2} \triangleq \mathbf{p}^\top \begin{bmatrix} m_1 & 0 \\ 0 & m_2 \end{bmatrix}^{-1} \mathbf{p} + \frac{1}{2} k(q_1 - q_2 - \ell)^2 + \frac{1}{2} k_g q_3^2 + \gamma[m_1, m_2] \mathbf{q}. \quad (3.26)$$

The port-Hamiltonian flow set-valued mapping can be then defined as in (3.12). The two flows happen, respectively if

$$(\mathbf{x}, s) \in \mathcal{C}_1 \times \{1\} \triangleq \{\mathbf{x} : \mathbf{q}_2 > 0\} \times \{1\}, \quad (3.27)$$

$$(\mathbf{x}, s) \in \mathcal{C}_2 \times \{2\} \triangleq \{\mathbf{x} : \mathbf{q}_2 \leq 0\} \times \{2\}. \quad (3.28)$$

Transitions between the two modes happen as follows:

$$\begin{bmatrix} \mathbf{x}^+ \\ s^+ \end{bmatrix} = \begin{bmatrix} \mathbf{x} \\ 2 \end{bmatrix} \quad \text{if } (\mathbf{x}, s) \in \mathcal{D}_1 \times \{1\} \triangleq \{\mathbf{x} : q_2 \leq 0\} \times \{1\}, \quad (3.29)$$

$$\begin{bmatrix} \mathbf{x}^+ \\ s^+ \end{bmatrix} = \begin{bmatrix} \mathbf{x} \\ 1 \end{bmatrix} \quad \text{if } (\mathbf{x}, s) \in \mathcal{D}_2 \times \{2\} \triangleq \{\mathbf{x} : q_2 > 0\} \times \{2\}. \quad (3.30)$$

Thus, the jump set and the jump set-valued mapping can be derived as in (3.18), (3.17). Finally, it can be noticed that the output is the same for each mode:

$$y = \mathcal{O}_{\text{PH}} \triangleq \mathbf{G}_1^\top \nabla \mathcal{H}_1(\mathbf{x}) = \mathbf{G}_2^\top \nabla \mathcal{H}_2(\mathbf{x}) = \dot{q}_1 - \dot{q}_2. \quad (3.31)$$

The concept of passivity, fundamental for the theory port-Hamiltonian systems, can be extended to the hybrid case in the following section.

### 3.3 Passivity

The concept and characterization of passivity for hybrid systems has been recently explored by Naldi and Sanfelice (2013).

**Definition 3.3.1** (Passive impulsive port–Hamiltonian system). *A system in the form (3.3) is passive if and only if it satisfies the following dissipation inequality*

$$\forall \mathbf{x} \in \mathcal{D}, \mathbf{g} \in \mathcal{G} \quad \mathcal{H}(\mathbf{g}(\mathbf{x})) - \mathcal{H}(\mathbf{x}) \leq 0. \quad (3.32)$$

Hereafter, necessary and sufficient condition for the passivity of a subclass systems of type (3.3) is given. Firstly, let us start with a basic definition.

**Definition 3.3.2** (Evenly  $\psi$ -diverging function). *Let  $\psi : \mathbb{R}^n \supseteq \text{dom}(\psi) \rightarrow \mathbb{R}^n$ . A map  $\mathcal{H} : \mathbb{R}^n \supseteq \text{dom}(\mathcal{H}) \rightarrow \mathbb{R}$  is evenly diverging with respect to  $\psi$  if*

$$\forall \xi \in \text{dom}(\psi) \quad \mathcal{H}(\psi(\xi)) - \mathcal{H}(\xi) \leq 0 \Leftrightarrow \|\psi(\xi)\|_2 - \|\xi\|_2 \leq 0. \quad (3.33)$$

**Proposition 3.3.3** (Condition for passivity of impulsive port–Hamiltonian systems). *Without any loss of generality, let us assume  $\mathbb{0}$  to be a minimum of  $\mathcal{H}(\mathbf{x})$ :*

$$\mathbb{0}_n = \min_{\mathbf{x} \in \mathcal{X}} \mathcal{H}(\mathbf{x}). \quad (3.34)$$

*A system (3.3) such that  $\mathcal{H}(\mathbf{x})$  is positive in  $\mathcal{X} \setminus \{\mathbb{0}_n\}$ ,  $\mathcal{H}(\mathbb{0}_n) = 0$  and  $\mathcal{H}$  is evenly diverging with respect to all  $\mathbf{g} \in \mathcal{G}$ , is passive if and only if*

$$\|\mathbf{g}\|_\infty \leq 1 \quad \forall \mathbf{g} \in \mathcal{G}. \quad (3.35)$$

*Proof.* If  $\mathcal{H}(\mathbf{x})$  is evenly diverging with respect to all the jump maps, it holds

$$\forall \mathbf{g} \in \mathcal{G}, \mathbf{x} \in \mathcal{X} \quad \mathcal{H}(\mathbf{g}(\mathbf{x})) - \mathcal{H}(\mathbf{x}) \leq 0 \Leftrightarrow \|\mathbf{g}(\mathbf{x})\|_2 \leq \|\mathbf{x}\|_2. \quad (3.36)$$

Then,

$$\mathcal{H}(\mathbf{g}(\mathbf{x})) - \mathcal{H}(\mathbf{x}) \leq 0 \quad \Leftrightarrow \quad \sup_{\mathbf{x} \neq 0} \frac{\|\mathbf{g}(\mathbf{x})\|_2}{\|\mathbf{x}\|_2} \triangleq \|\mathbf{g}\|_\infty \leq 1.$$

□

If  $\mathbf{g}$  is a linear function, i.e.  $\mathbf{g}(\mathbf{x}) = \mathbf{M}\mathbf{x}$  ( $\mathbf{M} \in \mathbb{R}^{n \times n}$ ), condition (3.35) requires that the maximum among the absolute value of the eigenvalues of  $\mathbf{M}$  is less or equal than one:

$$\forall k \in \mathbb{N}_{\leq n}^* \quad \max_k |\lambda_k|_2 \leq 1 \quad \lambda_k : \mathbf{M}\mathbf{v}_k = \lambda_k \mathbf{v}_k. \quad (3.37)$$

Note that this Proposition can be naturally extended to the case in which  $\mathcal{H}$  has a unique minimum in  $\mathbf{x}^*$  by a change of coordinates  $\mathbf{z} \triangleq \mathbf{x} - \mathbf{x}^*$  and requiring  $\mathcal{H} \circ \mathbf{z} : \mathcal{X} \rightarrow \mathbb{R}$  to be evenly diverging with respect to all  $\mathbf{g} \in \mathcal{G}$ .

Here, passivity corresponds to the property of no internal energy generation during jumps. In fact, during flows, the (continuous time) passivity is guaranteed by the port–Hamiltonian structure. Note that Definition 3.3.1 is analogous to the one of *flow-passivity* in Naldi and Sanfelice (2013) applied to single-flows hybrid inclusions with port–Hamiltonian flows.

**Remark 3.3.4.** *Recalling, example 3.2.2, it can be concluded that the impact pendulum model is passive for Proposition 3.3.3 if and only if the restitution coefficients  $c_l, c_u$  are all less than one.*

Passivity can also be defined for hybrid port–Hamiltonian systems by extending Definition 3.3.1 as follows.

**Definition 3.3.5** (Passive hybrid port–Hamiltonian system). *A system in the form (3.20) is passive if and only if it satisfies the following dissipation inequality*

$$\forall s \in \mathcal{M}, i \in \mathcal{M}, \mathbf{x} \in \mathcal{D}_{s \rightarrow i}, \mathbf{g} \in \mathcal{G}_{s \rightarrow i} \quad \mathcal{H}_i(\mathbf{g}(\mathbf{x})) - \mathcal{H}_s(\mathbf{x}) \leq 0. \quad (3.38)$$

Similarly, Proposition 3.3.3 can be also naturally extended to hybrid case. Note that this definition is consistent to the definition of dissipative hybrid automata in (Agarwal et al. , 2017).

**Remark 3.3.6.** *The hopping robot of Example 3.2.4 is passive since the jump maps are simply the identity and, thus, there is no energy variation during jumps (jump–lossless).*

Lyapunov stability of both, impulsive and hybrid port–Hamiltonian systems, will be addressed in the next section.

### 3.4 Lyapunov Stability of Autonomous Systems

The following theorem has been derived from Theorem 2.4.3.

**Theorem 3.4.1** (Lyapunov Stability of Impulsive port–Hamiltonian Systems). *Consider a system in the form (3.3) with  $\mathbf{u} = 0$  and a compact set  $\mathcal{A} \subset \mathcal{X}$  satisfying  $\mathcal{G}(\mathcal{D} \cap \mathcal{A}) \subset \mathcal{A}$ . If*

$$\mathcal{H}(\mathbf{x}) > 0 \quad \forall \mathbf{x} \in (\mathcal{C} \cup \mathcal{D}) \setminus \mathcal{A}, \quad (3.39a)$$

$$\mathcal{H}(\mathbf{g}(\mathbf{x})) - \mathcal{H}(\mathbf{x}) \leq 0 \quad \forall \mathbf{x} \in \mathcal{D} \setminus \mathcal{A}, \forall \mathbf{g} \in \mathcal{G}, \quad (3.39b)$$

then the set  $\mathcal{A}$  is stable.

*Proof.* The proof is obtained directly from Theorem 2.4.3. Firstly, let us assume  $\mathcal{H}$  to be the candidate Lyapunov function. Then, conditions (2.70a) and (2.70c) correspond, respectively to (3.39a), (3.39b). Finally, condition (2.70b) is automatically satisfied due to the port–Hamiltonian structure of the flows, i.e.

$$\langle \nabla \mathcal{H}(\mathbf{x}), \dot{\mathbf{x}} \rangle = \nabla \mathcal{H}^\top(\mathbf{x}) \mathbf{R}(\mathbf{x}) \nabla \mathcal{H}(\mathbf{x}) \leq 0. \quad (3.40)$$

Thus, if the conditions of this Theorem are satisfied, the system is Lyapunov stable according to Theorem 2.4.3.  $\square$

Note that the condition (3.39b) is automatically satisfied if (3.3) is passive.

**Corollary 3.4.2.** *Consider a system in the form (3.3) and assume it to be passive. If*

$$\exists \mathbf{x}^* : \forall \mathbf{x} \neq \mathbf{x}^* \quad \mathcal{H}(\mathbf{x}) > 0, \quad \mathcal{H}(\mathbf{x}^*) = 0, \quad (3.41)$$

then, for any  $\epsilon > 0$  there exists a Lyapunov stable set

$$\mathcal{A}_\epsilon = \{\mathbf{x} : \mathcal{H}(\mathbf{x}) \leq \epsilon\}. \quad (3.42)$$

Thus, every neighborhood of any strict minimum of  $\mathcal{H}$  is stable as long as (3.20) is passive.

**Remark 3.4.3.** *Regarding the impact pendulum of Example 3.2.2, any neighborhood  $\mathcal{B}_{0^+}$  of the origin,*

$$\mathcal{B}_{0^+} \triangleq \{(q, p) : 0 \leq q \leq \delta q \in \mathbb{R}^+ \wedge 0 \leq p \leq \delta p \in \mathbb{R}^+\}, \quad (3.43)$$

can be easily proven to be a Lyapunov stable set according to Theorem 3.4.1. Moreover, thanks to Corollary 3.4.2, it can be deduced that for all nonnegative  $\epsilon$ ,  $\mathcal{A}_\epsilon$  is Lyapunov stable.

It is trivial to extend also Lyapunov stability to the hybrid port–Hamiltonian case by means of multiple Lyapunov functions. However, only passive systems are worth to be considered.

Minima of the Hamiltonian function are known to be asymptotically stable fixed points of port–Hamiltonian systems with non–null dissipation. Along any trajectory,

the system will dissipate its energy eventually landing in one of the minima of the Hamiltonian.

Nevertheless, this holds also for hybrid port-Hamiltonian systems<sup>\*1</sup>. The main difference is that here energy is dissipated also during discrete jumps and thus, the state will eventually converge to one of the Hamiltonian minima of some system's mode.

Finally, it can also be proven that, if there exists a point  $\mathbf{x}^*$  being the unique strict minimum of each mode's Hamiltonian function, then  $\mathbf{x}^*$  is stable and globally attractive.

---

<sup>\*1</sup> Here we are taking for granted well-posedness and regularity (maximality) of solutions.

## 3.5 Summary

In this chapter, hybrid port–Hamiltonian systems have been defined. Both passivity and stability have also characterized.

As a final consideration, this chapter left opened the utility of this modeling framework for real applications, either in robotics or control theory.

Following, in the next chapters several applications are proposed, ranging from the control a ball–dribbling robot to the hybrid control of linear systems. Note that, in the latter case, explored in Chapter 5, the “hybrid” nature is not given by the physics of the system but from the controller.

## Chapter 4

# Iterative Energy Shaping of a Ball–Dribbling Robot

---

4.1	Introduction .....	48
4.2	Model of the Ball–Dribbling Robot.....	49
	4.2.1 Port-Hamiltonian Model of Flows.....	49
	4.2.2 Model of the Impacts .....	49
4.3	Analysis of the Autonomous Model .....	52
	4.3.1 Passivity and Autonomous Stability .....	52
	4.3.2 Chaotic Trajectories.....	52
4.4	Dribbling Control .....	57
4.5	Numerical Simulations.....	60
	4.5.1 Autonomous System .....	60
	4.5.2 Controlled System .....	60
	4.5.3 Numerical Stability and Robustnes Analysis .....	62
4.6	Summary .....	76

---

## 4.1 Introduction



CHALLENGING control problems are often the best and most direct way to prove the validity of a modeling framework. This chapter introduces a novel method for controlling a *ball–dribbling* robot. A representation of the controlled system is given in Figure 4.1.

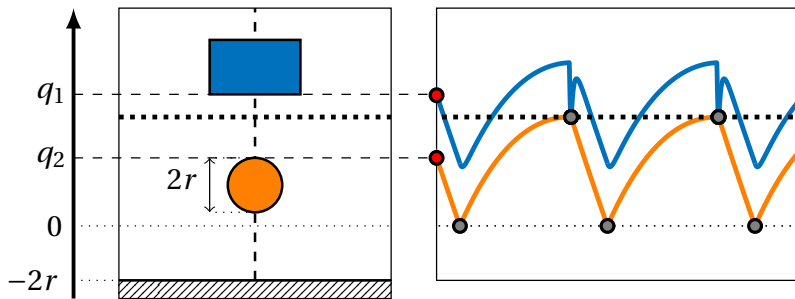


Fig. 4.1: One-dimensional ball–dribbling robotic system. The position of the robot (rectangle), is represented by the variable  $q_1$  while  $u$  is an input force applied to it. Moreover, the position of the ball (circle), of radius  $r$ , is represented by  $q_2$ .

This model belongs to the class of *impulsive port–Hamiltonian* systems. The ball–dribbling problem has been previously considered by Bätz et al. (2010). In their work authors assumed the absence of any viscous friction effect, the exact knowledge of the ball’s mass and the experimental estimation of the impacts’ restitution coefficients. Moreover, they assumed the end–effector of the robot to be elastic and thus no instantaneous robot–ball contacts were possible. A similar consideration can be done for the work presented in (Haddadin et al. , 2018), where the elastic potential energy stored in the robot end–effector was exploited to perform the dribbling task. While compared to the previous work, our method, relax all the assumption by considering the viscous friction and do not require the knowledge of any parameter characterizing the ball’s dynamics.

The proposed novel control technique attempts at casting energy shaping in a learning context. By “learning” here it is intended that the control law is adjusted on the bases of previous iterations. In chain, the concept of iterations, or trials, arise naturally in this context since for, the class of systems that are considered, the discontinuous dynamics separating the flows, can be used to implicitly recognize trials without introducing additional structure.

Numerical simulations, performed to steer the output of such a system along a periodic reference, successfully demonstrate the efficacy of the proposed approach. In particular, in the simulation experiments, the control task that is achieved is the periodic bouncing of the ball by means of impacts at a constant and prescribed height.

## 4.2 Model of the Ball–Dribbling Robot

### 4.2.1 Port-Hamiltonian Model of Flows

Let  $q_1$  be the position of the robot,  $q_2$  the position of the ball and  $p_1 \triangleq m_1 \dot{q}_1$ ,  $p_2 \triangleq m_2 \dot{q}_2$  the momenta of the robot and the ball respectively. The state-space model of the system is:

$$\begin{cases} \dot{q}_1 = \frac{1}{m_1} p_1, & \dot{p}_1 = -m_1 \gamma - \frac{\beta_1}{m_1} p_1 + u \\ \dot{q}_2 = \frac{1}{m_2} p_2, & \dot{p}_2 = -m_2 \gamma - \frac{\beta_2}{m_2} p_2 \end{cases}, \quad (4.1)$$

being  $\gamma$  the gravitational acceleration (i.e.,  $\gamma = 9.81 \text{ m/s}^2$ ), and  $\beta_1, \beta_2 > 0$  the viscous friction coefficients. Let  $\mathbf{q} \triangleq (q_1, q_2)$ ,  $\mathbf{p} \triangleq (p_1, p_2)$  and  $\mathbf{x} \triangleq (\mathbf{q}, \mathbf{p})$ . The system can be expressed in the canonical port–Hamiltonian form defining the Hamiltonian function as the total energy, i.e.

$$\mathcal{H}(\mathbf{q}, \mathbf{p}) \triangleq \frac{1}{2} \mathbf{p}^\top \mathbf{M}^{-1} \mathbf{p} + \mathcal{V}(\mathbf{q}), \quad (4.2)$$

where  $\mathbf{M} = \text{diag}(m_1, m_2)$  and  $\mathcal{V}(\mathbf{q}) = \gamma[m_1, m_2]\mathbf{q}$ . Then, the port–Hamiltonian dynamics are defined by the system matrices

$$\mathbf{J} \triangleq \begin{bmatrix} 0 & 0 & 1 & 0 \\ 0 & 0 & 0 & 1 \\ -1 & 0 & 0 & 0 \\ 0 & -1 & 0 & 0 \end{bmatrix}, \quad \mathbf{R} \triangleq \begin{bmatrix} 0 & 0 & 0 & 0 \\ 0 & 0 & 0 & 0 \\ 0 & 0 & \beta_1 & 0 \\ 0 & 0 & 0 & \beta_2 \end{bmatrix}, \quad \mathbf{G} \triangleq \begin{bmatrix} 0 \\ 0 \\ 1 \\ 0 \end{bmatrix}. \quad (4.3)$$

In this way, the natural pairing between input and output leads to

$$y = \mathbf{G}^\top \nabla \mathcal{H} = \frac{1}{m_1} p_1 = \dot{q}_1. \quad (4.4)$$

Indeed, the flow set  $\mathcal{C}$  is

$$\begin{aligned} \mathcal{C} \triangleq & \{\mathbf{x}: q_1 \geq q_2 \geq 0\} \setminus [\{\mathbf{x}: q_2 = 0 \wedge p_2 < 0\} \cup \\ & \cup \{\mathbf{x}: q_1 = q_2 \wedge (p_1 p_2 < 0 \vee m_2 p_1 < m_1 p_2)\}]. \end{aligned} \quad (4.5)$$

**Remark 4.2.1.** *The system is under-actuated as an input force can be applied only to the robot. Furthermore, from physical considerations, it can be derived that the behavior of the robot does not influence in any way the flow of the ball. However, the dynamics of the overall hybrid system will be coupled during jumps: the robot can influence the ball's motion (and vice versa) through impacts.*

### 4.2.2 Model of the Impacts

Considering the ball-dribbling robot, discontinuities of the system's state may happen in two situations: during the collision between ball and the floor or the one between

the robot and the ball. Here collisions are considered partially inelastic while both the robot and the ball, are modeled as rigid bodies.

### Ball-Floor Collisions

The collision of the ball with the ground will causes a sudden change of the ball's momentum:

$$p_2^+ = -c_g p_2, \quad (4.6)$$

where  $c_g \in (0, 1)$  is the *ball-ground restitution coefficient*. Therefore, the resulting jump map is

$$\mathbf{x}^+ = \mathbf{g}_1(\mathbf{x}) = \underbrace{\begin{bmatrix} 1 & 0 & 0 & 0 \\ 0 & 1 & 0 & 0 \\ 0 & 0 & 1 & 0 \\ 0 & 0 & 0 & -c_g \end{bmatrix}}_{\mathbf{M}_1} \mathbf{x}. \quad (4.7)$$

The jump happens if  $\mathbf{x} \in \mathcal{D}_1$ , where the jump set  $\mathcal{D}_1$  is the following sub-manifold of the state space:

$$\mathcal{D}_1 \triangleq \{\mathbf{x}: q_2 = 0 \wedge p_2 < 0\}. \quad (4.8)$$

### Robot-Ball Collisions

During the collisions between the robot and the ball, both the robot and ball momenta will change discontinuously as follows. The conservation law of the total momentum yields:

$$p_1^+ + p_2^+ = p_1 + p_2. \quad (4.9)$$

Considering the partial inelasticity of the impacts:

$$\frac{p_1^+}{m_1} - \frac{p_2^+}{m_2} = -c_i \left( \frac{p_1}{m_1} - \frac{p_2}{m_2} \right), \quad (4.10)$$

where  $c_i \in (0, 1)$  is the *robot-ball restitution coefficient*. It follows that

$$\begin{bmatrix} p_1^+ \\ p_2^+ \end{bmatrix} = \begin{bmatrix} p_1 - \mu(m_2 p_1 - m_1 p_2) \\ p_2 + \mu(m_2 p_1 - m_1 p_2) \end{bmatrix}, \quad \mu = \frac{c_i + 1}{m_1 + m_2}. \quad (4.11)$$

Thus, the corresponding jump map is

$$\mathbf{x}^+ = \mathbf{g}_2(\mathbf{x}) = \underbrace{\begin{bmatrix} 1 & 0 & 0 & 0 \\ 0 & 1 & 0 & 0 \\ 0 & 0 & 1 - \mu m_2 & \mu m_1 \\ 0 & 0 & \mu m_2 & 1 - \mu m_1 \end{bmatrix}}_{\mathbf{M}_1} \mathbf{x}. \quad (4.12)$$

The robot-ball collision happens if  $\mathbf{x} \in \mathcal{D}_2$ , where the jump set  $\mathcal{D}_2$  is:

$$\mathcal{D}_2 \triangleq \{\mathbf{x}: q_1 = q_2 \wedge (p_1 p_2 < 0 \vee m_2 p_1 < m_1 p_2)\}. \quad (4.13)$$

The overall jump set  $\mathcal{D}$  is defined as  $\mathcal{D} \triangleq \mathcal{D}_1 \cup \mathcal{D}_2$  and the resultant set-valued mapping of the jumps is

$$\mathcal{G} \triangleq \{\mathbf{g}_i : \mathbf{x} \in \mathcal{D}_i \Rightarrow \mathbf{x}^+ = \mathbf{g}_i(\mathbf{x}), i = 1, 2\}. \quad (4.14)$$

The final hybrid system can be then written in the form (3.3). Note that the state-space manifold  $\mathcal{X}$  is:

$$\mathcal{X} \triangleq \mathcal{C} \cup \mathcal{D} = \{\mathbf{x}: q_1 \geq q_2 \geq 0\}. \quad (4.15)$$

and that

$$\forall \mathbf{x} \in \mathcal{X} \setminus \{\mathbf{0}_4\} \quad \mathcal{H}(\mathbf{x}) > 0 \quad \wedge \quad \mathcal{H}(\mathbf{0}_4) = 0. \quad (4.16)$$

In Fig. 4.2 the *hybrid automata* of the autonomous system ( $u = 0$ ), is represented.

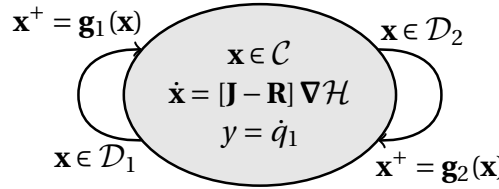


Fig. 4.2: Hybrid automata of the autonomous system. It has a single mode for flows, described by an autonomous port-Hamiltonian system, and it has two jumps:  $\mathbf{g}_1$  resets the states during *ball-ground* collisions ( $\mathbf{x} \in \mathcal{D}_1$ ) while  $\mathbf{g}_2$  resets the states during *robot-ball* collisions ( $\mathbf{x} \in \mathcal{D}_2$ ).

## 4.3 Analysis of the Autonomous Model

### 4.3.1 Passivity and Autonomous Stability

**Proposition 4.3.1.** *The ball–dribbling robot is passive.*

*Proof.* Let  $\hat{q}_1, \hat{q}_2, \hat{p}_1, \hat{p}_2$  be the versors of the axes  $q_1, q_2, p_1, p_2$ .  $\mathcal{H}(\mathbf{x})$  is nondecreasing along the eigendirections of  $\mathbf{g}_1, \mathbf{g}_2$  which are, respectively, the one of the axis  $(\hat{q}_1, \hat{q}_2, \hat{p}_1, \hat{p}_2)$  and  $(\hat{q}_1, \hat{q}_2, m_2\hat{p}_1 + m_1\hat{p}_2, \hat{p}_1 - \hat{p}_2)$ , i.e.  $\mathcal{H}$  is evenly diverging with respect to  $\mathbf{g}_1, \mathbf{g}_2$ . Thus, the ball–dribbling robot is passive for Proposition 3.3.3 as  $\mathbf{M}_1$  has eigenvalues  $\lambda_{1,2,3} = 1, \lambda_4 = -c_g$  and  $\mathbf{M}_2$  has eigenvalues  $\lambda_{1,2,3} = 1, \lambda_4 = -c_i$ , whose norms are indeed all less or equal than one.  $\square$

Moreover, it is very straightforward to prove that in the case of the autonomous system ( $u = 0$ ), any neighborhood of the origin  $\mathbb{0}_4$  is a Lyapunov stable set.

### 4.3.2 Chaotic Trajectories

Let us consider the uncontrolled system and set the physical parameters so that the system is conservative, i.e.  $c_i = c_g = 1, \beta_1 = \beta_2 = 0$ . In this case, the Hamiltonian is constant,

$$\forall t \geq 0, \mathbf{x} \in \mathcal{C} \quad \dot{\mathcal{H}}(\mathbf{x}(t)) = 0, \quad (4.17)$$

$$\forall t \geq 0, \mathbf{x} \in \mathcal{D}, \mathbf{g} \in \mathcal{G} \quad \mathcal{H}(\mathbf{g}(\mathbf{x}(t))) - \mathcal{H}(\mathbf{x}(t)) = 0. \quad (4.18)$$

Thus, trajectories lie on foliations of level sets Hamiltonian corresponding to possible initial conditions  $\mathbf{x}_0$ :

$$\forall t \geq 0 \quad \mathbf{x}(t) \in \{\mathbf{x}: \mathcal{H}(\mathbf{x}) = \mathcal{H}(\mathbf{x}_0)\} \quad (4.19)$$

and the Liouville theorem (a reference is necessary HERE) (in the form of Boltzmann equation) also guarantees conservation of the phase–space measure.

However, although the system is linear, chaos emerges due to the presence of impacts. The system is in fact characterized by an exceptional sensitivity to the initial condition: trajectories starting “very close” tend to diverge in time (within the limited phase–space).

With the aim of revealing the dawn of chaos, a numerical experiment has been performed in the modus operandi of a Monte Carlo simulation. The system has been integrated for 3000 different initial conditions  $\mathbf{x}_0^i$  sampled by a multivariate normal distribution centered in a nominal initial condition  $\mathbf{x}_0$  and with variance  $\sigma = 10^{-6}$ :

$$\mathbf{x}_0^i \sim \mathcal{N}(\mathbf{x}_0, \sigma \mathbb{I}_n). \quad (4.20)$$

Choosing  $\mathbf{x}_0 \triangleq (2, 1.5, 0, 0)$ ,  $m_1 = 1\text{Kg}$  and  $m_2 = 0.15\text{Kg}$ , the nominal trajectory and the other 3000 ones have been integrated for  $t = 20\text{s}$ . The experiments have been carried out with the *Hybrid Equations (HyEQ) Toolbox* (Sanfelice et al. , 2013) for the MATLAB

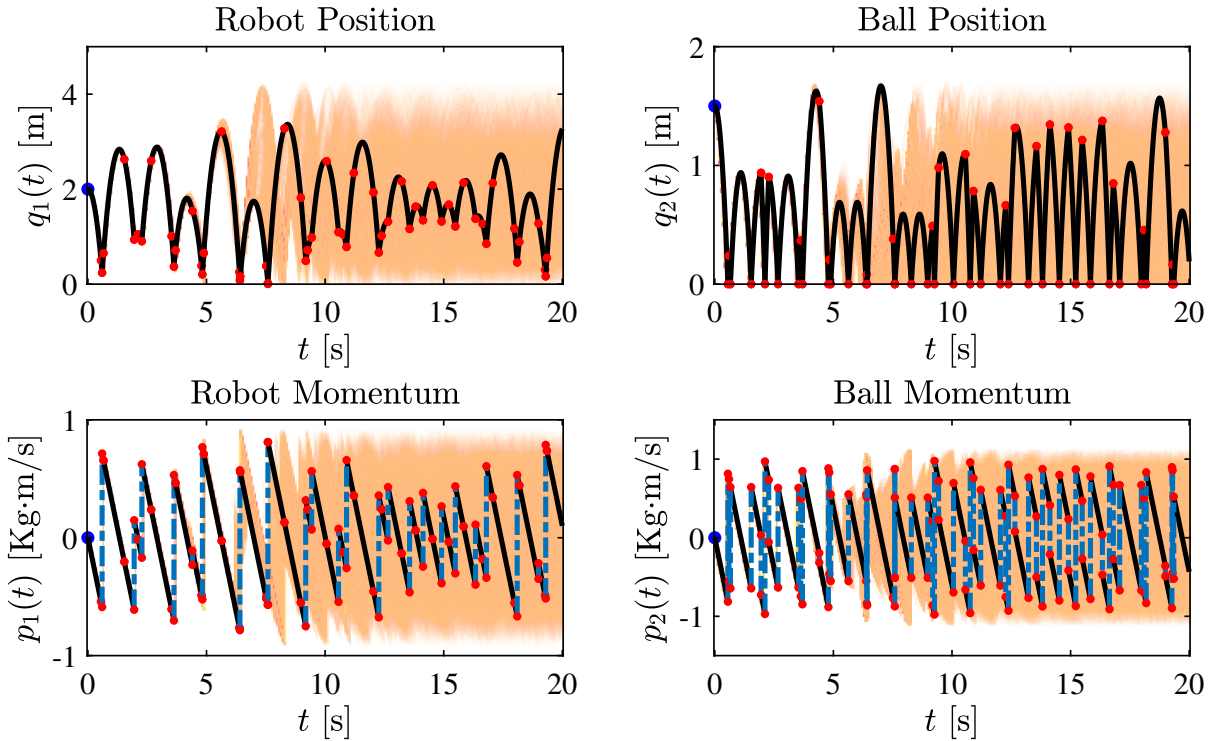


Fig. 4.3: Time evolution of the autonomous system's state in the Monte Carlo simulation. The black trajectory is the nominal one (starting from  $\mathbf{x}_0$ ), where red dots and dashed blue lines indicate discrete events (impacts) and the value of the state after the events, respectively. Orange lines show the traces of all the other trajectories of the Monte Carlo runs (with initial condition sampled from  $\mathcal{N}(\mathbf{x}_0, \sigma \mathbb{I}_n)$ ). The blue dots at  $t = 0$  are the initial conditions. It can be noticed how trajectories, starting very close, diverge, densely covering the state-space.

environment. The time evolution of the system's state in all the trials is shown in Fig. 4.3. The black trajectory represents the nominal one (starting from  $\mathbf{x}_0$ ), where red dots and dashed blue lines indicate discrete events (impacts) and the value of the state after the events, respectively. Orange lines show the traces of all other trajectories for each Monte Carlo run. The blue dots at  $t = 0$  are the initial conditions. It can be noticed how trajectories, starting indistinguishably close, diverge, densely covering to the state-space.

This phenomenon is further emphasized in Fig. 4.4, which shows the phase-space trajectories of the robot and the ball, respectively.

The time evolution of the energy (Hamiltonian function) among the Monte Carlo runs is also shown in Fig. 4.5. As expected, the energy is conserved through time.

The experiment which has been done here numerically can be formalized as follows. Instead of an initial condition  $\mathbf{x}_0$ , an initial (probability) density of the state in space

$$\psi(\mathbf{x}_0) = \mathcal{N}(\mathbf{x}_0, \sigma \mathbb{I}_n) \quad (4.21)$$

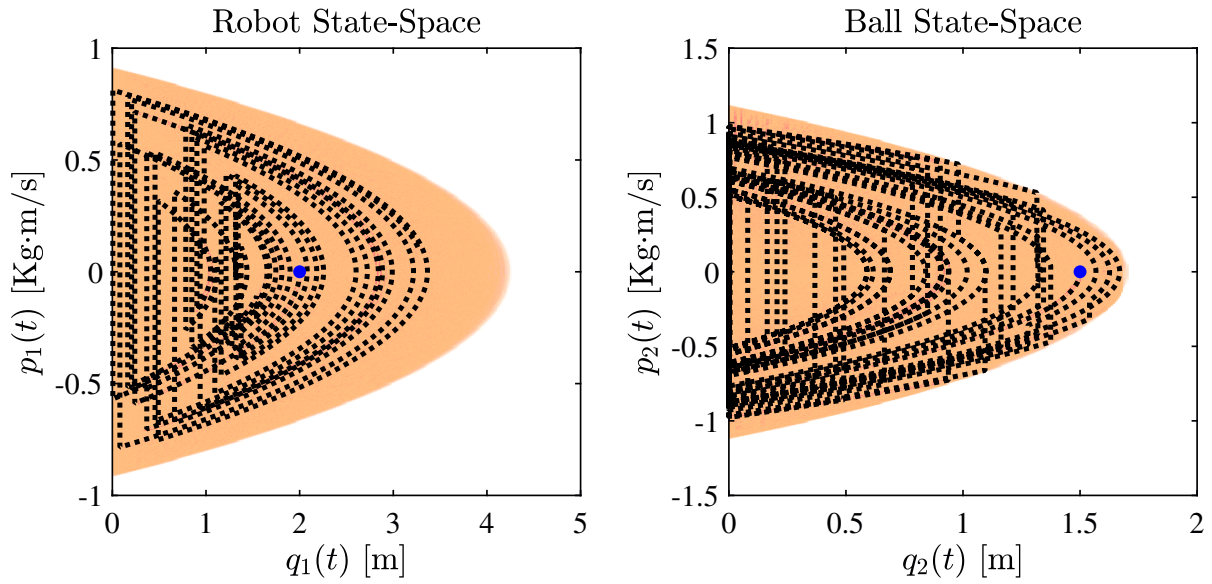


Fig. 4.4: Phase–space trajectory of the autonomous system in the Monte Carlo simulation. The dashed black line is the nominal one (starting from  $\mathbf{x}_0$ ). Orange lines show the traces of all the other trajectories of the Monte Carlo runs (with initial condition sampled from  $\mathcal{N}(\mathbf{x}_0, \sigma \mathbb{I}_n)$ ). The blue dots at  $t = 0$  are the initial conditions. It can be noticed how trajectories, starting very close, diverge, densely covering the state–space.

has been considered and the evolution in time of this distribution has been observed through the dynamics of the system, i.e. the solution of a distributed parameters sys-

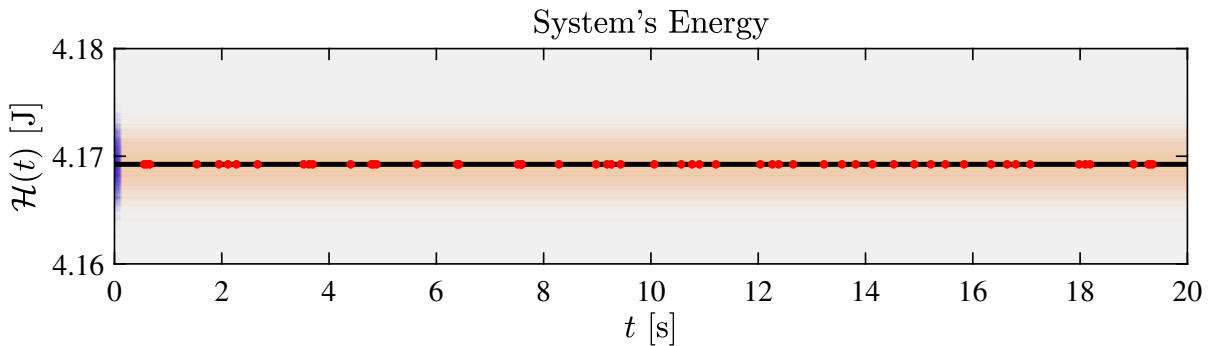


Fig. 4.5: Time evolution of the energy in the Monte Carlo simulation. The black trajectory is the nominal one (starting from  $\mathbf{x}_0$ ), where red dots indicate discrete events (impacts). Orange lines show the traces of all the other trajectories of the Monte Carlo runs (with initial condition sampled from  $\mathcal{N}(\mathbf{x}_0, \sigma \mathbb{I}_n)$ ). The blue dots at  $t = 0$  are the initial energies of each Monte Carlo run. It can be noticed how, regardless the initial condition, energy is conserved in time.

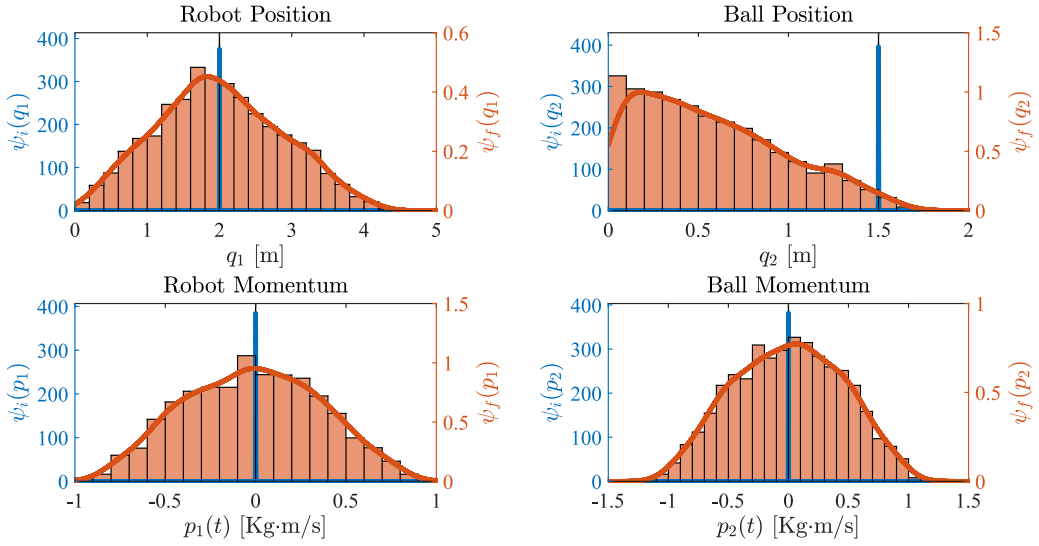


Fig. 4.6: Histograms and reconstructed spatial (probability) density functions of the state. Blue and orange histograms (lines) represent, respectively, initial and final spatial densities of each state.

tem has been numerically approximated.

From the numerical experiment's results, the histograms of state density in space at each time instant have been built. The initial and final spatial density functions

$$\psi_i \triangleq \psi(\mathbf{x}_0) = \mathcal{N}(\mathbf{x}_0, \sigma \mathbb{I}_n), \quad \psi_f = \psi(\mathbf{x}(t = 20s)) \quad (4.22)$$

displayed in Fig. 4.6.

The time evolution of state probability distribution <sup>\*1</sup> have been plotted (in a phaseogram) for each state of the system. Results are reported in Figure 4.7.

At  $t = 0$  the state probability is just a *spike* across the nominal initial condition. Throughout time, however, the spatial (probability) of each state relaxes to a function with much larger variance. This experiment demonstrated that, although all trajectories started very close one to each other, after a short period of time, the state can be almost everywhere in the state-space. Thus, the essence of the autonomous conservative ball-dribbling robot, resembles the one of a stochastic process, despite the fact that it is deterministic in nature.

<sup>\*1</sup> i.e. the probability of finding the state of the system somewhere in the state-space.

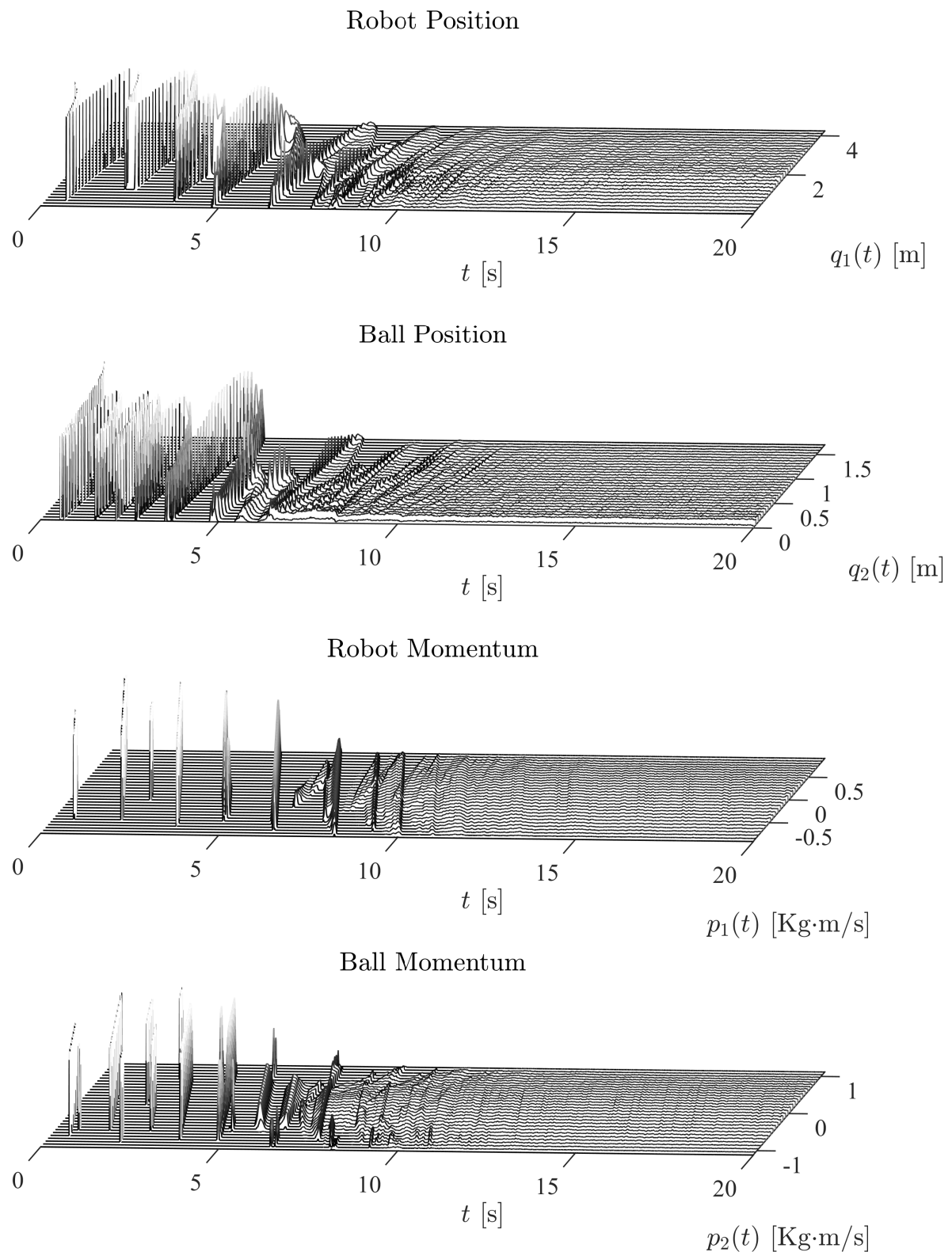


Fig. 4.7: Phase-gram of the state spatial (probability) density function computed from the Monte Carlo experiment. At  $t = 0$  the state spatial density is just a spike across the initial condition. Throughout time, the density relaxes to a function with larger variance.

## 4.4 Dribbling Control

Let us consider the control task of continuously hitting the ball such that it reaches, at every cycle, the same maximum height  $q_{2,max}^*$ . In order to address this control problem, it is possible to design an hybrid controller with two modes, i.e., a *wait mode* ( $S_w$ ) and a *hit mode* ( $S_h$ ). In the wait state, the robot must stay at a constant height above the ball, to overcome any interference between its motion and the one of the ball and, at the same time, stay close enough to the ball to hit it quickly at the right time. Then, in the hit state, the controller must move the robot toward the ball so that the exchanged impulse during the impact would lead the ball to come back to the desired peak  $q_{2,max}^*$ . In particular, the system would enter in the hit state whenever the ball reaches the peak of its bounce and switch back to the wait mode immediately after the impact between the two bodies. In both modes, it is desirable to exploit the passivity-based control theory. Besides, the system is under-actuated and the flows are decoupled. Therefore, it is impossible to shape the total energy of system setting its minimum in a desired configuration different from the origin. Although it is not possible to modify the energy of the ball, it is however possible to partially shape the Hamiltonian, i.e. the part relative to the robot. If

$$\mathcal{H}(\mathbf{x}) = \mathcal{H}_1(q_1, p_1) + \mathcal{H}_2(q_2, p_2), \quad (4.23)$$

it is possible to obtained a desired-shape Hamiltonian

$$\mathcal{H}^*(\mathbf{x}) = \mathcal{H}_1^*(q_1, p_1) + \mathcal{H}_2(q_2, p_2), \quad (4.24)$$

allowing to bring the robot in a desired configuration  $q_1^*$ . This might be achieved through an *energy-balancing passivity-based controller*<sup>\*2</sup> (Ortega et al. , 2001, 2008; Secchi et al. , 2007) described in Chapter 2:

$$u = \beta(\mathbf{x}) + v = \beta(\mathbf{x}) - k_d y \quad (4.25)$$

$$= \frac{\partial V_1(q_1)}{\partial q_1} - k_p(q_1 - q_1^*) - k_d \dot{q}_1 \quad (4.26)$$

$$= \gamma m_1 q_1 - k_p(q_1 - q_1^*) - k_d \dot{q}_1. \quad (4.27)$$

As pointed out before, the controller has two separate modes and the control parameters  $k_p$ ,  $k_d$ ,  $q_1^*$  should be changed during the state transitions. For this reason, let us collect the control parameters in a vector

$$\boldsymbol{\omega} = (k_p, k_d, q_1^*) \quad (4.28)$$

<sup>\*2</sup> In this case  $q_1^*$  becomes a strict minimum of  $\mathcal{H}_1^*$  and asymptotic stabilization must be achieved with  $p_1 = 0$  at steady-state

and consider it as part of the state vector. The augmented model of the controlled system can be then rewritten as follows:

$$\begin{cases} \begin{bmatrix} \dot{\mathbf{x}} \\ \dot{\boldsymbol{\omega}} \end{bmatrix} = \begin{bmatrix} [\mathbf{J} - \mathbf{R}] \nabla \mathcal{H}^*(\mathbf{x}) + \mathbf{G} v(\mathbf{x}, \boldsymbol{\omega}) \\ 0_3 \end{bmatrix} & (\mathbf{x}, \boldsymbol{\omega}, v) \in \mathcal{C} \times \Omega \times \mathcal{U} \\ \begin{bmatrix} \mathbf{x}^+ \\ \boldsymbol{\omega}^+ \end{bmatrix} \in \mathcal{G} \times \Lambda & (\mathbf{x}, \boldsymbol{\omega}) \in \mathcal{D} \times \Omega \\ y = \mathbf{G}^\top \nabla \mathcal{H}^*(\mathbf{x}) \end{cases}, \quad (4.29)$$

where  $\Omega$  is the space of admissible parameters values and  $\Lambda$  is the jump set-valued mapping of the control parameters. The shaped Hamiltonian  $\mathcal{H}^*(\mathbf{x}, \boldsymbol{\omega})$ , results to be

$$\mathcal{H}^*(\mathbf{x}, \boldsymbol{\omega}) = \frac{1}{2} \mathbf{p}^\top \mathbf{M}^{-1} \mathbf{p} + \frac{1}{2} k_p (q_1 - q_1^*)^2 + \gamma m_2 q_2. \quad (4.30)$$

Notice that the choice of the control parameters influences both the closed-loop energy  $\mathcal{H}^*$  (with  $k_p$  and  $q_1^*$ ) and the output feedback  $v$  (with  $k_d$ ). Let us define a jump set  $\mathcal{D}_3$  corresponding to the sub-manifold of the state-space where the ball reaches the peak  $q_{2,max}$  of its bounce:  $\mathcal{D}_3 = \{\mathbf{x}: p_2 = 0\}$ . It is clear that during the time evolution of the system, the state will cyclically enter in  $\mathcal{D}_3$  and therefore the controller will periodically switch to  $S_h$  where the robot moves toward the ball until they collide, i.e.  $\mathbf{x} \in \mathcal{D}_2$ , when the controller switches back to  $S_w$  where the robot waits above the ball at a distance  $\delta$ . The jumps maps resetting the control parameters are the following:

$$\boldsymbol{\omega}^+ = \mathbf{v}_3(\mathbf{x}, \boldsymbol{\omega}) = [k_{p,h} \quad k_{d,h} \quad q_2]^\top \quad \mathbf{x} \in \mathcal{D}_3, \quad (4.31)$$

$$\boldsymbol{\omega}^+ = \mathbf{v}_2(\mathbf{x}, \boldsymbol{\omega}) = [k_{p,w} \quad k_{d,w} \quad q_2 + \delta]^\top \quad \mathbf{x} \in \mathcal{D}_2, \quad (4.32)$$

$$\boldsymbol{\omega}^+ = \mathbf{v}_1(\mathbf{x}, \boldsymbol{\omega}) = \boldsymbol{\omega} \quad \mathbf{x} \in \mathcal{D}_1. \quad (4.33)$$

Therefore,

$$\Lambda \triangleq \{\mathbf{v}_i : \mathbf{x} \in \mathcal{D}_i \Rightarrow \boldsymbol{\omega}^+ = \mathbf{v}_i(\boldsymbol{\omega}, \mathbf{x}), i = 1, 2, 3\}. \quad (4.34)$$

Figure 4.8 shows the finite-state machine representing the controller. When  $\mathbf{x} \in \mathcal{D}_3$ , the state of the system does not jump, i.e.  $\mathbf{x}^+ = \mathbf{g}_3(\mathbf{x}) = \mathbf{x}$  if  $\mathbf{x} \in \mathcal{D}_3$ . The set-valued mapping  $\mathcal{G}$  is redefined considering  $\mathbf{g}_3$ .

**Remark 4.4.1.** *The behavior of the system strongly depends on the choice of the control parameters. Furthermore, unless a solution of (4.29) is derived, it is not possible to find analytically two sets of control parameters (one for  $S_w$  and one for  $S_h$ ) which solve the control problem, i.e. ensuring that the ball bounces continuously reaching each time the desired peak  $q_{2,max}^*$ .*

For the reasons stated in previous remark, a new paradigm of energy based control, which combines the traditional energy shaping approach with a basic form of iterative learning control: the *iterative energy shaping*, has been introduced.

**Definition 4.4.2** (Iterative Energy Shaping Control).

*First, let us define some further control parameters which are needed for the design. Let  $\xi$  be a counter of the number of cycles of the system, i.e., the number of complete bounces of the*

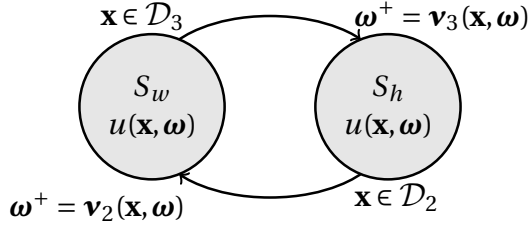


Fig. 4.8: Finite state machine of the controller. It has an *hit* state \$S\_h\$ in which it forces the robot to move toward the ball and a *wait* state \$S\_w\$ in which it keeps the robot at a constant distance \$\delta\$ from the ball. The transitions happen as follows: \$S\_h \rightarrow S\_w\$ when the robot hits the ball, \$S\_w \rightarrow S\_h\$ when the ball reaches the peak of its bounce.

ball. Let initialize \$\xi\$ to one. Let \$e(\xi) = q\_{2,max}^\* - q\_{2,max}\$ computed when \$\mathbf{x} \in \mathcal{D}\_3\$ be the tracking error of the iterative energy shaping control loop. Thus, the control parameters vector can be redefined as

$$\boldsymbol{\omega} \triangleq (k_p, k_d, q_1^*, \xi). \quad (4.35)$$

The iterative energy shaping control law is defined by means of the following control parameters jump maps:

$$\boldsymbol{\omega}^+ \triangleq \mathbf{v}_3(\mathbf{x}, \boldsymbol{\omega}) = [k_0 \varphi_\xi(e) \quad k_{d,h} \quad q_2 \quad \xi + 1]^\top \quad \mathbf{x} \in \mathcal{D}_3, \quad (4.36)$$

$$\boldsymbol{\omega}^+ \triangleq \mathbf{v}_2(\mathbf{x}, \boldsymbol{\omega}) = [k_{p,w} \quad k_{d,w} \quad q_2 + \delta \quad \xi]^\top \quad \mathbf{x} \in \mathcal{D}_2, \quad (4.37)$$

where \$\sigma > 0\$ is a constant scalar and \$\varphi\_\xi(e)\$ is a scalar function of the error. When the controller is in the hit state, the resulting shaped Hamiltonian assumes the following form:

$$\mathcal{H}^*(\mathbf{x}, \boldsymbol{\omega}) = \frac{1}{2} \mathbf{p}^\top \mathbf{M}^{-1} \mathbf{p} + \frac{1}{2} k_0 \varphi_\xi(e) (q_1 - q_1^*)^2 + \gamma m_2 q_2. \quad (4.38)$$

A representation of the *hybrid automata* corresponding to the final controlled system is pictured in Fig. 4.9. The main idea is to iteratively adjust the slope (steepness) of the energy of the system as function of the error. For instance, when \$e > 0\$, it can be derived that the robot had hit the ball with not enough momentum. Thus, at the next cycle, the energy function should be steeper so that the robot will accelerate faster toward the ball, since the dissipation rate \$k\_d\$ of the damping injection didn't change. The same concept can be adopted for \$e < 0\$, by making the the energy function less steep. A possible choice of \$\varphi\_\xi(e)\$ is

$$\varphi_\xi(e) \triangleq \varphi_0 + a \cdot e(\xi) + b \cdot \sum_{i=1}^{\xi} e(i), \quad (4.39)$$

which provides a proportional and integral action with a constant offset \$\varphi\_0\$ in response to the error. The integral action should ensure zero steady state error.

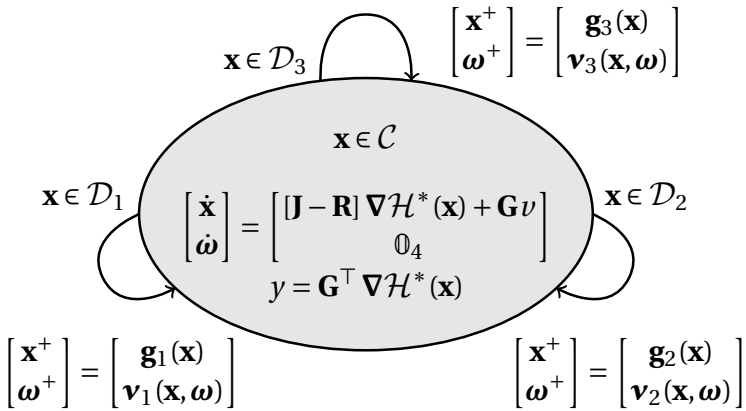


Fig. 4.9: Hybrid automata representing the controlled system. Although the *iterative energy shaping* controller has two modes, the controlled system is still an impulsive port–Hamiltonian system

## 4.5 Numerical Simulations

To validate the proposed control scheme, numerical simulations have been performed. The physical parameters of the system have been chosen as  $m_1 = 0.1\text{Kg}$ ,  $m_2 = 0.05\text{Kg}$ ,  $\beta_1 = 0.2\text{N}\cdot\text{s/m}$ ,  $\beta_2 = 0.3\text{N}\cdot\text{s/m}$ ,  $c_g = c_i = 0.8$ . The initial conditions have been set to  $q_1(0) = 2\text{m}$ ,  $q_2(0) = 1.5\text{m}$ ,  $p_1(0) = p_2(0) = 0\text{Kg}\cdot\text{m/s}$ . Note that the mass of the ball  $m_2$  has been chosen similar to the one of a standard golf ball ( $\approx 46\text{g}$ ).

### 4.5.1 Autonomous System

Firstly, the behavior of the uncontrolled system has been simulated. The time evolution of the state variables are shown in Fig. 4.10. The phase-space trajectory of the autonomous system over the energy of the system is represented in Fig. 4.11.

Fig. 4.12 pictures the time evolution of the Hamiltonian function while Fig. 4.13 shows how the energy is distributed within the system during its time evolution. It can be noticed that  $\mathcal{H}$  presents a monotonically decreasing trend, in both flows (due to the viscous friction terms) and jumps (since the restitution coefficients are less than one). In fact, trajectories decrease on level–sets of  $\mathcal{H}$ , even if  $\mathcal{H}_1$  and  $\mathcal{H}_2$  may locally increase after some ball–robot impacts. Moreover, from the figures it is easily to verify the asymptotic stability and attractivity of the origin ( $x = 4$ ) and the *Zeno behavior* of the autonomous system (see Goebel et al. (2009b)).

### 4.5.2 Controlled System

Simulations of the system controlled via iterative energy shaping have also been performed. The control parameters have been chosen as:  $k_{p,w} = 10^4$ ,  $k_{d,w} = 10^3$ ,  $\delta = 0.05\text{m}$ ,

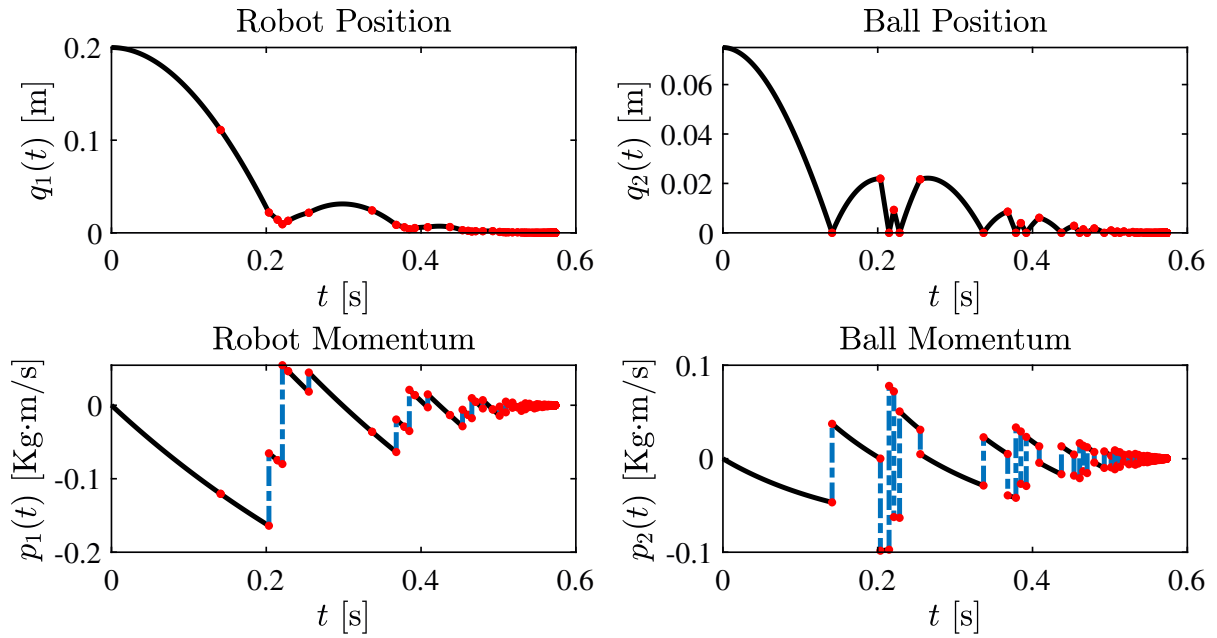


Fig. 4.10: Uncontrolled system: time evolution of the robot and ball position states (position and momentum). Red dots correspond to system's jumps while dashed blue lines highlight discontinuous state changes. Notice that both the position and velocity go asymptotically to zero.

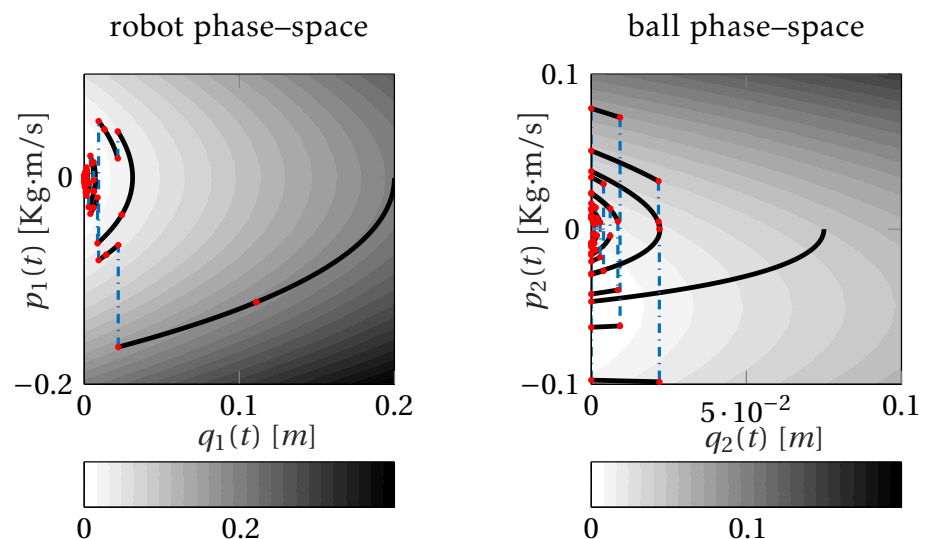


Fig. 4.11: Uncontrolled system: Phase-space trajectory over the energy function. Red dots correspond to system's jumps while dashed blue lines highlight discontinuous state changes. Notice that both, the position and velocity go asymptotically to zero.

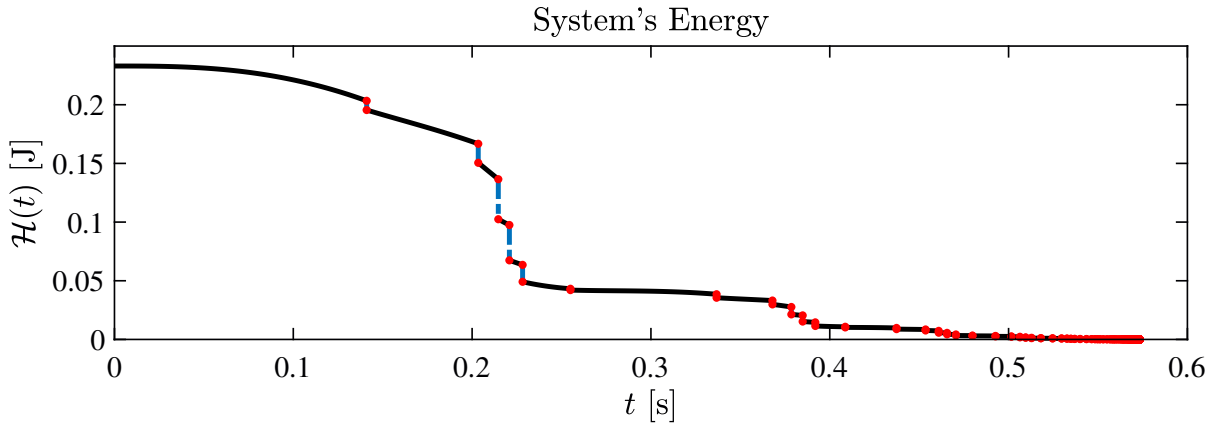


Fig. 4.12: Uncontrolled system: time evolution of the Hamiltonian function. Due to system's passivity, the energy monotonically decreases to zero both during flow and jumps.

$k_0 = 10$ ,  $k_{d,h} = 0$ ,  $\varphi_\xi(e) = 10e + 100\sum_{i=1}^{\xi} e(i)$ ,  $q_{2,max}^* = 0.1\text{m}$ . The time evolution of the state variables are shown in Fig. 4.14 and Fig. 4.15. Notice that the trajectory of the ball becomes periodic (asymptotically), reaching at each bounce the desired peak  $q_{2,max}^*$ , proving the effectiveness of the proposed control scheme. Furthermore, the time evolution of the energy function is shown in Fig. 4.16 and Figs. 4.17 while Fig. 4.18 and Figs. 4.19 show how the energy flows across the system during each period. As expected, also the energy becomes periodic. In fact, the energy at the beginning and at the end of each cycle (bounce) assumes exactly the same value. Moreover, it can be noticed that, at steady state, during the ball–robot impact, the robot transfers to the ball the exact amount of energy necessary to reach the desired bounce peak. Finally, as shown in Fig. 4.20 the error goes to zero with the number of cycles. On the other hand, the function  $\varphi_\xi(e)$  converges exponentially to a positive constant value. A final consideration about the convergence of the system to the desired periodic trajectory can be made from the phase-space portrait of the system's trajectory (Fig. 4.21). Being the time represented by the color transition, it can be noticed that the system approaches a limit cycle, an attractive asymptotically periodic trajectory, in which the tracking error is zero.

### 4.5.3 Numerical Stability and Robustnes Analysis

#### Robustness to Initial Condition

In order to numerically prove the stability and robustness of the proposed control scheme, a Monte Carlo experiment similar to the one presented in Section 4.3, has been performed. In particular, choosing as physical parameters  $m_1 = 0.1\text{Kg}$ ,  $m_2 = 0.15\text{Kg}$ ,  $\beta_1 = 0.2$ ,  $\beta_2 = 0.3$ ,  $c_1 = c_2 = 0.8$  and control parameters  $k_{p,w} = 10^4$ ,  $k_{d,w} = 10^3$ ,  $\delta = 0.5$ ,  $\sigma = 10$ ,  $k_{d,h} = 10^2$ ,  $\varphi_\xi(e) = 3000 + 10e + 300\sum_{i=1}^{\xi} e(i)$ ,  $q_{2,max}^* = 1$ , a total of 3000 trajectories have

been computed starting from initial conditions  $\mathbf{x}_0^i$  sampled by the normal distribution

$$\mathcal{N}(\mathbf{x}_0, \sigma \mathbb{I}_n), \quad (4.40)$$

with  $\mathbf{x}_0 \triangleq (2, 1.5, 0, 0)$  and  $\sigma = 1^{*3}$ . The time evolution of the system's state in the nominal case ( $\mathbf{x}(t=0) = \mathbf{x}_0$ ) and all the Monte Carlo trials are displayed in Fig. 4.22.

It can be noticed how even if the trajectories start far from each other, are all asymptotically periodic and converge to the nominal trajectory. This means that the controller generates an attractive *limit cycle* in the closed-loop system. This is further highlighted in Fig. 4.23 where the phase-space trajectories are represented.

The time evolution of the energy (Hamiltonian function) among the Monte Carlo runs is also shown in Fig. 4.24.

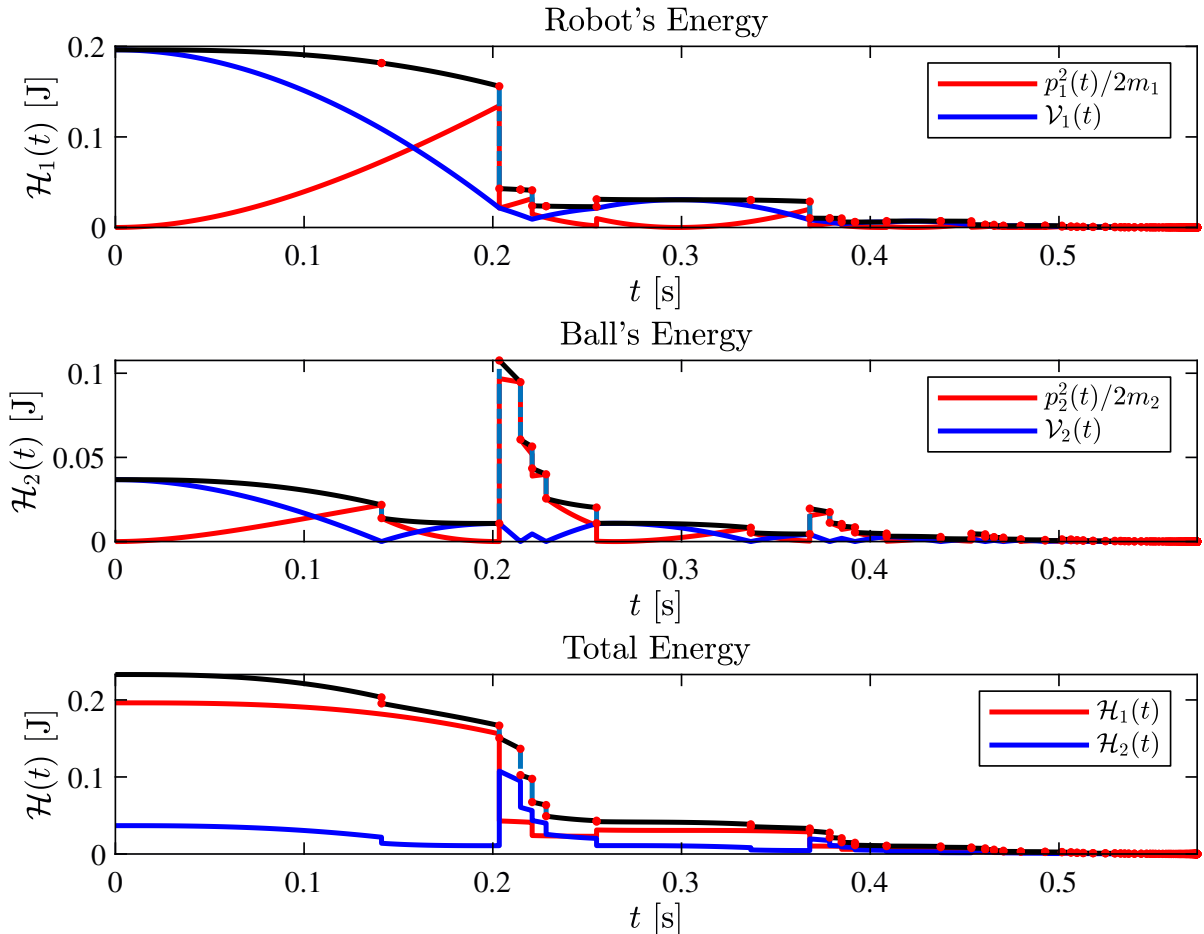


Fig. 4.13: Uncontrolled system: Energy distribution within the system. Trajectories decrease on level-sets of  $\mathcal{H}$ , even if  $\mathcal{H}_1$  and  $\mathcal{H}_2$  may locally increase after some ball–robot impacts.

<sup>\*3</sup> To minimize the effects of numerical instabilities of the *HyEq* solver, larger physical and control parameters respect to the one used in the previous section have been chosen in this case.

The stability and attractivity to the nominal trajectory of the iterative energy shaping controlled system is shown in Fig. 4.25, which pictures the convergence of the tracking error and energy shaping gain. It is worth to underline that the mean of both, the error and gain among the Monte Carlo runs is almost identical to the nominal one. Further investigations might be interesting to be performed in order to analyse this phenomenon.

### Robustness to Change of Parameters

To prove the robustness against sudden changes of physical parameters of the system, several simulations have been performed with the same model and control parameters used in Subsection 4.5.2 and, changing at time  $t = 2.5\text{s}$  some parameter of the model. Firstly the reference have been setted from  $0.1\text{m}$  to  $0.05\text{m}$  (-50%). Then, the mass of the ball  $m_2$  has been changed from  $0.05\text{Kg}$  to  $0.25\text{Kg}$  (+400%). Finally, the restitution coefficient of the ball–robot collision has been changed from 0.8 to 0.99 (+23.75%). The resulting states trajectories, tracking error, learned gains and energy are reported in Figs. 4.26, 4.27 and 4.28.

Results demonstrated that the controller presents excellent robustness properties. In all three situations, the system recovers swiftly from the parameter change, adapting itself to the new value.

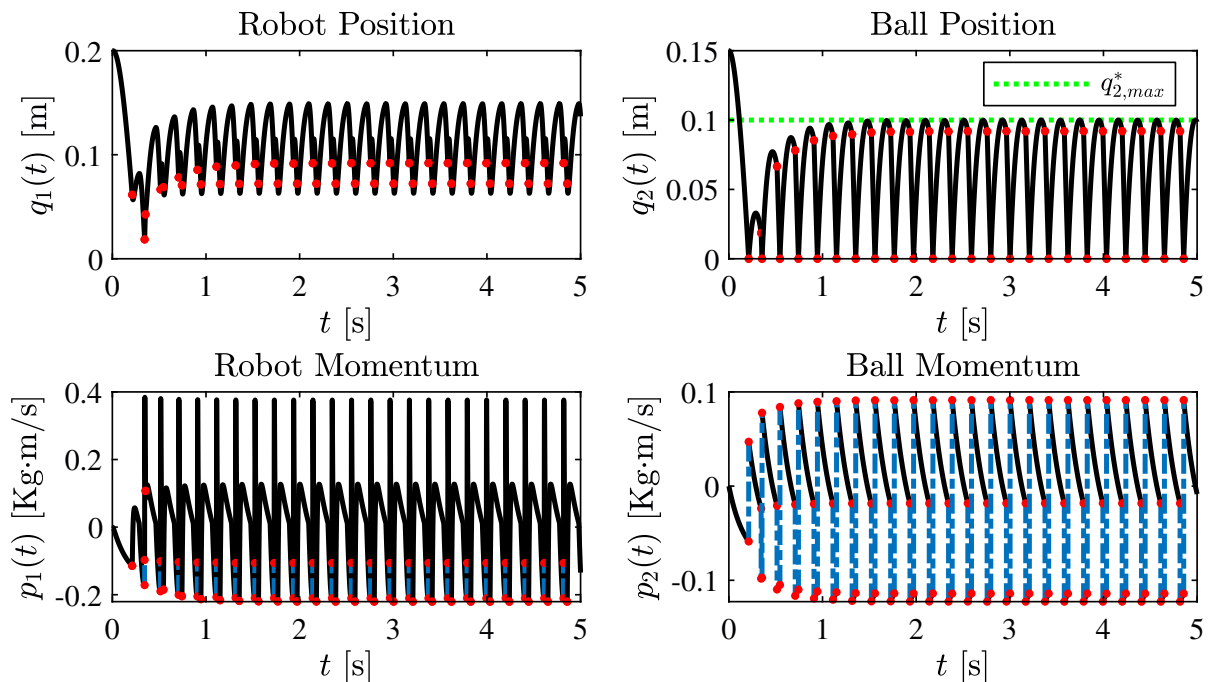


Fig. 4.14: Iterative energy shaping control: time evolution of the robot and ball states (position and momentum). Red dots correspond to system's jumps while dashed blue lines highlight discontinuous state changes. Notice that the ball states converge on a periodic trajectory reaching at each bounce the desired peak  $q_{2,max}^*$  (dotted green line).

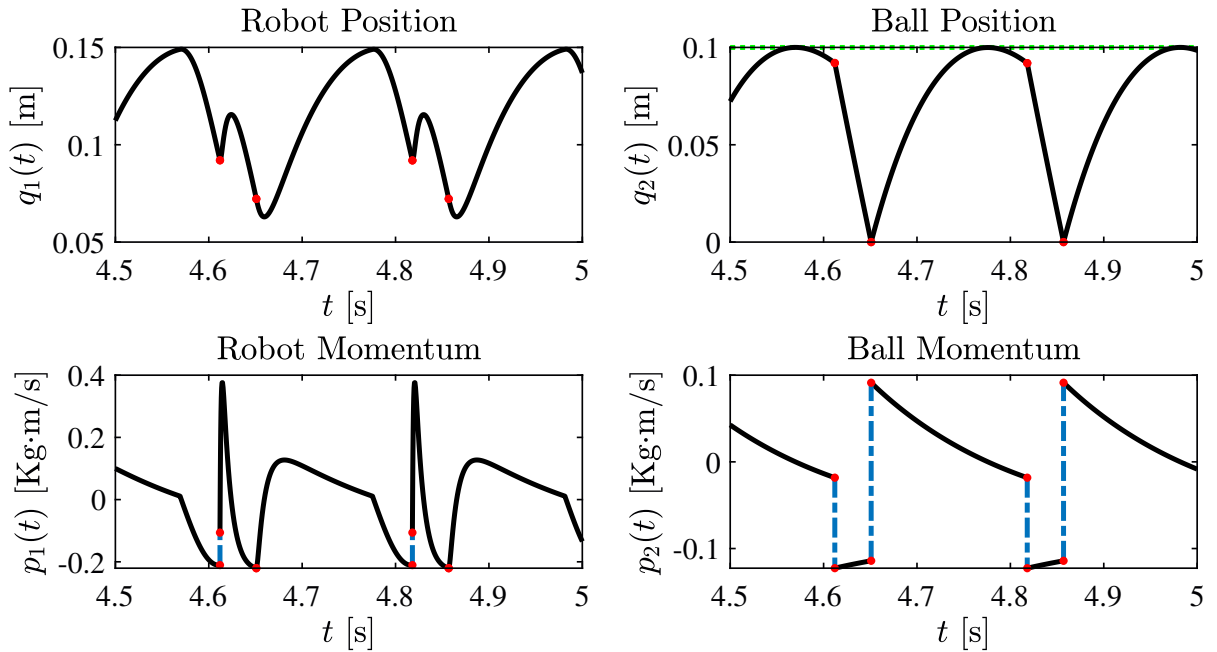


Fig. 4.15: Iterative energy shaping control: detailed view of the time evolution of the ball and robot positions at steady state.

In particular, when the reference is changed from 0.1m to 0.05m, all the physical properties of the system are conserved, e.g. dissipation during flows and jumps. However, to stabilize the ball on the desired trajectory, the robot needs to transfer less momentum to the ball during their collision. The system thus adapts itself to those new conditions by decreasing the energy shaping gain in the hit state.

Instead, when the mass of the ball is increased from 0.05Kg to 0.25Kg, its momentum

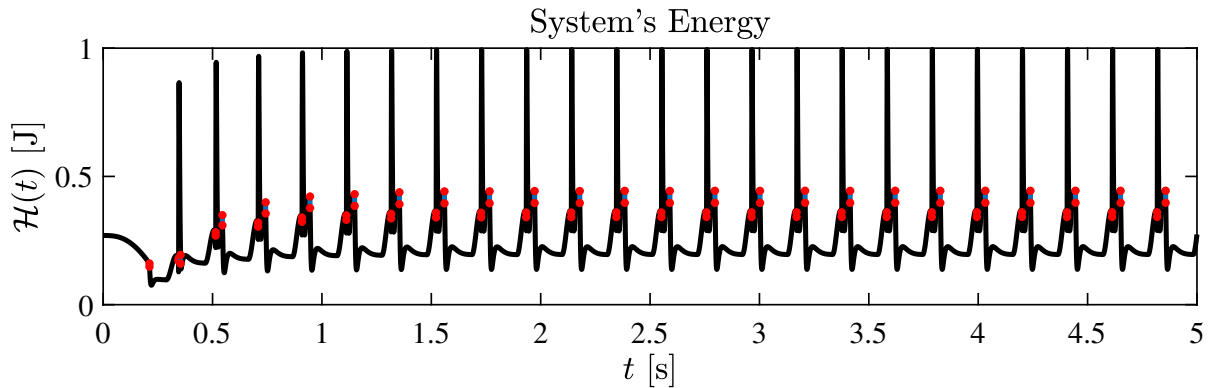


Fig. 4.16: Iterative energy shaping control: the time evolution of the Hamiltonian function. After a short transient also the system's energy becomes periodic.

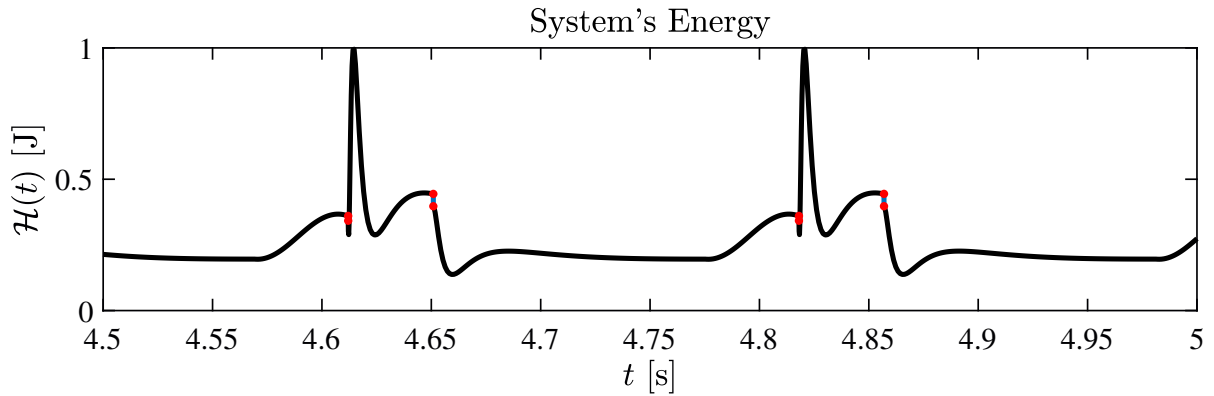


Fig. 4.17: Iterative energy shaping control: detailed view of the time evolution of the Hamiltonian function at steady-state to highlight its (asymptotic) periodicity.

per unit of speed grows and thus, the conservation of momentum during the ball–robot collision requires an inresing of the robot’s speed which will allow to transfer the same momentum to the ball. In turn, the acceleration of the robot during the hit mode is also controlled by the energy shaping gain. Consequently, it automatically increases and adapat itself towards the value of zero tracking error.

Finally, when the the ball–robot collision’s restitution coefficient is increased from 0.8 to 0.99, the percentage of momentum that the robot transfers to the ball, i.e elasticity of impact, increases. Consequently, the energy shaping gain became lower. Robustness to changes in the robot mass, friction coefficients and ball–ground restitution coefficients have also been tested. Results shown the effectiveness of the proposed solution.

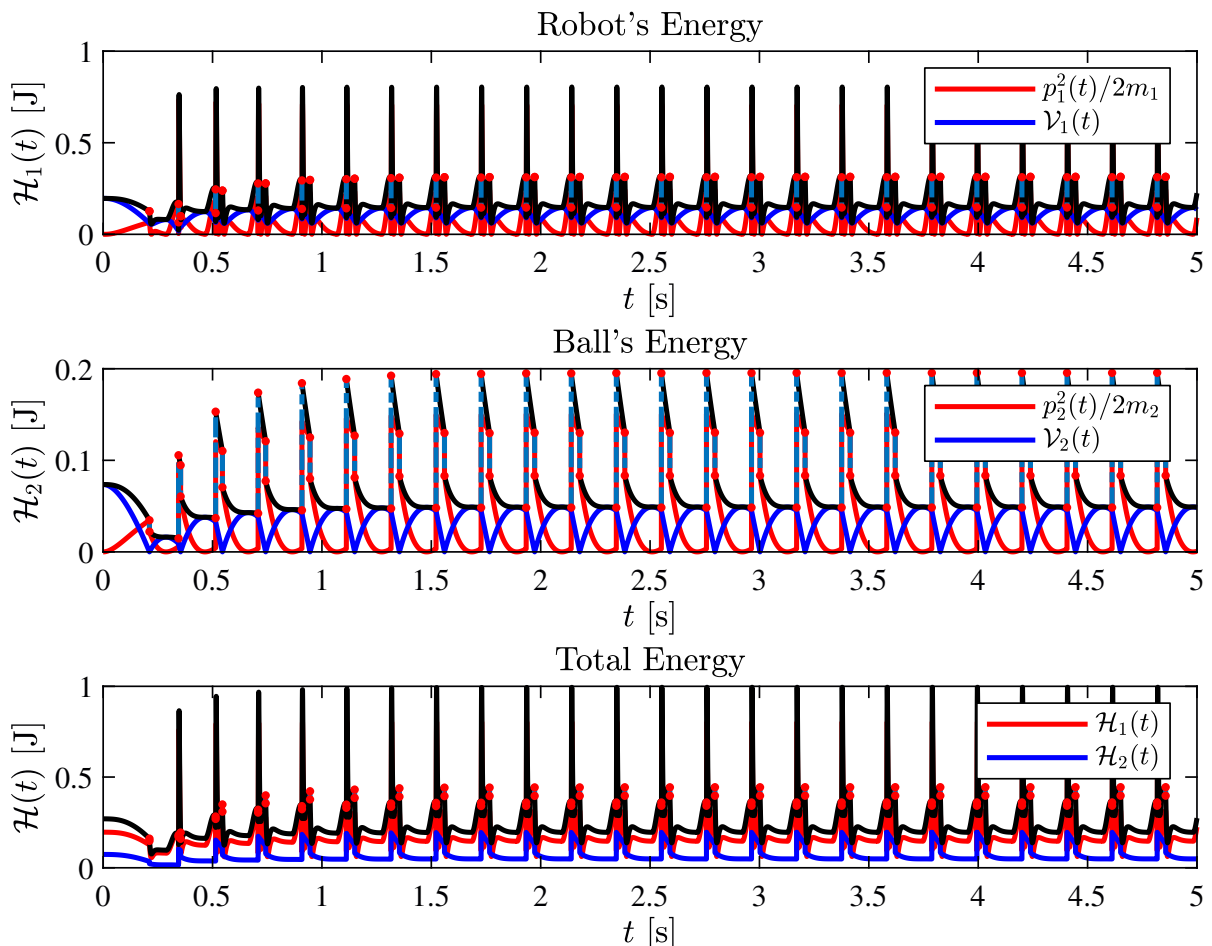


Fig. 4.18: Iterative energy shaping control: Distribution of the energy across the system's components and time. After a short transient also the system's energy becomes periodic.

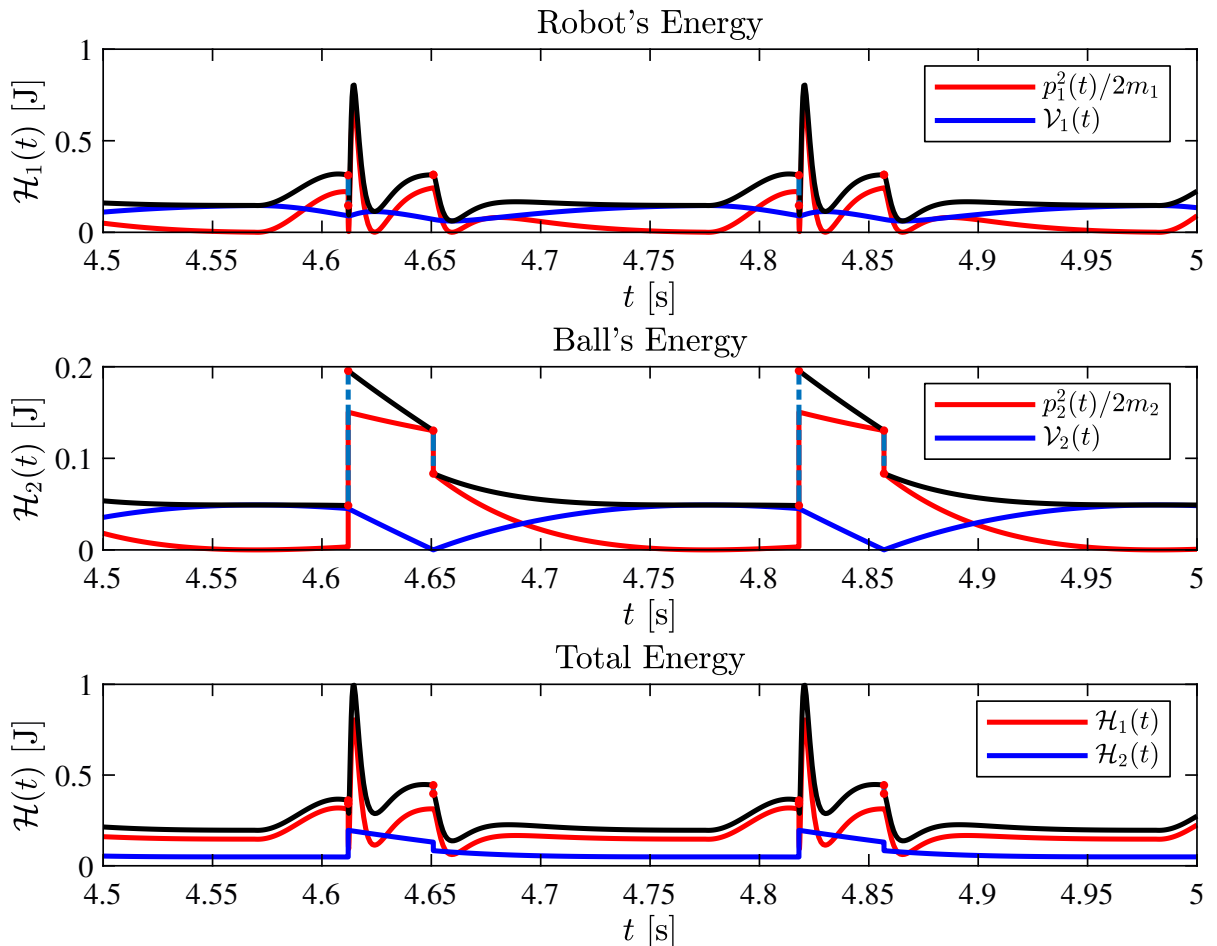


Fig. 4.19: Iterative energy shaping control: detailed view of the energy distribution across the system’s components and time. at steady state to highlight its (asymptotic) periodicity.

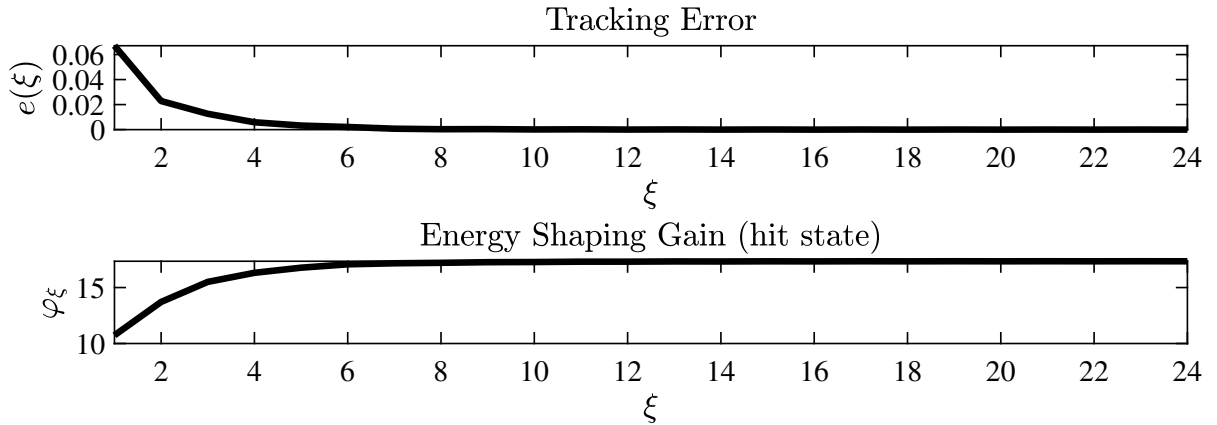


Fig. 4.20: Iterative energy shaping control: (discrete) time evolution of the tracking error  $e$  and of the energy shaping gain  $\varphi_\xi(e)$ . As the number of cycles  $\xi$  increases, the tracking error  $e$ , i.e. the difference between the desired and ball's bounce peak, goes asymptotically to zero. At the same time, the energy shaping gain converges, increasing monotonically, to a constant value.

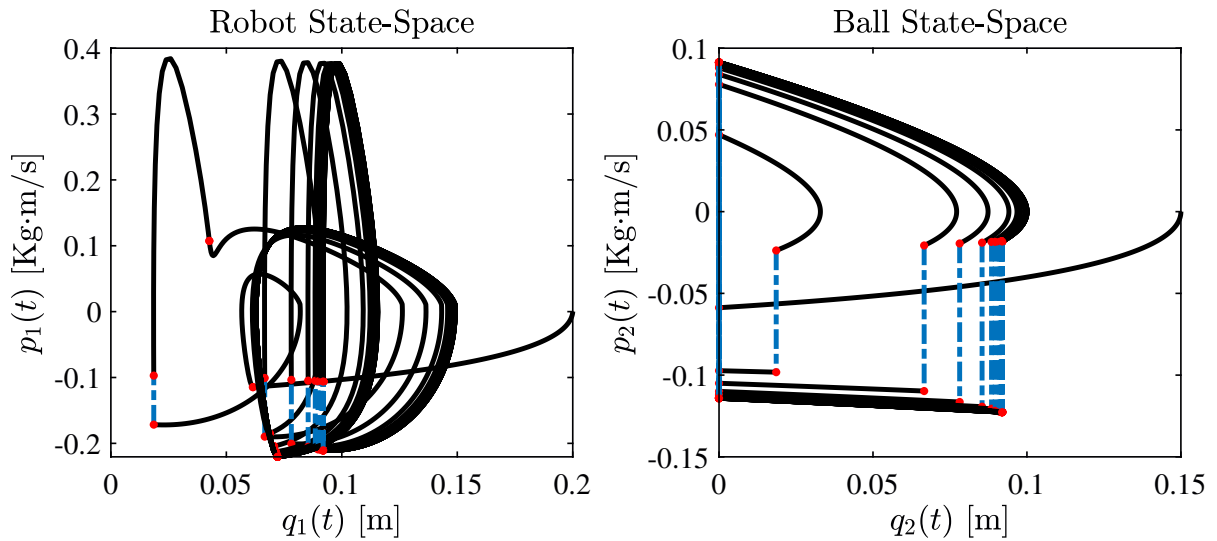


Fig. 4.21: Iterative energy shaping control: projections on the  $q_1 - p_1$  plane and the  $q_2 - p_2$  plane of the phase-space trajectory of the system. The system converges to a hybrid limit cycle in which  $e = 0$ .

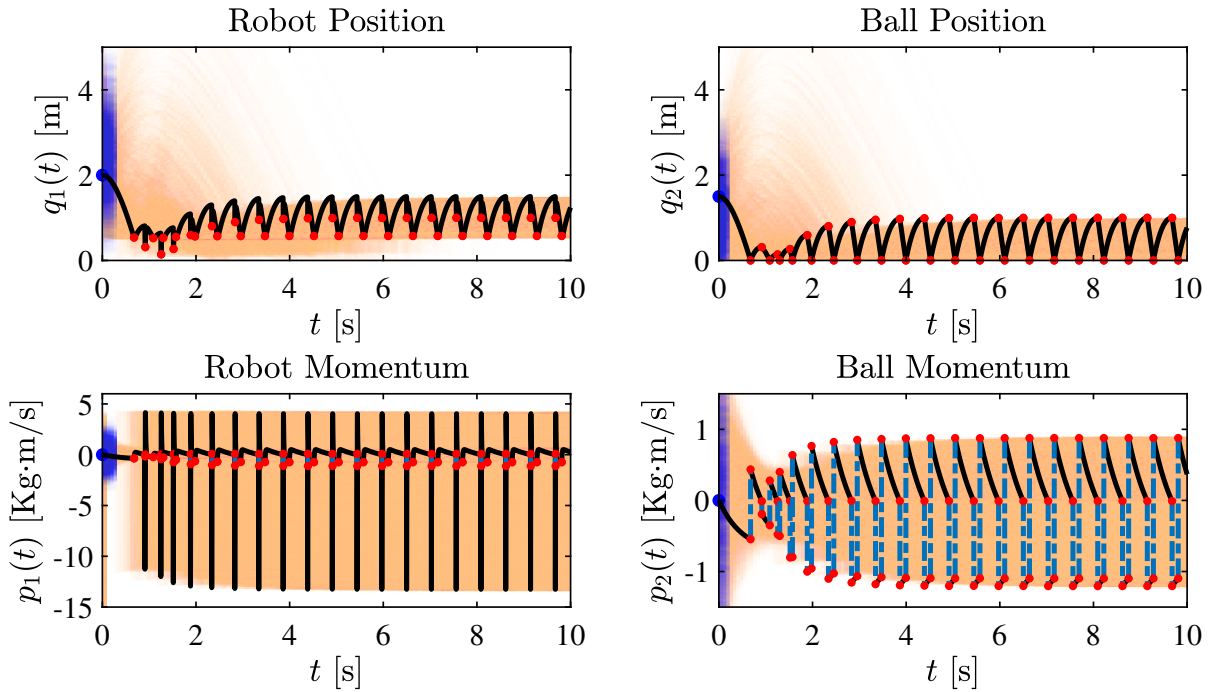


Fig. 4.22: Time evolution of the controlled system’s state in the Monte Carlo simulation. The black trajectory is the nominal one (starting from  $\mathbf{x}_0$ ), where red dots and dashed blue lines indicate discrete events (impacts) and value of the state after the events, respectively. Orange lines show the traces of all the other trajectories of the Monte Carlo runs (with initial condition sampled from  $\mathcal{N}(\mathbf{x}_0, \sigma \mathbb{I}_n)$ ). The blue dots at  $t = 0$  are the initial conditions. It can be noticed how trajectories, starting far from each other, converge to the nominal trajectory.

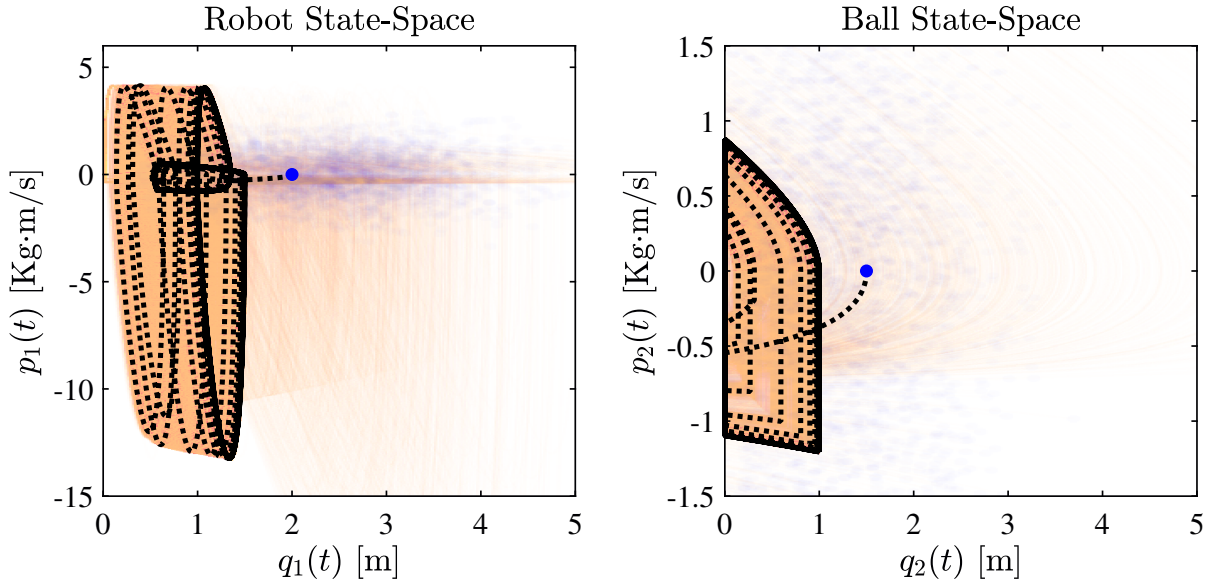


Fig. 4.23: Phase–space trajectory of the controlled system in the Monte Carlo simulation. The dashed black line is the nominal one (starting from  $\mathbf{x}_0$ ). Orange lines show the traces of all the other trajectories of the Monte Carlo runs (with initial condition sampled from  $\mathcal{N}(\mathbf{x}_0, \sigma \mathbb{I}_n)$ ). The blue dots at are the initial conditions. It can be noticed how trajectories, starting far from each other, converge to the nominal trajectory.

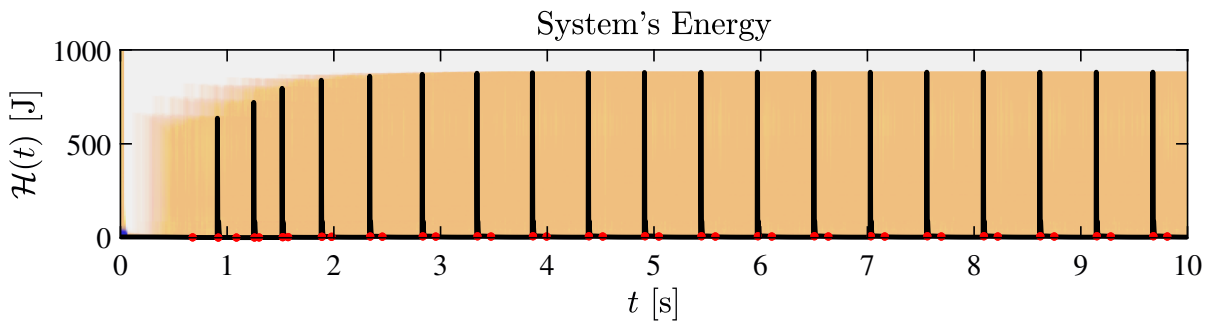


Fig. 4.24: Time evolution of the energy in the Monte Carlo simulation. The black trajectory is the nominal one (starting from  $\mathbf{x}_0$ ), where red dots indicate discrete events (impacts). Orange lines show the traces of all the other trajectories of the Monte Carlo runs (with initial condition sampled from  $\mathcal{N}(\mathbf{x}_0, \sigma \mathbb{I}_n)$ ). The blue dots at  $t = 0$  are the initial energies of each Monte Carlo run.

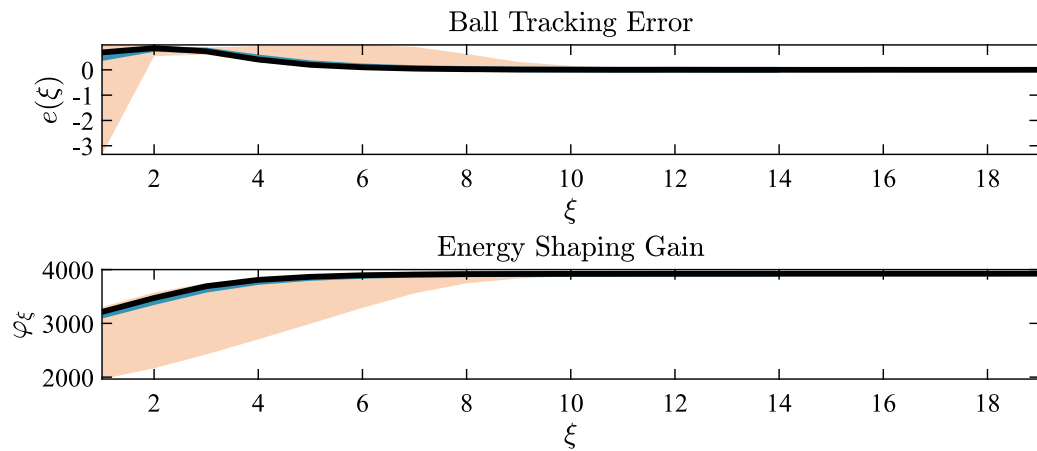


Fig. 4.25: Convergence of the tracking error and energy shaping gain (hit state) in the Monte Carlo simulation. The black line indicates the nominal case. The orange area bounds the minimum and maximum among the values of each Monte Carlo runs while the blue line represents their average.

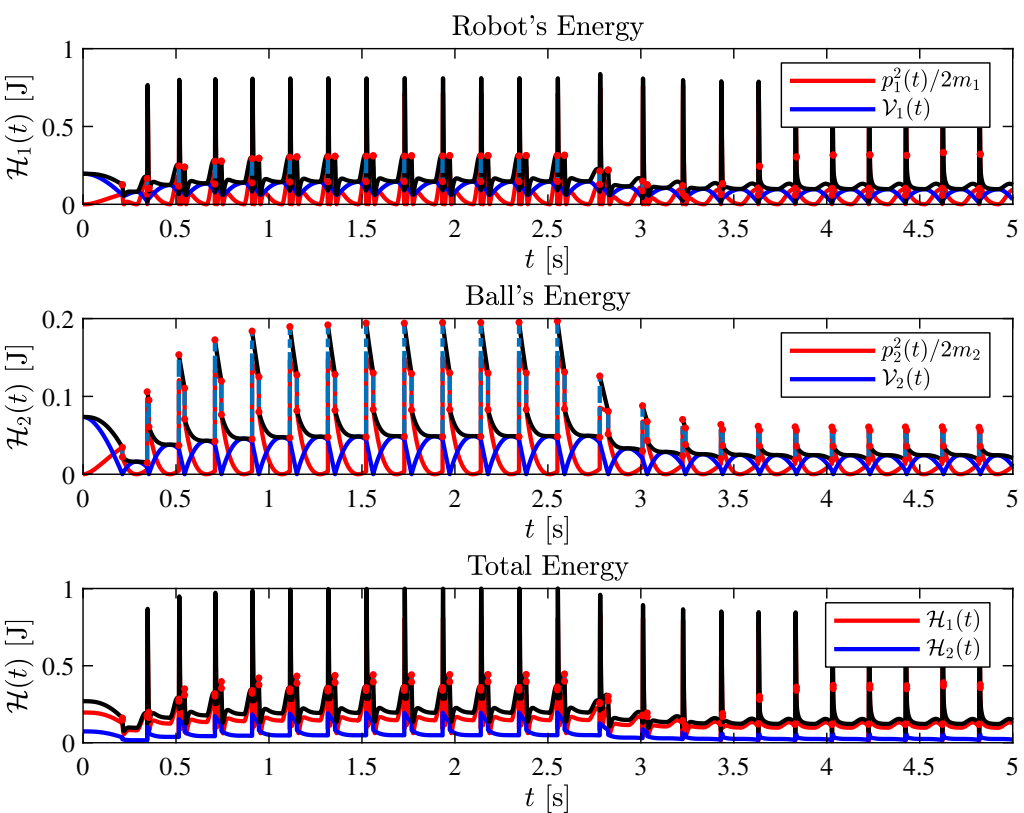
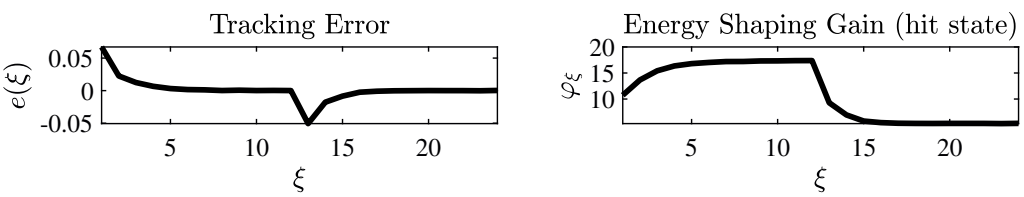
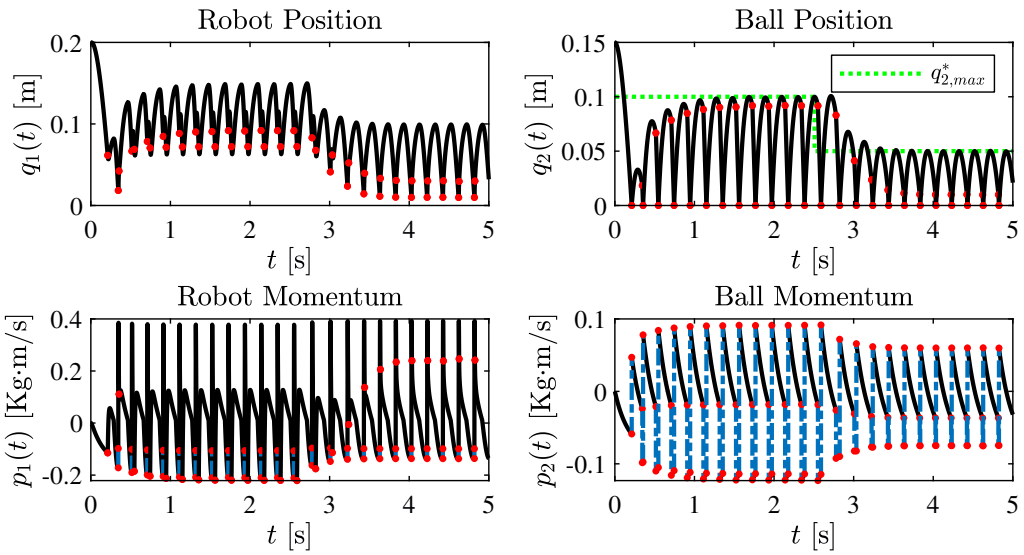


Fig. 4.26: Robustness to parameters variations: change on the reference position.  
73

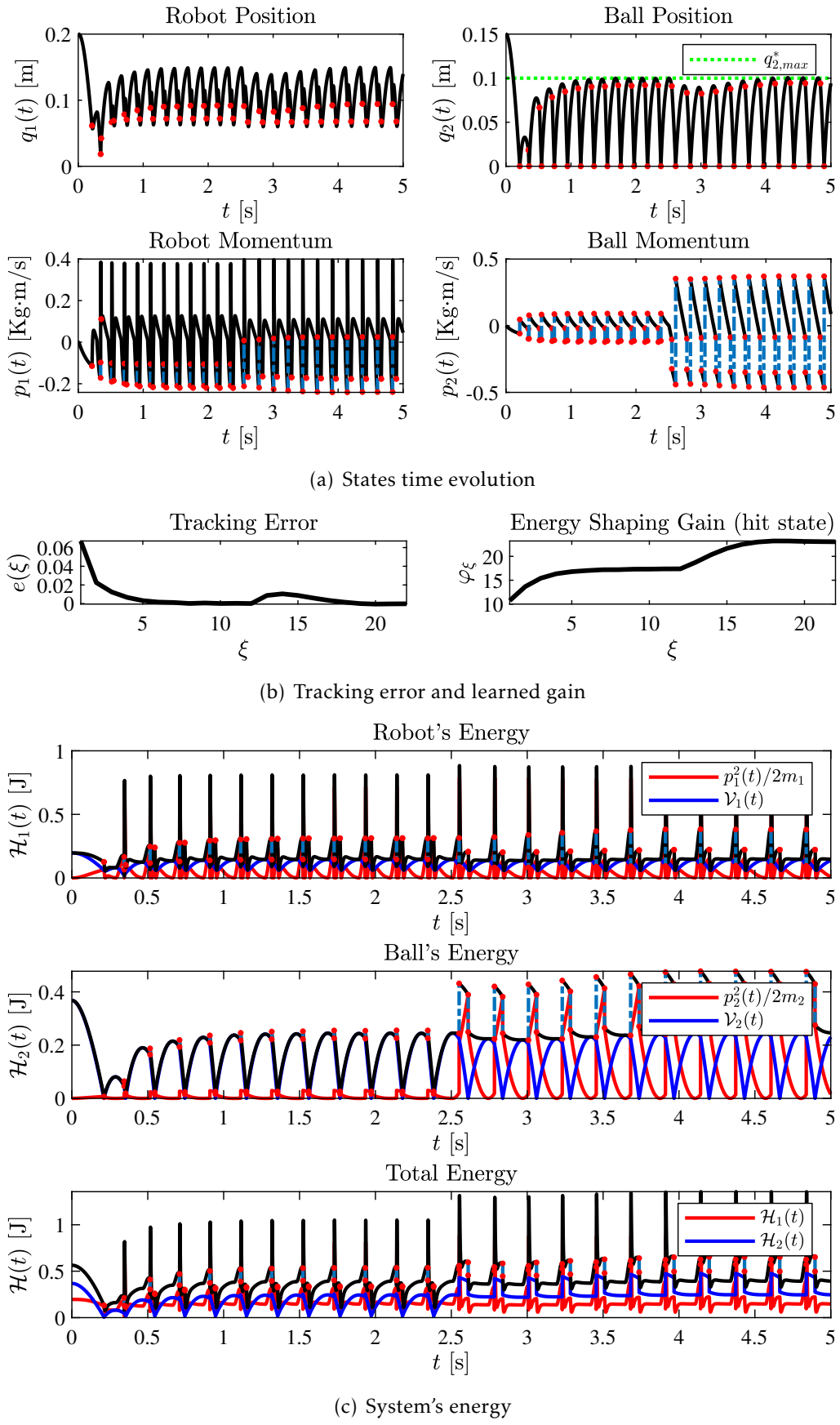


Fig. 4.27: Robustness to parameters variations: change on the ball's mass.  
74

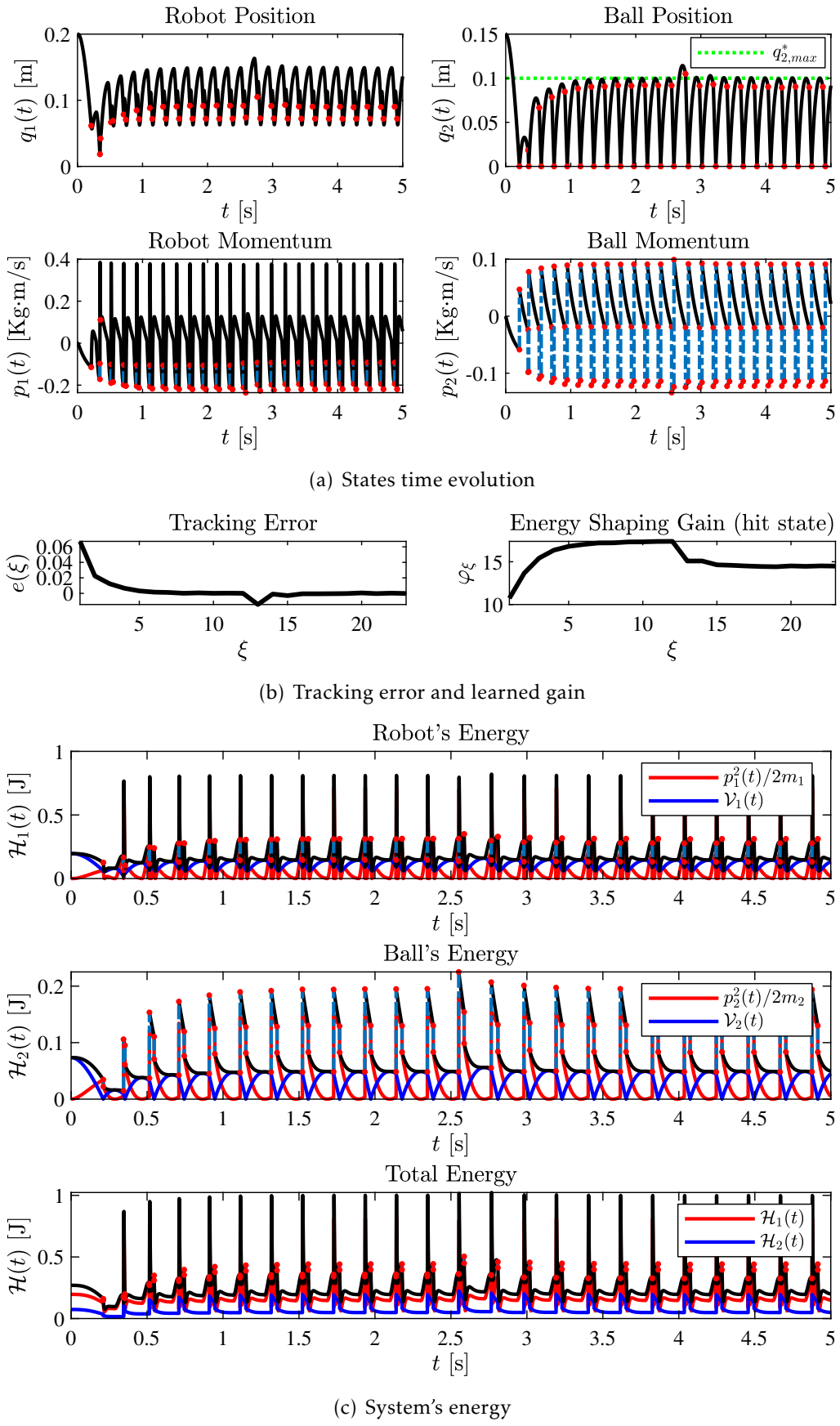


Fig. 4.28: Robustness to parameters variations: change on the restitution coefficients.

## 4.6 Summary

In this chapter, inspired by the theory developed in Chapter 3, a new paradigm of energy based control for the ball–dribbling robot, the *iterative energy shaping*, has been introduced.

Firstly, the hybrid port–Hamiltonian model of the ball–dribbling robot has been derived and characterized. Then, its passivity and autonomous stability have been confirmed. It has been shown how chaotic behaviors arise in the autonomous model.

A new paradigm of energy–based control, the *iterative energy shaping*, has been then introduced. Numerical simulations have been performed to prove the effectiveness of the proposed control scheme as well as its robustness to uncertain initial conditions and sudden changes to some physical parameters.

The aim of the next chapter is to give an idea of the ubiquity of the hybrid port–Hamiltonian framework is. A novel hybrid nonlinear controller is developed to solve a theoretical problem for linear system. Then, it is shown that the controlled system belongs to the class of hybrid port–Hamiltonian systems.

# Chapter 5

## Multistable Energy Shaping of Linear–Time–Invariant Systems

---

5.1	Introduction .....	78
5.2	Multistable Energy Shaping of LTI Systems .....	80
5.2.1	Passivity of LTI Systems .....	80
5.2.2	Multistable Passivity-Based Control of LTI Systems .....	81
5.2.3	Application Example .....	83
5.2.4	Choice of the Dissipation Rate: Shaping the Basins of Attraction .	84
5.3	Hybrid Mode Selector.....	88
5.3.1	Impulse generation .....	88
5.3.2	Overall Hybrid System .....	89
5.4	Hybrid Port–Hamiltonian Model and Stability .....	90
5.5	Numerical Simulation.....	92
5.6	Summary .....	95

---

## 5.1 Introduction

 EXPONENTIALLY stable linear-time-invariant (LTI) systems admit an unique equilibrium point, while in many practical situations, they have to operate in a finite number of *working modes* (fixed values of voltages, positions, etc.). Thus, with standard linear control techniques, a continuous exogenous reference signal must be constantly provided in order to achieve the desired behavior, e.g. asymptotic stabilisation of a desired set points. The block diagram of classical PID Control scheme is reported in Fig. 5.1. In order to embed in the controlled system

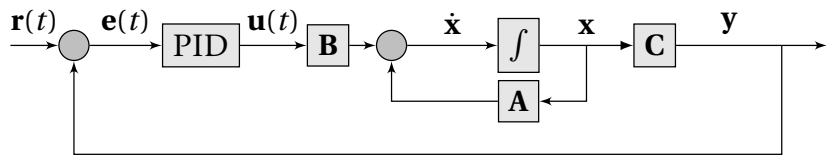


Fig. 5.1: A block representation of a classic feedback control system.  $\mathbf{x}$  is the state of the system,  $\mathbf{A}$ ,  $\mathbf{B}$ ,  $\mathbf{C}$  are the system's matrices,  $\mathbf{y}$  is the output, and  $\mathbf{r}(t)$  is a desired reference signal. In classic linear control the tracking error  $\mathbf{e}$  is obtained by comparing the reference and the output. The error is then processed by a PID controller which computes the control input.

the information on the desired working modes, a nonlinear controller is employed to simultaneously stabilise multiple points, i.e. achieve *multistability* and avoid the need of external reference signals. The introduction of the nonlinear terms gives rise to interesting properties of the controlled system, e.g. the possibility of shaping the basins of attraction of the different fixed points. Appealing studies on the inverse problem, i.e., turning *monostable* a multistable nonlinear system, have already been presented by Pisarchik and Feudel (2014).

In this chapter, considering that stable LTI system can be made passive through an opportune choice of input and output (Byrnes et al. (1991a)), a nonlinear controller able to stabilize multiple points is designed following a port-Hamiltonian paradigm, (Ortega and Mareels (2000); Secchi et al. (2007); Ortega et al. (2008); Van Der Schaft et al. (2014)). Then, in order to switch among the working modes, a *mode selector* is developed exploiting the theory of hybrid dynamical systems (Van Der Schaft and Schumacher (2000); Goebel et al. (2009a)). A graphical representation of a state-space trajectory for the proposed controlled system is shown in Fig. 5.2.

Moreover, it is shown that the controlled system falls in the framework of hybrid port–Hamiltonian systems, proving the generality and applicability of the newly developed theory.

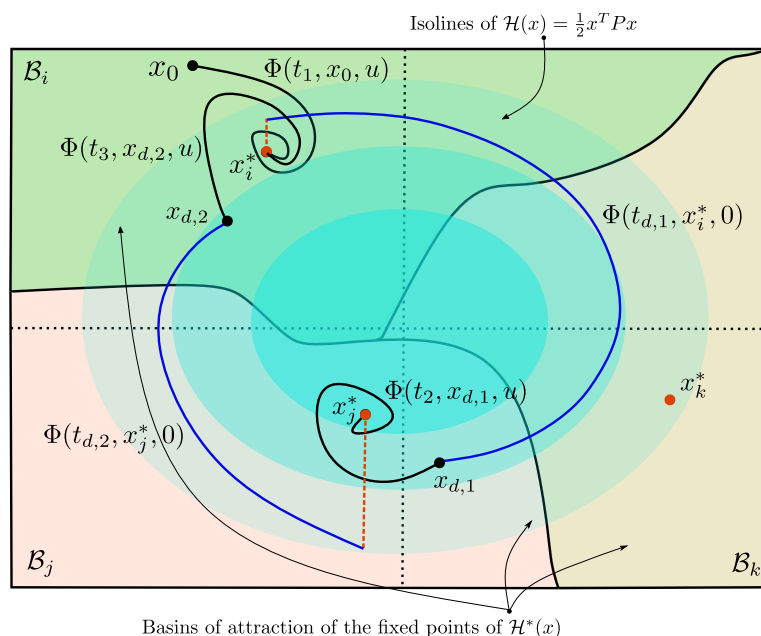


Fig. 5.2: Graphical representation of a state-space trajectory of the controlled system. The controlled system will have two logical states: a stabilization state (black lines) and a mode switching state (blue lines).

## 5.2 Multistable Energy Shaping of LTI Systems

In this section a nonlinear feedback law for a LTI system is designed to stabilise multiple fixed points. Passivity and the properties of passive LTI systems are briefly discussed.

### 5.2.1 Passivity of LTI Systems

Let us consider the stable LTI specialization of (2.7), i.e. the standard system with state space realization

$$\begin{cases} \dot{\mathbf{x}}(t) = \mathbf{A}\mathbf{x}(t) + \mathbf{B}\mathbf{u}(t) \\ \mathbf{y}(t) = \mathbf{C}\mathbf{x}(t) \end{cases}, \quad (5.1)$$

with system matrices  $(\mathbf{A}, \mathbf{B}, \mathbf{C})$  of appropriate dimensions and let  $\mathbf{A}$  be Hurwitz. It is easy to verify that, once system (5.1) is equipped with a quadratic storage function

$$\mathcal{H}(\mathbf{x}) = \frac{1}{2}\mathbf{x}^\top \mathbf{P}\mathbf{x}, \quad \mathbf{P} = \mathbf{P}^\top > 0, \quad (5.2)$$

it enjoys the KPY property, i.e. it is passive, if and only if

$$\mathbf{A}^\top \mathbf{P} + \mathbf{P}\mathbf{A} \leq 0 \quad \mathbf{B}^\top \mathbf{P} = \mathbf{C}. \quad (5.3)$$

**Remark 5.2.1.** *It is worth to be noticed that passivity could just be tested by the definition:  $(\mathbf{A}, \mathbf{B}, \mathbf{C})$  is passive if and only if it is dissipative with respect to the supply rate  $\langle \mathbf{y}, \mathbf{u} \rangle \triangleq \mathbf{y}^\top \mathbf{u}$ , i.e., if and only if there exists  $\mathcal{H} \in \mathcal{C}^1$ ,*

$$\dot{\mathcal{H}} \leq \mathbf{y}^\top \mathbf{u}, \quad (5.4)$$

Thus, it yields,

$$\dot{\mathcal{H}} = \frac{1}{2}\mathbf{x}^\top (\mathbf{A}^\top \mathbf{P} + \mathbf{P}\mathbf{A})\mathbf{x} + \mathbf{x}^\top \mathbf{P}\mathbf{B}\mathbf{u} \leq \mathbf{x}^\top \mathbf{C}^\top \mathbf{u}, \quad (5.5)$$

which is true if and only if (5.3) hold.

Furthermore, for system (5.1) with  $\mathbf{A}$  stable and  $\mathbf{u} = \mathbf{0}_m$ , the storage function is non increasing along trajectories, i.e.

$$\dot{\mathcal{H}}(\mathbf{x}) = \frac{1}{2}\mathbf{x}^\top (\mathbf{A}^\top \mathbf{P} + \mathbf{P}\mathbf{A})\mathbf{x} \leq 0 \quad \forall \mathbf{x} \in \mathcal{X}. \quad (5.6)$$

This means that the *natural* dissipation inferred by the choice of  $\mathbf{P}$  of the autonomous system corresponds to  $\frac{1}{2}\mathbf{x}^\top (\mathbf{A}^\top \mathbf{P} + \mathbf{P}\mathbf{A})\mathbf{x}$  where  $\mathbf{A}^\top \mathbf{P} + \mathbf{P}\mathbf{A} \leq 0$ . In order to present clearly the upcoming concepts, the following prototype linear system has been chosen as example to be invoked throughout the chapter.

**Example 5.2.2.** Consider a forced mass–spring–damper system of example 2.3.3 with unitary mass, i.e.  $k > 0$ ,  $m = 1$ ,  $p = \dot{q}$  and  $\mathbf{x} \triangleq (q, p)$ . The LTI state–space (5.1) representation is

$$\dot{\mathbf{x}} = \underbrace{\begin{bmatrix} 0 & 1 \\ -k & -b \end{bmatrix}}_{\mathbf{A}} \mathbf{x} + \underbrace{\begin{bmatrix} 0 \\ 1 \end{bmatrix}}_{\mathbf{B}} u. \quad (5.7)$$

The autonomous system is exponentially stable if  $b > 0$ . Let  $\mathbf{P} = \text{diag}(k, 1)$ . Indeed  $\mathbf{P} = \mathbf{P}^\top > 0$  and  $\mathbf{A}^\top \mathbf{P} + \mathbf{P} \mathbf{A} < 0$ . Thus, the system is passified (with storage function  $\mathcal{H} = \frac{1}{2}\mathbf{x}^\top \mathbf{P} \mathbf{x}$ ) choosing the linear output as  $\mathbf{y} \triangleq \mathbf{B}^\top \mathbf{P} \mathbf{x} = \dot{q}$ , as also derived by first principles in Chapter 2. Note that  $\mathcal{H}$  is the total energy of the system. In general, any mechanical systems is passive with its total energy as storage function by choosing as input(s) the (generalised) forces and as output(s) the (generalised) momenta.

### 5.2.2 Multistable Passivity-Based Control of LTI Systems

Any passive LTI system (5.1) with storage function  $\mathcal{H}(\mathbf{x}) = \frac{1}{2}\mathbf{x}^\top \mathbf{P} \mathbf{x}$  such that  $\text{null}(\mathbf{P}) \subseteq \text{null}(\mathbf{A})$  admits a port-Hamiltonian representation<sup>\*1</sup>:

$$\begin{cases} \dot{\mathbf{x}} = [\mathbf{J} - \mathbf{R}] \mathbf{P} \mathbf{x} + \mathbf{B} \mathbf{u} \\ \mathbf{y} = \mathbf{B}^\top \mathbf{P} \mathbf{x} \end{cases}, \quad (5.8)$$

where

$$\mathbf{J} \triangleq \frac{1}{2}(\mathbf{A}\mathbf{P}^{-1} - \mathbf{P}^{-1}\mathbf{A}^\top), \quad \mathbf{R} \triangleq -\frac{1}{2}(\mathbf{A}\mathbf{P}^{-1} + \mathbf{P}^{-1}\mathbf{A}^\top), \quad (5.9)$$

are derived by the following relations:

$$\mathbf{A} = [\mathbf{J} - \mathbf{R}] \mathbf{P}, \quad (5.10)$$

$$(\mathbf{J} - \mathbf{R})^\top + (\mathbf{J} - \mathbf{R}) = -2\mathbf{R}. \quad (5.11)$$

Thus, for a LTI system, the energy balancing control law (2.44) becomes

$$\boldsymbol{\beta}(\mathbf{x}) = -(\mathbf{B}^\top \mathbf{B})^{-1} \mathbf{B}^\top \mathbf{P}^{-1} \mathbf{A}^\top \nabla \mathcal{H}_a, \quad (5.12)$$

with

$$\mathcal{H}_a \triangleq \mathcal{H}^* - \frac{1}{2}\mathbf{x}^\top \mathbf{P} \mathbf{x} \quad (5.13)$$

and the matching conditions:

$$\begin{bmatrix} \mathbf{B}^\perp & [\mathbf{J} - \mathbf{R}]^\top \\ \mathbf{B}^\top \end{bmatrix} \nabla \mathcal{H}_a = \mathbf{0}_{n+m}. \quad (5.14)$$

---

<sup>\*1</sup> Since  $\mathbf{P} > 0$ , this condition does not represent a loss of generality, i.e. any system (5.1) can be written in PH form.

**Proposition 5.2.3** (Multistable EB–PBC of LTI System). *Consider a passive LTI system (5.1) equipped with a quadratic storage function  $\mathcal{H}(\mathbf{x}) = \frac{1}{2}\mathbf{x}^\top \mathbf{P}\mathbf{x}$ . Let  $\mathcal{H}^* \in \mathcal{C}^2$  be a desired storage (energy) function with  $p$  minima corresponding to  $p$  desired equilibrium points  $\mathbf{x}_i^*$ , i.e.*

$$\nabla \mathcal{H}^*|_{\mathbf{x}=\mathbf{x}_i^*} = \mathbb{0}_n, \quad \nabla^2 \mathcal{H}^*|_{\mathbf{x}=\mathbf{x}_i^*} > 0 \quad \forall i = 1, \dots, p. \quad (5.15)$$

*The EB–PBC control action (5.12) stabilises the desired equilibrium points  $\mathbf{x}_i^*$  if (5.14) holds true for the chosen  $\mathcal{H}^*$ .*

*Proof.* The proof follows similarly to (Ortega et al. , 2008). Indeed, the minimum points of  $\mathcal{H}^*$  will result to be Lyapunov stable equilibria in the same way in which EB–PBC acts on a single fixed point. It follows that if  $\mathbf{A}$  is Hurwitz, the new “shaped” energy  $\mathcal{H}^*$  will be monotonically decreasing along any trajectory since  $\mathbf{A}^\top \mathbf{P} + \mathbf{P}\mathbf{A} < 0$  and, thus, if it is bounded from below the system will reach asymptotically one of the minima of  $\mathcal{H}^*$ . However, if the linear system is only stable, i.e.  $\mathbf{A}^\top \mathbf{P} + \mathbf{P}\mathbf{A} \leq 0$ , then locally invariant sets have to be examined by means of La Salle’s invariance theorem to check asymptotic stability (Khalil and Grizzle, 2002).  $\square$

**Remark 5.2.4.** *Deeper evaluations and considerations on Lyapunov functions for multistable nonlinear systems are reported in Efimov (2012). It has to be underlined that, in order to have an energy function with multiple minima, it is necessary to have the presence of local maxima, which however do not affect global behavior of the system, since those are just unstable fixed points of the closed loop system.*

Furthermore, in the case of LTI systems, the damping injection takes the form

$$\mathbf{v} = -\mathbf{K}_d \mathbf{B}^\top \mathbf{P} \mathbf{x}. \quad (5.16)$$

A block diagram picturing the overall control scheme is represented in Fig. 5.3.

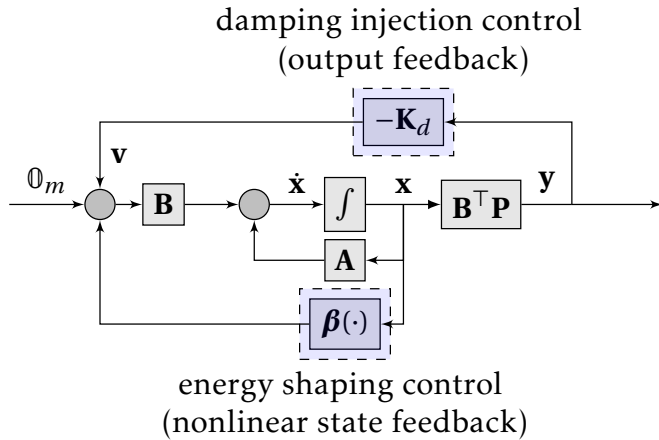


Fig. 5.3: A block representation of the controlled system. Here, the energy shaping and damping injection control actions asymptotically stabilize all the desired working modes of the system, i.e. the minima of the new energy function.

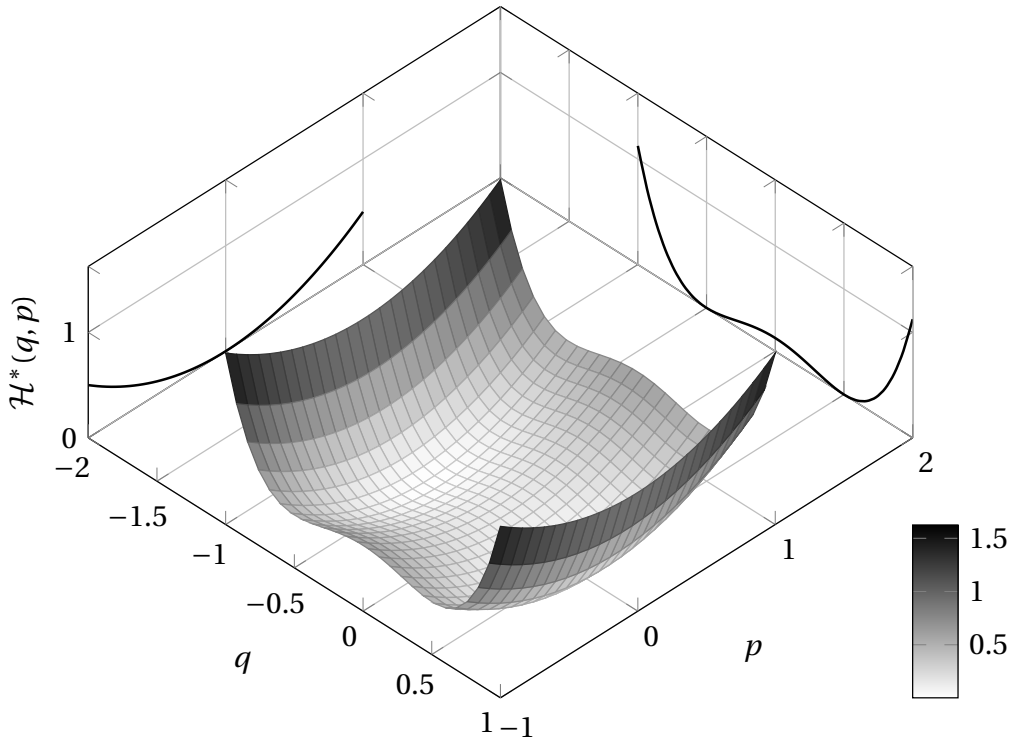


Fig. 5.4: Desired shaped energy function  $\mathcal{H}^*(q, p) = \lambda q^4 - \mu q^2 + \frac{1}{2} p^2 + \frac{\mu^2}{4\lambda}$

### 5.2.3 Application Example

Consider the system in Example 5.2.2 and let the desired energy function have two symmetrically distributed minima on the displacement axes, e.g.,

$$\mathcal{H}^*(q, p) = \lambda q^4 - \mu q^2 + \frac{1}{2} p^2 + \frac{\mu^2}{4\lambda} \quad \lambda, \mu > 0, \quad (5.17)$$

which has two minima in  $[\pm\sqrt{\mu/2\lambda}, 0]^\top$  and a local maximum in  $[0, 0]^\top$ . The desired energy function is plotted in Figure 5.4. Thus,

$$\mathcal{H}_a = \mathcal{H}^* - \mathcal{H} \quad (5.18)$$

$$= \lambda q^4 - (\mu + \frac{1}{2}\kappa) q^2 + \frac{1}{2} p^2 + \frac{\mu^2}{4\lambda} \quad (5.19)$$

and, therefore

$$\nabla \mathcal{H}_a = (4\lambda q^3 - (2\mu + k)q, p). \quad (5.20)$$

It is easy to proof that the matching conditions (5.14) of the EB-PBC are satisfied for  $\mathcal{H}_a$ . The energy shaping control law becomes

$$\beta(q) = -[0 \quad 1] \begin{bmatrix} 0 & -1 \\ 1 & -b \end{bmatrix} \begin{bmatrix} 4\lambda q^3 - (2\mu + k)q \\ p \end{bmatrix} \quad (5.21)$$

$$= -4\lambda q^3 + (2\mu + k)q. \quad (5.22)$$

A numerical simulation of the proposed control scheme has been performed with  $k = 1$ ,  $b = 0.5$ . The parameters  $\lambda$  and  $\mu$  have been set to 2 and 1 respectively, placing the minima of  $\mathcal{H}^*$  in  $[\pm 0.5, 0]^\top$ . No damping injection actions has been added as the asymptotic stability is already guaranteed by the natural dissipation of the autonomous linear system. Starting in the initial position  $\mathbf{x}_0 \triangleq (-0.9, 0)$  the system has been simulated for both the autonomous and the multistable EB-PBC controlled system for 40s. The resulting phase-space portraits are reported in Fig. 5.5.

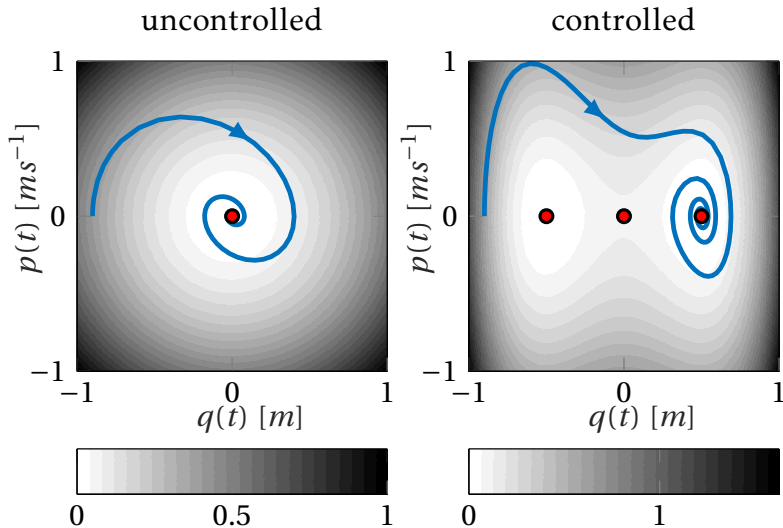


Fig. 5.5: Comparison of the phase–space portraits of the autonomous and the multistable EB–PBC controlled system with  $k = 1$ ,  $b = 0.5$ ,  $\lambda = 2$ ,  $\mu = 1$ . The phase–space portraits are represents over contour plots of the corresponding energy functions, i.e.,  $\mathcal{H} = \frac{1}{2}(kq + p)$  and  $\mathcal{H}^* = 2q^4 - q^2 + \frac{1}{2}p + \frac{1}{8}$ . The red dots indicates the critical points of  $\mathcal{H}$  and  $\mathcal{H}^*$ .

#### 5.2.4 Choice of the Dissipation Rate: Shaping the Basins of Attraction

In this section it is shown how, by tuning the dissipation rate  $\mathbf{K}_d$ , it is possible to shape the basins of attraction of the designed stable fixed points of the closed–loop system.

**Definition 5.2.5.** *The basin of attraction  $\mathcal{B}$  of a fixed point  $\mathbf{x}^*$  of a system (2.7) is the set of all initial conditions  $\mathbf{x}_0$  leading to long–time behavior that approaches that fixed point, i.e.*

$$\mathcal{B} \triangleq \left\{ \mathbf{x}_0 \in \mathcal{X} \mid \lim_{t \rightarrow \infty} \boldsymbol{\phi}(t, \mathbf{x}_0, \mathbf{u}) = \mathbf{x}^* \right\}. \quad (5.23)$$

The designed feedback control law (5.21) allows to fix multiple stable points for the closed–loop system. The damping injection component of the overall control action

can be used to “shape” their basins of attraction. This property allows to have interesting control actions which will be qualitatively shown. Consider the system of Example 5.2.2 controlled by the energy shaping control law (5.21). The closed-loop system in the form (2.7) can be expressed as

$$\begin{cases} \dot{\mathbf{x}} = \begin{bmatrix} p \\ -4\lambda q^3 + 2\mu q - bp \end{bmatrix} + \mathbf{B}\nu \\ y = \mathbf{B}^\top \mathbf{P}\mathbf{x} \end{cases}. \quad (5.24)$$

If  $\nu = 0$  the system has two asymptotically stable fixed points in  $[\pm\sqrt{\mu/2\lambda}, 0]^\top$ . Let  $\mathbf{K}_d \triangleq k_d$ . The output feedback controller  $\nu = -k_d y = -k_d p$  does not change the location of the fixed points. In fact, it only changes the overall friction of the system from  $b$  to  $b + k_d$ , i.e. the natural dissipation of the closed-loop system from  $bp^2$  to  $(b + k_d)p^2$ . Besides, the respective basins of attraction strongly depend on the choice of the controller, i.e., on the value of  $k_d$ . In Fig. 5.6 the basins of attraction of the two fixed points are shown for different values of  $k_d$  in the region  $[-1, 1] \times [-1, 1]$  of the state space with  $b = 0$ ,  $\lambda = 2$ ,  $\mu = 1$ . It is evident that the higher the dissipation rate is, the lower is the number of transitions between basins of attraction.

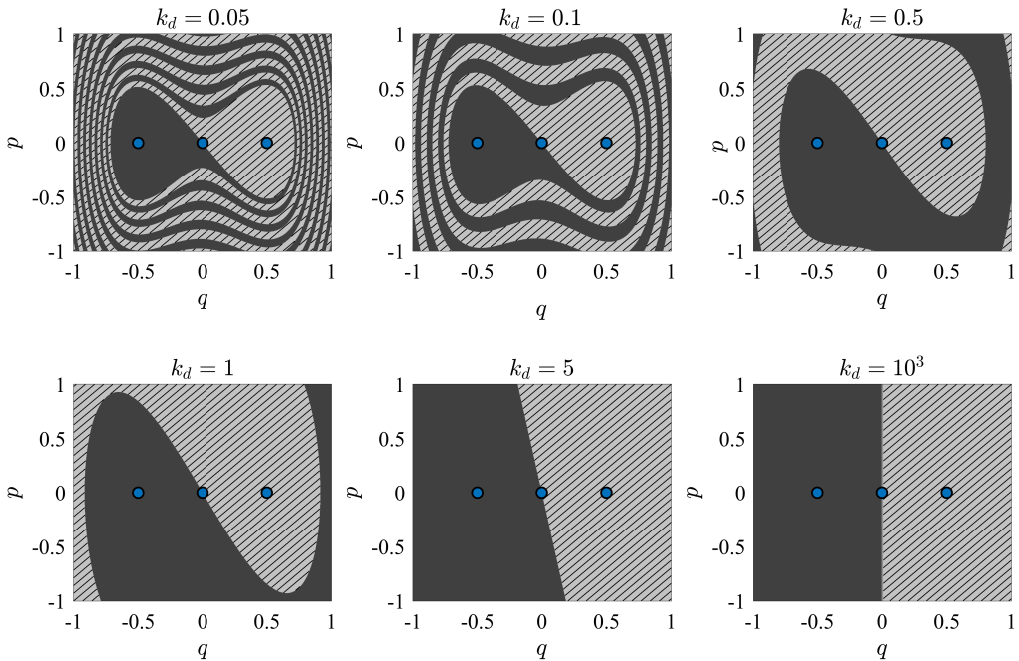


Fig. 5.6: Basins of attraction of the fixed points of the system for different values of  $k_d$  in the region  $[-1, 1] \times [-1, 1]$ . The basin of attraction of the minima [blue points] are represented in dark gray (for  $(-0.5, 0)$ ) and light hatched gray (for  $(0.5, 0)$ ). The blue point in  $(0, 0)$  is the local maximum of  $\mathcal{H}^*$ .

Therefore, given an initial condition  $\mathbf{x}_0$ , and a desired set point  $\mathbf{x}_i^*$ , corresponding to one of the minima of  $\mathcal{H}^*$ , we would be interested in choosing a dissipation rate  $\mathbf{K}_d = \mathbf{K}_d^\top \succeq 0$  such that  $\mathbf{x}_0$  belongs to the basin of attraction  $\mathcal{B}_i$  of  $\mathbf{x}_i^*$ .

From now on, we will consider the topology on  $\mathbb{R}^n$  to be the *standard* one, i.e. the one induced by the euclidian metric. Furthermore, given an open set  $\mathcal{S} \subset \mathbb{R}^n$ , let us denote its closure with  $\bar{\mathcal{S}}$ .

**Theorem 5.2.6.** (*Necessity*) Let  $c$  be the initial energy,  $c = \mathcal{H}^*(\mathbf{x}_0)$ . Let  $\Lambda_c$  be the  $c$ -level set of  $\mathcal{H}^*$ ,  $L_c \mathcal{H}^* = \{\mathbf{x} : \mathcal{H}^*(\mathbf{x}) = c\} \subset \mathbb{R}^n$ . If there exists a  $\mathbf{K}_d = \mathbf{K}_d^\top \succeq 0$  such that  $\mathbf{x}_0 \in \mathcal{B}_i$ , then one of the following is necessarily satisfied:

1.  $L_c \mathcal{H}^*$  is connected and

$$\exists \Gamma : \partial \Gamma = L_c \mathcal{H}^* \wedge \mathbf{x}_i^* \in \bar{\Gamma}. \quad (5.25)$$

2.  $L_c \mathcal{H}^*$  is not connected but it is the union of  $r$  connected sets  $L_c^1 \mathcal{H}^*, \dots, L_c^r \mathcal{H}^*$  and

$$\exists \Gamma_j : \partial \Gamma_j = L_c^j \mathcal{H}^* \wedge \mathbf{x}_0, \mathbf{x}_i^* \in \bar{\Gamma}_j. \quad (5.26)$$

*Proof.* Due to dissipativity of the controlled system, i.e.

$$\dot{\mathcal{H}}^* \leq \mathbf{y}^\top \mathbf{v} = -\mathbf{x}^\top \mathbf{P} \mathbf{B} \mathbf{K}_d \mathbf{B}^\top \mathbf{P} \mathbf{x} \leq 0 \quad \forall \mathbf{K}_d = \mathbf{K}_d^\top \succeq 0, \quad (5.27)$$

the any trajectory with initial condition will lie inside the closure of the set  $\Gamma$  defined as

$$\partial \Gamma \triangleq L_c \mathcal{H}^*, \quad (5.28)$$

regardless on the choice of  $\mathbf{K}_d$ , i.e.,

$$\forall t, \forall \mathbf{K}_d = \mathbf{K}_d^\top \succeq 0 \quad \phi(t, \mathbf{x}_0, \mathbf{u}) \in \bar{\Gamma}. \quad (5.29)$$

Therefore, if  $\mathbf{x}_i^* \notin \bar{\Gamma}$ , it is impossible to reach it, i.e.,

$$\mathbf{x}_i^* \notin \bar{\Gamma} \Rightarrow \nexists \mathbf{K}_d = \mathbf{K}_d^\top \succeq 0 : \mathbf{x}_0 \in \mathcal{B}_i. \quad (5.30)$$

If  $L_c \mathcal{H}^*$  is connected also  $\bar{\Gamma}$  is connected and  $\mathbf{x}_0 \in \partial \Gamma \subset \bar{\Gamma}$ , then the necessary condition for the existence of a  $\mathbf{K}_d = \mathbf{K}_d^\top \succeq 0$  such that  $\mathbf{x}_0 \in \mathcal{B}_i$  is simply:  $\mathbf{x}_i^* \in \bar{\Gamma}$ . On the other hand if  $L_c \mathcal{H}^*$  is not connected but it is the union of connected sets, the trajectory will never leave the set  $\bar{\Gamma}_j$  defined by

$$\partial \Gamma_j \triangleq L_c^j \mathcal{H}^*, \quad (5.31)$$

where

$$L_c \mathcal{H}^* = \bigcup_{k=1}^m L_c^k \mathcal{H}^* \text{ and } \mathbf{x}_0 \in L_c^j \mathcal{H}^* \quad (5.32)$$

Thus, the necessary condition is that also  $\mathbf{x}_i^*$  belongs to  $\bar{\Gamma}_j$ .  $\square$

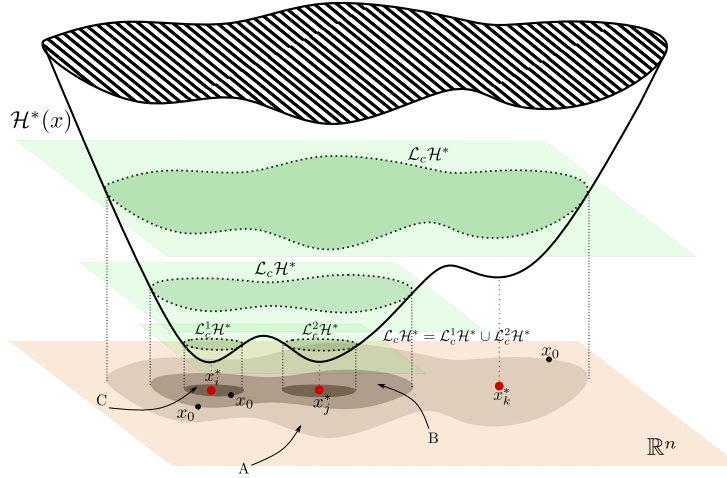


Fig. 5.7: Graphical representation of the necessary condition given by Theorem 5.2.6. Case (A): the condition is satisfied for all the stable fixed points  $\mathbf{x}_i^*$ ,  $\mathbf{x}_j^*$  and  $\mathbf{x}_k^*$ . Case (B): the condition is satisfied for  $\mathbf{x}_i^*$ ,  $\mathbf{x}_j^*$  but not for  $\mathbf{x}_k^*$ . Case (C): the condition is satisfied only for  $\mathbf{x}_i^*$ .

A graphical representation of this necessary condition is given in Fig. 5.7.

In order to choose among the possibly infinite values of  $\mathbf{K}_d$  such that  $\mathbf{x}_0 \in \mathcal{B}_i$ , one could minimize both the approaching time and the damping injection control effort needed to bring  $\mathbf{x}(t)$  from  $\mathbf{x}_0$  to  $\mathbf{x}_i^*$ , i.e.,

$$\begin{aligned} & \text{minimize}_{\mathbf{K}_d} \quad \int_0^\infty \left( (\mathbf{x}(s) - \mathbf{x}_i^*)^\top \mathbf{Q} (\mathbf{x}(s) - \mathbf{x}_i^*) + \mathbf{x}(s)^\top \mathbf{P} \mathbf{B} \mathbf{K}_d \mathbf{S} \mathbf{K}_d^\top \mathbf{B}^\top \mathbf{P} \mathbf{x}(s) \right) ds \\ & \text{subject to} \quad \lim_{t \rightarrow \infty} \boldsymbol{\phi}(t, \mathbf{x}_0, \boldsymbol{\beta}(\mathbf{x}) - \mathbf{K}_d \mathbf{B}^\top \mathbf{P} \mathbf{x}) = \mathbf{x}_i^* \end{aligned}, \quad (5.33)$$

with  $\mathbf{Q} = \mathbf{Q}^\top \succeq 0$ ,  $\mathbf{S} = \mathbf{S}^\top \succeq 0$ .

## 5.3 Hybrid Mode Selector

Once the feedback law and the damping injection are designed to produce the desired working modes and to shape their basins of attraction, the proposed strategy aims to switch from a working mode to another. In particular, considering the system to be in one of the working modes  $\mathbf{x}_i^*$ , a control action which moves the system to another desired mode,  $\mathbf{x}_j^*$ , is designed. The strategy reckons on the following actions:

1. Switch-off the energy shaping controller (the system turns back linear);
2. Give an impulse to the system to bring the state inside the basin of attraction of  $\mathbf{x}_j^*$ ;
3. Switch on again the energy shaping controller.

### 5.3.1 Impulse generation

When the nonlinear controller  $\mathbf{u} = \boldsymbol{\beta}(\mathbf{x}) + \mathbf{v}$  is switched off, i.e.  $\mathbf{u} = \mathbf{0}_m$ , the system turns back in the LTI form (5.1). Without loss of generality, let  $t = 0$  and let the LTI system be controllable. The response of the system to a weighted impulse input

$$\mathbf{u}(t) = \mathbf{v}\delta(t), \quad (5.34)$$

where  $\mathbf{v} \in \mathbb{R}^m$  distributes the Dirac delta function  $\delta(t)$  among the  $m$  inputs, is

$$\begin{aligned} \mathbf{x}(t) &= e^{t\mathbf{A}}\mathbf{x}_0 + \int_0^t e^{(t-s)\mathbf{A}}\mathbf{B}\mathbf{u}(s)ds = \\ &= e^{t\mathbf{A}}\mathbf{x}_0 + \int_0^t e^{(t-s)\mathbf{A}}\mathbf{B}\mathbf{v}\delta(s)ds \\ &= e^{t\mathbf{A}}\mathbf{x}_0 + e^{t\mathbf{A}}\mathbf{B}\mathbf{v} \end{aligned} \quad (5.35)$$

$$= e^{t\mathbf{A}}(\mathbf{x}_0 + \mathbf{B}\mathbf{v}). \quad (5.36)$$

Since the control objective is to move the system from  $\mathbf{x}_i^*$  to  $\mathbf{x}_j^*$  in a time  $t^*$ , it is tempting to impose the desired behavior in (5.35) by requiring:

$$\mathbf{x}_j^* \triangleq \mathbf{x}(t^*) = e^{t^*\mathbf{A}}(\mathbf{x}_i^* + \mathbf{B}\mathbf{v}). \quad (5.37)$$

Therefore,  $\mathbf{v}$  might be obtained as

$$\mathbf{v} = (\mathbf{B}^\top \mathbf{B})^{-1} \mathbf{B}^\top (e^{-t^*\mathbf{A}} \mathbf{x}_j^* - \mathbf{x}_i^*). \quad (5.38)$$

However, unless  $m = n$ , (5.37) is over-determined, i.e.  $n$  (scalar) equations with only  $m$  unknowns (the components of  $\mathbf{v}$ ). To overcome this issue, the design of the impulse controller is achieved by solving the following optimization problem: find  $t^*$ ,  $\mathbf{v}$  such that

$$[t^*, \mathbf{v}] = \underset{t^*, \mathbf{v}}{\operatorname{argmin}} \gamma \|\mathbf{v}\|_2^2 + \rho \left\| \mathbf{x}_j^* - e^{t^*\mathbf{A}}(\mathbf{x}_i^* + \mathbf{B}\mathbf{v}) \right\|_2^2, \quad (5.39)$$

subject to  $\boldsymbol{\phi}(t^*, \mathbf{x}_i^*, \mathbf{v}\delta(t)) \in \mathcal{B}_j$

where  $\gamma, \rho \in \mathbb{R}^+$  are two arbitrary weights and  $\mathcal{B}_j$  is the basin of attraction of  $\mathbf{x}_j^*$ . The term  $\gamma \|\mathbf{v}\|_2^2$  has been introduced for regularization since, in some cases, it might be convenient to simultaneously minimize also the squared norm of the impulse weights.

The solution of (5.39), provides an impulsive input  $\mathbf{u} = \mathbf{v}\delta$  which guarantees that the system will arrive in  $\mathcal{B}_j$  in a time  $t^*$ . For the sake of a latter numerical implementation, the constraint was defined as

$$\left\| \hat{\boldsymbol{\phi}}(t_\infty, e^{t^* \mathbf{A}}(\mathbf{x}_i^* + \mathbf{B}\mathbf{v}), \boldsymbol{\beta}(\mathbf{x}) - \mathbf{K}_d \mathbf{B}^\top \mathbf{P} \mathbf{x}) - \mathbf{x}_j^* \right\|_2 \leq \varepsilon, \quad (5.40)$$

where  $\hat{\boldsymbol{\phi}}$  is the numerically integrated trajectory of the system,  $t_\infty \gg 1$  is the integration time and  $0 \leq \varepsilon \ll 1$  is a chosen threshold.

**Remark 5.3.1.** Assuming that the switch is performed only at steady-state, the optimization of  $\mathbf{v}$  and  $t^*$  for each pair of fixed points  $\mathbf{x}_i, \mathbf{x}_j$  can be performed off-line.

### 5.3.2 Overall Hybrid System

If an impulse is applied to the system at time  $t$  in order to reach the desired destination  $\mathbf{x}_j^*$ , in the instant of time in which the impulse is applied, the state undergoes to a discontinuous jump

$$\mathbf{x}^+ = \mathbf{x}(t) + \mathbf{B}\mathbf{v}. \quad (5.41)$$

Therefore, the controlled system can be described as an *hybrid automata*, with two logic states  $S_1$  and  $S_2$ . In  $S_1$  the system is controlled with the multistable EB-PBC and in  $S_2$  the system is completely uncontrolled. Thus, by introducing a timer  $\tau$  and an external asynchronous signal  $r$  (initialized to 0), the transition from  $S_1$  to  $S_2$  will happen when  $r$  changes from 0 to the index of the desired fixed point, i.e.,  $r \in \{0, 1, \dots, p\}$ , with a state jump described by (5.41) and resetting the timer  $\tau$  to 0. Then the system will remain uncontrolled (and thus linear) for a time  $t^*$ , i.e.  $\tau = t^*$  after which the logic state will switch back from  $S_2$  to  $S_1$  and the timer and the external signal  $r$  will be reset. A graphical representation of the designed hybrid automata is given in Fig. 5.8.

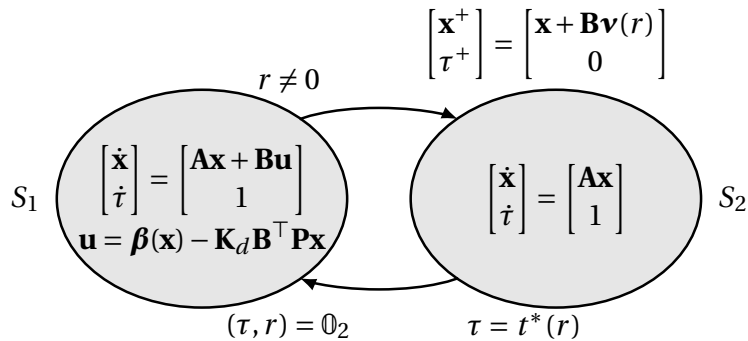


Fig. 5.8: Hybrid automata representing the overall controlled system with the hybrid mode selector.

## 5.4 Hybrid Port–Hamiltonian Model and Stability

A brief analysis of the overall hybrid model of the system controlled with the proposed *multistable energy shaping* with mode selector leads to the following consideration: the system can be formalized as the interconnection (see Sanfelice (2011)) between a hybrid port Hamiltonian system and an auxiliary hybrid system as represented in Fig. 5.9. The hybrid port–Hamiltonian model has two modes (similarly to the *hopping robot*

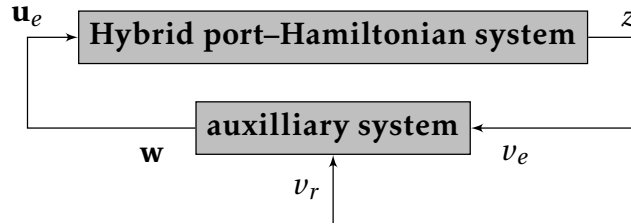


Fig. 5.9: A block representation of interconnection of the hybrid systems.

described in Chapter 3). Let  $\mathcal{H}_1(\mathbf{x}) \triangleq \mathcal{H}^*(\mathbf{x})$ ,  $\mathcal{H}_2(\mathbf{x}) = \mathcal{H}(\mathbf{x})$  and let  $s \in \mathcal{M} \triangleq \{1, 2\}$  be the indicates the current mode of the system. The flows of the systems are, respectively

$$\dot{\mathbf{x}} = \mathbf{A}\mathbf{P}^{-1}\nabla\mathcal{H}_1(\mathbf{x}) - \mathbf{B}\mathbf{K}_d\mathbf{B}^\top\mathbf{P}\mathbf{x} \quad \text{if } (\mathbf{x}, s) \in \mathcal{C}_1 \times \{1\}, \quad (5.42)$$

$$\dot{\mathbf{x}} = \mathbf{A}\mathbf{P}^{-1}\nabla\mathcal{H}_2(\mathbf{x}) \quad \text{if } (\mathbf{x}, s) \in \mathcal{C}_2 \times \{2\}, \quad (5.43)$$

where  $\mathcal{C}_1 \equiv \mathcal{C}_2 \triangleq \mathcal{X}$  and  $\mathcal{X}$  is the state–space of the linear system (5.1). Thus,

$$\mathcal{C} = \bigcup_{i=1}^2 \mathcal{C}_i \times \{i\}. \quad (5.44)$$

Note that, in both modes,

$$\mathbf{y} = \mathbf{B}^\top\mathbf{P}\mathbf{x}. \quad (5.45)$$

Let us also define an *auxiliary output*  $z \triangleq s$ . The jumps of the systems happen as

$$\begin{bmatrix} \mathbf{x}^+ \\ s^+ \end{bmatrix} = \begin{bmatrix} \mathbf{x} + \mathbf{B}\mathbf{v}(\mathbf{u}_e) \\ 2 \end{bmatrix} \quad \text{if } (\mathbf{x}, s, \mathbf{u}_e) \in \mathcal{D}_1 \triangleq \mathcal{X} \times \{1\} \times \mathcal{U}_e^1, \quad (5.46)$$

$$\begin{bmatrix} \mathbf{x}^+ \\ s^+ \end{bmatrix} = \begin{bmatrix} \mathbf{x} \\ 1 \end{bmatrix} \quad \text{if } (\mathbf{x}, s, \mathbf{u}_e) \in \mathcal{D}_2 \triangleq \mathcal{X} \times \{2\} \times \mathcal{U}_e^2, \quad (5.47)$$

where  $\mathbf{u}_e$  is the *auxiliary input* and

$$\mathcal{U}_e^1 \triangleq \mathbb{R} \times \mathbb{N}^*, \quad \mathcal{U}_e^2 \triangleq \{t^*(r)\} \times \mathbb{N}^*. \quad (5.48)$$

Let  $\mathcal{D} \triangleq \mathcal{D}_1 \cup \mathcal{D}_2$  and  $\mathcal{F}_{\text{PH}}, \mathcal{G}_{\text{PH}}$  are defined as in (3.12), (3.17).

To complete the model, let us define the *auxiliary hybrid system* which formalize the behavior of  $\tau$  and  $r$ :

$$\begin{cases} \begin{bmatrix} \dot{\tau} \\ \dot{r} \end{bmatrix} = \begin{bmatrix} 1 \\ 0 \end{bmatrix} & (\tau, r) \times \mathbb{R} \times \mathbb{N} \\ \\ \begin{bmatrix} \tau^+ \\ r^+ \end{bmatrix} = \begin{cases} \begin{bmatrix} \tau \\ v_r \end{bmatrix} & \text{if } (\tau, r, v_r, v_e) \in \mathbb{R} \times \mathbb{N} \times \mathbb{N}^* \times \{1\} \\ \begin{bmatrix} 0 \\ r \end{bmatrix} & \text{if } (\tau, r, v_r, v_e) \in \mathbb{R} \times \mathbb{N}^* \times \{0\} \times \{1\} \\ \begin{bmatrix} 0 \\ 0 \end{bmatrix} & \text{if } (\tau, r, v_r, v_e) \in \{t^*(r)\} \times \mathbb{N}^* \times \mathbb{N} \times \{2\} \end{cases} & , \end{cases} \quad (5.49)$$

where  $v_r$  is the *mode change* triggering signal which is supposed to take positive integer values corresponding to the index of the selected minima of  $\mathcal{H}^*$  and to be active in zero-measure time intervals. The output of the auxiliary system is defined as  $\mathbf{w} \triangleq (\tau, r)$ .

The final interconnected system is realized by imposing that the (auxiliary) output of the hybrid port–Hamiltonian system corresponds to the input  $v_e$  of the auxiliary system and vice versa, i.e.

$$v_e \equiv z, \quad \mathbf{u}_e \equiv \mathbf{w}. \quad (5.50)$$

The hybrid port–Hamiltonian system defined above is not passive. In fact, there is no guarantees that

$$\forall (\mathbf{x}, s, \mathbf{u}_e) \in \mathcal{D}_1 \quad \mathcal{H}(\mathbf{x} + \mathbf{B}\mathbf{v}(\mathbf{u}_e)) \leq \mathcal{H}^*(\mathbf{x}) \quad \text{and} \quad \forall (\mathbf{x}, s, \mathbf{u}_e) \in \mathcal{D}_2 \quad \mathcal{H}^*(\mathbf{x}) \leq \mathcal{H}(\mathbf{x}). \quad (5.51)$$

Nevertheless, it is reasonable to assume  $\|\mathbf{v}(r)\|_2$  bounded from above. In such case, it is possible to prove that the state–space of the controlled system is limited and does not “explode”.

## 5.5 Numerical Simulation

A numerical simulation of the overall controlled system has been performed to validate the proposed control scheme. The whole procedure has been implemented in the MATLAB® environment. The system introduced in Example 5.2.2 has been controlled with the multistable energy shaping (5.21) and the damping injection  $\nu = -\kappa\dot{\zeta}$ . The system parameters have been chosen as  $k = 5$ ,  $b = 0.5$  and, as in the example in Section 5.2, the minima of  $\mathcal{H}^*$  have been positioned in  $[\pm 0.5, 0]^\top$  by setting  $\lambda = 2$  and  $\mu = 1$ . To implement the asynchronous external control signal  $r$ , the two fixed points have been denoted with  $\mathbf{x}_1^* = [-0.5, 0]^\top$  and  $\mathbf{x}_2^* = [0.5, 0]^\top$ . The dissipation rate  $k_d$  has been set to 4.5. The *fmincon* solver of the *global optimization toolbox* of MATLAB® has been employed to solve the optimization problem (5.39). The optimization parameters have been chosen as  $t_\infty = 10^3$ ,  $\varepsilon = 10^{-5}$ , considering an absolute tolerance of  $10^{-6}$  for the numerical integration (ODE45). Starting from the initial state  $\mathbf{x}_0 \triangleq [-0.8, 0]^\top$ , the system, controlled with the nonlinear state feedback and the damping injection, has been integrated until secured convergence to  $\mathbf{x}_1^*$  (5s). Then,  $r$  has been set to 2 in order to trigger the change of working mode, i.e. to bring the state to  $\mathbf{x}_2^*$ . After the jump, the system has been let flowing uncontrolled for a time  $t^*$  and then the nonlinear controller has been turned on again. After other 5s the procedure has been repeated, by setting  $r$  to 1 and bring the state back in  $\mathbf{x}_1^*$ . This simulation has been performed twice, with different values of  $\gamma$  for the impulse design process (performed off-line);  $\rho$  has been set to 1 in both cases.

First,  $\gamma$  has been set to  $10^{-3}$  to emphasize the minimization of the norm of the error

$$\|\mathbf{e}\|_2^2 = \left\| \mathbf{x}_j^* - e^{t^*\mathbf{A}} (\mathbf{x}_i^* + \mathbf{B}\mathbf{v}) \right\|_2^2. \quad (5.52)$$

Then,  $\gamma$  has been set to 2, accentuating the minimization of the squared norm  $\|\mathbf{v}\|_2^2$  of the impulse weights vector (in this case  $\mathbf{v} \in \mathbb{R}$ ). The numerical results of the optimization are reported in Table 5.1 while the system trajectories are shown in Figs. 5.10 and 5.11. In the first case ( $\gamma = 10^{-3}$ ), the transient from  $\mathbf{x}_1^*$  to  $\mathbf{x}_2^*$  (and vice versa) is very fast

Table 5.1: Hybrid controller optimization results.

(a) 1 <sup>st</sup> impulse ( $x_1^* \rightarrow \mathcal{B}_2$ )				(b) 2 <sup>nd</sup> impulse ( $x_2^* \rightarrow \mathcal{B}_1$ )			
$\gamma$	$\ \mathbf{e}\ _2^2$	$\nu$	$t^*$	$\gamma$	$\ \mathbf{e}\ _2^2$	$\nu$	$t^*$
$10^{-3}$	0.00	1.05	1.04	$10^{-3}$	0.00	1.05	-1.05
2	0.15	0.00	1.41	2	0.15	0.00	1.42

and without any oscillation in the displacement, due to the high dissipation rate and the minimized error norm: when the EB–PBC controller is switched–on again the state is very close to the desired energy minimum. However, the price of this performance is the impulse, i.e. state jump, that has to be generated. On the other hand, when  $\gamma = 2$ ,

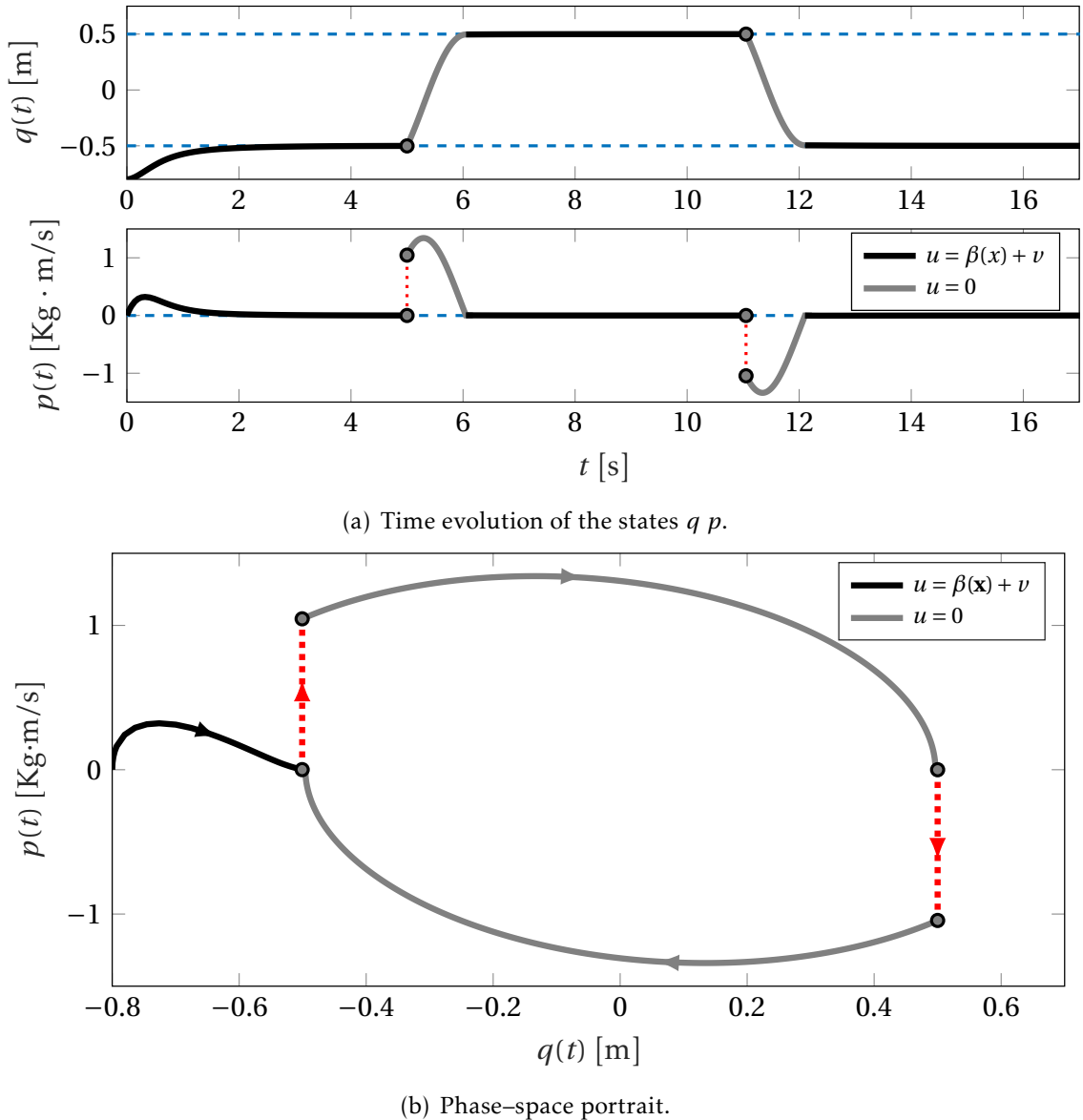


Fig. 5.10: Simulation experiment of the overall hybrid system carried out by settling  $\gamma = 10^{-3}$ . The system parameters were  $k = 5$ ,  $b = 0.5$ ,  $\lambda = 2$ ,  $\mu = 1$ ,  $k_d = 4.5$  and  $\mathbf{x}_0 = (-0.8, 0)$ . Two switching signals have been given to the system in order to trigger the change of fixed point at  $t = 5$ s and  $t = 11.03$ s. Black solid lines are parts of the system's trajectory with the nonlinear controller, red dashed lines indicate state discontinuities and the blue solid lines denote that the system was flowing uncontrolled. The dashed green lines are the the fixed points.

no state discontinuity is needed to change working mode, but at the cost of a slower transient.

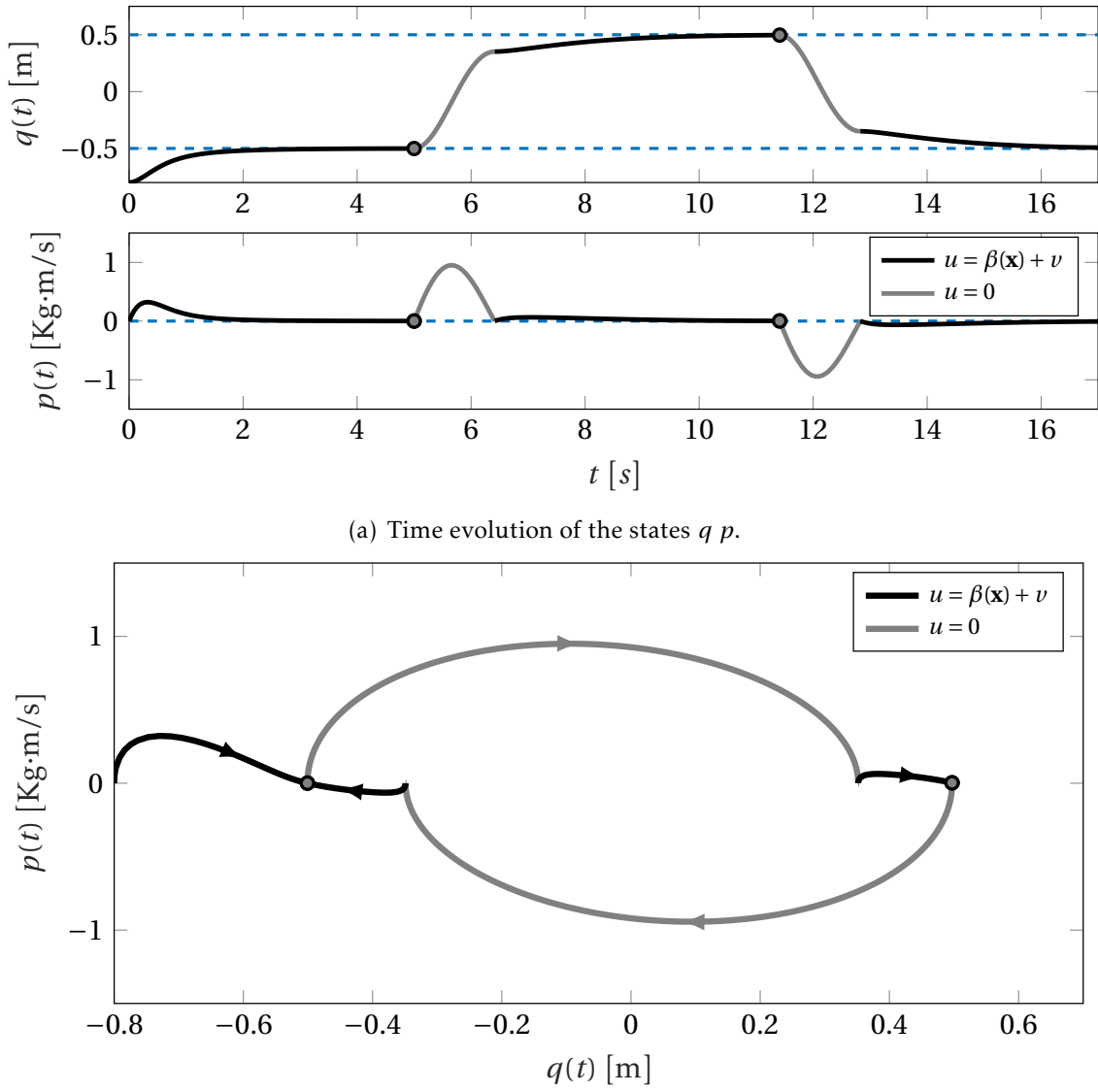


Fig. 5.11: Simulation experiment of the overall hybrid system carried out by settling  $\gamma = 2$ . The system parameters were  $k = 5$ ,  $b = 0.5$ ,  $\lambda = 2$ ,  $\mu = 1$ ,  $k_d = 4.5$  and  $\mathbf{x}_0 = (-0.8, 0)$ . Two switching signals have been given to the system in order to trigger the change of fixed point. The first one at time  $t = 5\text{s}$  and the second one at time  $t = 11.43\text{s}$ . Black solid lines are parts of the system's trajectory with the nonlinear controller and the blue solid lines denote that the system was flowing uncontrolled. The dashed green lines are the the fixed points.

## 5.6 Summary

In this chapter, a novel technique for controlling stable linear time invariant systems which operate in a finite number of working modes has been presented.

The theory of passivity-based control and port-Hamiltonian systems has been used to stabilize multiple fixed points of the closed-loop system. The proposed method allows then to switch among the desired working modes by engaging a hybrid mode selector triggered asynchronously by an external logic signal. Simulations have been performed to prove the validity of the control scheme.

The final closed-loop system is hybrid in nature due to the applied control technique. Furthermore, it belongs to the class of hybrid port-Hamiltonian systems described in Chapter 3, with a model similar to the *hopping robot* (see Fig. 3.2).



# Chapter 6

## Identification of a Class of Hybrid Dynamical Systems

---

6.1	Introduction .....	98
6.2	Problem Setting .....	99
6.3	Jump Detection.....	101
6.4	Identification Procedure .....	104
6.4.1	Approximation of the Smoothness Bound .....	104
6.4.2	Parameters Estimation .....	105
6.4.3	Reduced Order Identification .....	106
6.4.4	Flow and Jump Sets Approximation .....	108
6.5	Simulation Experiments .....	110
6.5.1	Case of Study: Impact Mass-Spring-Damper System .....	110
6.5.2	Numerical Simulation .....	112
6.6	Summary .....	118

---

## 6.1 Introduction



In this chapter, the identification problem for a class of hybrid dynamical systems is addressed. The majority of the literature on identification of HDS is related to classes of Piece Wise Affine systems (PWA), i.e. systems which are defined by subdividing the space into polyhedral regions which have associated an affine state update equation.

It is possible to discern four main different identification procedures for PWA systems: Bayesian, algebraic, clustering-based and bounded-error approaches. Qualitative comparison between the performance of those methodologies is reported in (Juloski et al. , 2005a; Paoletti et al. , 2007). Identification of piecewise affine (PWARX), hinging hyperplanes (HHARX), and Wiener piecewise affine (WPWARX) autoregressive exogenous models of hybrid dynamical systems have been addressed in (Bemporad et al. , 2001). Although in this work global convergence is provided through a mixed-integer linear or quadratic programming, the performance of the proposed solution strictly depends on the choice of the input signal  $u$ . Picewise affine identification of submodels and the valid polyhedral partitions of the domain of hybrid systems are evaluated by combining clustering, classification and linear identification techniques in the work proposed in (Ferrari-Trecate et al. , 2001). The particular behavior of each procedures is assessed via experimental evaluation of the electronic components of a pick-and-place device. Even if experimental results shown the validity of the proposed solution, it requires strict assumptions on the working space and error bounds. A pick-and-place machine has also been used in (Juloski et al. , 2005b) to evaluate a Bayesian scheme which model the unknown parameters as random variables described with probability distribution functions an implemented with particle filtering methodologies.

Researchers also tried to implement on-line identification of electronic components with fuzzy clustering (Sepasi and Sadrnia, 2008) and machine learning techniques. Feed-forward neural networks have been used for identification of a class of hybrid systems by Messai et al. (2008, 2006). The networks, characterized by continuous inputs, continuous outputs and binary discrete inputs, use a black-box approach to track all the mode of the system. Results are promising but highly dependent on the input sequence.

Compared to previous works, here the aim is to solve the identification problem for a class of HDS in the form of *hybrid inclusions*. This is justified by the necessity of performing systematic identification of the physical parameters characterizing *hybrid port Hamiltonian systems* in order to obtain reliable models from data and implement the developed control techniques.

In particular, here hybrid inclusions with one *flow* and one *jump* are considered, i.e. one constrained differential equation for the continuous-time part and one con-

strained difference equation for the discrete-time part. This class of systems includes *ball-juggling* mechanisms (see, e.g., Tian et al. , 2013), impact pendulums and other systems from the *nonsmooth mechanics* framework (Brogliato, 1999). Furthermore, with respect to previous works, the autonomous case is treated, in which no input-output relations are defined, with the assumption of being able to collect measurements of the state during a trajectory and linearity of the flow and jump maps with respect to two distinct sets of unknown parameters.

The proposed method relies on the Lipschitz continuity assumption of the flow map to determine from observations whether the state undergoes to a discontinuity, acknowledging that a jump happened. A linear recursive estimator is then used to estimate both the flow and jump parameters while the flow and jump sets are approximated by convex hulls.

The majority of the content of this Chapter is inspired by [c6].

## 6.2 Problem Setting

Let us consider an autonomous hybrid dynamical system represented by the following equations:

$$\begin{cases} \dot{\mathbf{x}} = \mathbf{f}(\mathbf{x}) & \mathbf{x} \in \mathcal{C} \\ \mathbf{x}^+ = \mathbf{g}(\mathbf{x}) & \mathbf{x} \in \mathcal{D} \end{cases}, \quad (6.1)$$

where  $\mathbf{x} \in \mathbb{R}^n$  is the state of the system,  $\mathbf{f}: \mathbb{R}^n \rightarrow \mathbb{R}^n$  and  $\mathbf{g}: \mathbb{R}^n \rightarrow \mathbb{R}^n$  are vector fields,  $\mathcal{C}$  and  $\mathcal{D}$  are closed subsets of  $\mathbb{R}^n$ . The system can be also represented by means of the *hybrid automata* in Fig. 6.1. System (6.1) is the single-flow single-jump specialization of the more general *hybrid inclusions* whose framework is deeply explored in Chapters 2, 3.

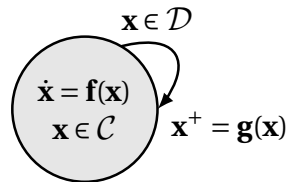


Fig. 6.1: Hybrid automata: Conceptual representation of the hybrid system  $\mathcal{H}$  characterized by a single flow map  $f$  and one jump map  $g$ . Only one state and one reset branch are needed to picture the behaviour of the system.

Let us suppose that the flow map  $\mathbf{f}$  and the jump map  $\mathbf{g}$  depend on two sets of *unknown parameters*  $\boldsymbol{\alpha} \in \mathbb{R}^{m_f}$  and  $\boldsymbol{\beta} \in \mathbb{R}^{m_g}$ , i.e.

$$\mathbf{f} = \mathbf{f}(\mathbf{x}, \boldsymbol{\alpha}) \quad \mathbf{g} = \mathbf{g}(\mathbf{x}, \boldsymbol{\beta})$$

and that no *a priori* knowledge of both, the flow set  $\mathcal{C}$  and the jump set  $\mathcal{D}$ , is available. Assume that the system is observable, i.e. it is possible to measure and collect samples of the state  $\mathbf{x}$ .

In order to correctly simulate the system or design a controller for it, it is necessary to identify the parameters in  $\boldsymbol{\alpha}$ ,  $\boldsymbol{\beta}$  and estimate the sets  $\mathcal{C}$  and  $\mathcal{D}$  from measurements of the state  $\mathbf{x}$ .

Hereafter, the basic assumptions required to develop the proposed identification method are presented. Firstly, as a very general hypothesis, both the flow and jump maps are assumed to be linear in the parameters. However,  $f$  and  $g$  are usually nonlinear with respect to the states. Thanks to this assumption, it is possible to employ linear identification techniques to estimate the unknown parameters.

**Assumption 6.2.1** (Linearity in the parameters). *The maps  $f$  and  $g$  are linear with respect to constant parameters collected in the vectors  $\boldsymbol{\alpha} \in \mathbb{R}^{m_f}$  and  $\boldsymbol{\beta} \in \mathbb{R}^{m_j}$  respectively, i.e., there exist  $\Phi: \mathbb{R}^n \rightarrow \mathbb{R}^{n \times m_f}$  and  $\Psi: \mathbb{R}^n \rightarrow \mathbb{R}^{n \times m_j}$  such that*

$$\begin{cases} \dot{\mathbf{x}} = \mathbf{f}(\mathbf{x}) = \Phi(\mathbf{x})\boldsymbol{\alpha} & \mathbf{x} \in \mathcal{C} \\ \mathbf{x}^+ = \mathbf{g}(\mathbf{x}) = \Psi(\mathbf{x})\boldsymbol{\beta} & \mathbf{x} \in \mathcal{D} \end{cases}, \quad (6.2)$$

The maps  $\Phi$ ,  $\Psi$  are assumed to be known a priori.

The second assumption deals with the regularity of the flow map.

**Assumption 6.2.2** (Smoothness and Lipschitzness of the flow map). *The following properties hold for the flow map  $\mathbf{f}$ :*

- i)  $\mathbf{f}$  is globally Lipschitz continuous on  $\mathcal{C}$ , i.e., there exists a constant  $k \geq 0$  such that

$$\forall \mathbf{x}_1, \mathbf{x}_2 \in \mathcal{C} \quad \|\mathbf{f}(\mathbf{x}_1) - \mathbf{f}(\mathbf{x}_2)\|_2 \leq k \|\mathbf{x}_1 - \mathbf{x}_2\|_2. \quad (6.3)$$

*k is referred as the Lipschitz constant;*

- ii)  $\mathbf{f}$  is differentiable almost everywhere in  $\mathcal{C}$ ;
- iii)  $\mathbf{f}$  admits a fixed point in the origin which is inside  $\mathcal{C}$ , i.e.  $\mathbf{f}(\mathbf{0}_n) = \mathbf{0}_n$ ,  $\{\mathbf{0}_n\} \in \mathcal{C}$ .

## 6.3 Jump Detection

**Definition 6.3.1** (Euler derivative norm). *Given the hybrid system  $(\mathbf{f}, \mathbf{g}, \mathcal{C}, \mathcal{D})$  and a time interval  $\delta t > 0$ , the norm of the Euler derivative of the state is defined as*

$$D_{\delta t} \mathbf{x}(t) = \frac{\|\mathbf{x}(t) - \mathbf{x}(t - \delta t)\|_2}{\delta t}. \quad (6.4)$$

**Definition 6.3.2** (Bounded-norm Euler derivative). *The Euler derivative of a hybrid system  $(\mathbf{f}, \mathbf{g}, \mathcal{C}, \mathcal{D})$  has bounded–norm if there exists  $\tau(t) \geq 0$  such that*

$$\forall \delta t > 0, t \in \mathbb{R}^+ \wedge \forall \mathbf{x} \in \mathcal{C} \quad D_{\delta t} \mathbf{x}(t) \leq \tau. \quad (6.5)$$

**Theorem 6.3.3** (Criteria for the norm bound of the Euler derivative). *Consider the hybrid system  $(\mathbf{f}, \mathbf{g}, \mathcal{C}, \mathcal{D})$ . If  $\mathbf{f}(\mathbf{x})$  satisfies Assumption 6.2.2<sup>\*1</sup> and  $\mathbf{x}(t) \in \mathcal{C} \forall t \in [t - \delta t, t]$ , then the system has bounded–norm Euler derivative with upper bound*

$$\tau(t) = \frac{1}{\delta t} \int_{t-\delta t}^t k \|\mathbf{x}(s)\|_2 ds. \quad (6.6)$$

*Proof.* Since

$$\dot{\mathbf{x}} = \mathbf{f}(\mathbf{x}) \quad \forall \mathbf{x} \in \mathcal{C}, \quad (6.7)$$

integrating both sides of the equation between  $t - \delta t$  and  $t$ , yields

$$\mathbf{x}(t) - \mathbf{x}(t - \delta t) = \int_{t-\delta t}^t \mathbf{f}(\mathbf{x}(s)) ds. \quad (6.8)$$

Therefore,

$$D_{\delta t} \mathbf{x}(t) = \frac{1}{\delta t} \|\mathbf{x}(t) - \mathbf{x}(t - \delta t)\|_2 = \frac{1}{\delta t} \left\| \int_{t-\delta t}^t \mathbf{f}(\mathbf{x}(s)) ds \right\|_2. \quad (6.9)$$

Considering the right hand side of the equation, it follows that

$$\frac{1}{\delta t} \left\| \int_{t-\delta t}^t \mathbf{f}(\mathbf{x}(s)) ds \right\|_2 \leq \frac{1}{\delta t} \int_{t-\delta t}^t \|\mathbf{f}(\mathbf{x}(s))\|_2 ds. \quad (6.10)$$

Since  $f$  is globally Lipschitz in  $\mathcal{C}$  and  $\mathbf{f}(\mathbb{0}_n) = \mathbb{0}_n$ ,

$$\frac{1}{\delta t} \int_{t-\delta t}^t \|\mathbf{f}(\mathbf{x}(s))\|_2 ds = \frac{1}{\delta t} \int_{t-\delta t}^t \|\mathbf{f}(\mathbf{x}(s)) - \mathbf{f}(\mathbb{0}_n)\|_2 ds \quad (6.11)$$

$$\leq \frac{1}{\delta t} \int_{t-\delta t}^t k \|\mathbf{x}(s)\|_2 ds < \infty, \quad (6.12)$$

<sup>\*1</sup> Notice that Assumption 6.2.2(ii) is not necessary for Theorem 6.3.3. However, it will become of fundamental importance later on.

where  $k$  is the Lipschitz constant. Thus, there exists a  $\tau \geq 0$  such that, for all  $t$ , it holds

$$D_{\delta t} \mathbf{x}(t) \leq \frac{1}{\delta t} \int_{t-\delta t}^t k \|\mathbf{x}(s)\|_2 ds \triangleq \tau(t, \delta t). \quad (6.13)$$

The above integral is always limited since, from global Lipschitz continuity of  $\mathbf{f}(\cdot)$ , global existence of trajectories  $\mathbf{x}(t)$  is assured in  $\mathcal{C}$ . It follows that on any compact time interval,  $[t - \delta t, t]$ , where the state does not leave the flow set, the quantity

$$\int_{t-\delta t}^t \|\mathbf{x}(s)\|_2 ds, \quad (6.14)$$

is limited, providing the result.  $\square$

From now on let us refer to  $\tau(t)$  as the *smoothness bound*.

**Example 6.3.4.** Consider an hybrid system with the flow described by

$$\dot{x} = f(x) = \sin(x) \quad x \in \mathcal{C}, \quad (6.15)$$

where  $\mathcal{C} \triangleq [0, 2\pi]$ .  $f$  clearly satisfies Assumption 6.2.2 and its Lipschitz constant  $k$  can be found as

$$k = \sup_{x \in \mathcal{C}} \left\| \frac{df}{dx} \right\|_2 = \sup_{x \in \mathcal{C}} \|\cos(x)\|_2 = 1. \quad (6.16)$$

Furthermore, the solution of the ordinary differential equation with  $x(0) = x_0$  is

$$x(t) = 2 \tan^{-1} \left( e^{t - \ln(\cot(x_0/2))} \right). \quad (6.17)$$

Since  $\mathbf{f}(0) = 0$  ( $\{0\} \in \mathcal{C}$ ) Theorem 6.3.3 holds and, for any  $\delta t > 0$  yields

$$D_{\delta t} x(t) = \frac{1}{\delta t} \|x(t) - x(t - \delta t)\| \leq \frac{1}{\delta t} \int_{t-\delta t}^t \|x(s)\|_2 ds = \tau(t). \quad (6.18)$$

Figure 6.2 shows in a numerical example with  $x_0 = 10^{-2}$  and  $\delta t = 0.5$ .

Thanks to Assumption 6.2.2 and the criteria provided by Theorem 6.3.3, any jump, i.e. state discontinuities, can be detected from a series of state measurements by inspecting the norm of the Euler derivative. In particular, the system can be considered to be jumping if  $D_{\delta t} \mathbf{x}(t)$  is above an empirically estimated smoothness bound  $\hat{\tau}(t)$  and the following assumption is always satisfied.

**Assumption 6.3.5** (Discontinuities and sampling time). For the chosen  $\delta t$  and  $\hat{\tau}$ , it holds:

- i)  $\mathbf{g}(\mathbf{x}) \in \mathcal{C} \quad \forall \mathbf{x} \in \mathcal{D}$ ;
- ii) If there exists a time instant  $s \in [t - \delta t, t]$  such that  $\mathbf{x}(s) \in \mathcal{D}$ , then  $s$  is unique;
- iii) Let  $\mathbf{x}(s) \in \mathcal{D}$ ,  $s \in (t - \delta t, t)$ . Then,

$$D_{\delta t} \mathbf{x}(t) \geq \hat{\tau}(t, \delta t). \quad (6.19)$$

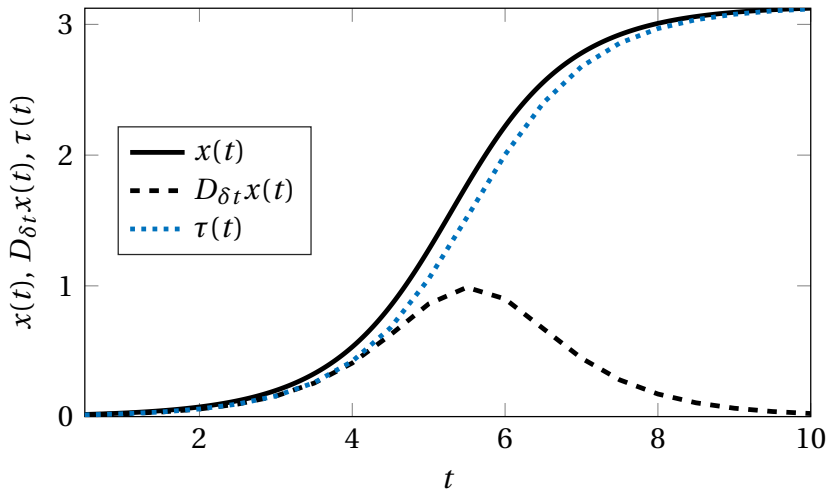


Fig. 6.2: Example 6.3.4. Time evolution of  $x(t)$ ,  $D_{\delta t}x(t)$ ,  $\tau(t)$  for  $x_0 = 10^{-2}$  and  $\delta t = 0.5$ . This figure shows an application example of Theorem 6.3.3. Notice that, as predicted by (6.18), along the whole trajectory  $D_{\delta t}x(t)$  is bounded from above by  $\tau(t)$ .

It is worth to clarify that Assumption 6.3.5(i) is needed to ensure that after a jump, the state will go back to the flow set. Moreover, 6.3.5(ii) ensures that the sampling time is small enough such that only one jump may happen within one time interval. Finally, 6.3.5(iii) requires that the sampling time and the estimated smoothness bounds are chosen such that a jump can be detected looking at the Euler derivative norm.

Therefore, a *jump detection function* can be defined as

$$\gamma(t) \triangleq \begin{cases} 0 & \frac{1}{\delta t} \|\mathbf{x}(t) - \mathbf{x}(t - \delta t)\|_2 \leq \hat{\tau}(t) \\ 1 & \text{otherwise} \end{cases}, \quad (6.20)$$

which is zero during the flows of the system and assumes the value 1 during the jumps.

At any instant of time  $\gamma(t)$  allows to determine whether the system is *jumping* or *flowing*;  $\hat{\tau}$  can be adaptively changed as function of the state and/or time. Note that  $\gamma(t) = 1$  indicates that the jump just happened and thus the system's state had been inside the jump set  $\mathcal{D}$  during the time interval  $[t - \delta t, t]$ .

**Remark 6.3.6.** Assumption 6.3.5 ensures two important properties. Firstly, that only one jump is possible between two samples of the state. Secondly, that the discontinuities created by jumps always make the Euler derivative norm to exceed the estimated smoothness bound for the chosen sampling time.

## 6.4 Identification Procedure

### 6.4.1 Approximation of the Smoothness Bound

In order to estimate on-line the smoothness bound (6.6), it is necessary to approximate the Lipschitz constant  $k$  and then numerically integrate the norm of the state between two sampling instants. At any time instant  $t$ , the estimated flow map  $\hat{\mathbf{f}}(\mathbf{x}, t)$  is defined as

$$\hat{\mathbf{f}}(\mathbf{x}, t) = \Phi(\mathbf{x})\hat{\boldsymbol{\alpha}}(t), \quad (6.21)$$

where  $\hat{\boldsymbol{\alpha}}(t)$  is the estimated vector of flow parameters at time  $t$ . Thanks to Assumption 6.2.2,  $\mathbf{f}(\mathbf{x})$  is differentiable (and so is  $\hat{\mathbf{f}}(\mathbf{x}, t)$ ) and globally Lipschitz on  $\mathcal{C}$ , the Lipschitz constant will bound from above the supremum of the norm of the Jacobian of  $\mathbf{f}(\mathbf{x})$  in the flow set  $\mathcal{C}$ :

$$k \geq \sup_{\mathbf{x} \in \mathcal{C}} \left\| \frac{\partial \mathbf{f}(\mathbf{x})}{\partial \mathbf{x}} \right\|_2. \quad (6.22)$$

Since  $\mathbf{f}(\mathbf{x})$  is not known a priori ( $\boldsymbol{\alpha}$  is unknown), the estimation of  $k$  must be carried out employing the estimated flow map  $\hat{\mathbf{f}}(\mathbf{x}, t)$ . In this work, as an estimate of the Lipschitz constant, the following quantity is considered:

$$\hat{k} = r \sup_{\mathbf{x} \in \mathcal{C}} \left\| \frac{\partial \hat{\mathbf{f}}(\mathbf{x}, t)}{\partial \mathbf{x}} \right\|_2 \quad r > 1. \quad (6.23)$$

Therefore, the estimated smoothness bound  $\hat{\tau}(t)$  is given by

$$\hat{\tau}(t) = \frac{\hat{k}}{\delta t} \int_{t-\delta t}^t \|\mathbf{x}(s)\|_2 ds = \quad (6.24)$$

$$= \frac{r}{\delta t} \sup_{\mathbf{x} \in \mathcal{C}} \left\| \frac{\partial \hat{\mathbf{f}}(\mathbf{x}, t)}{\partial \mathbf{x}} \right\|_2 \int_{t-\delta t}^t \|\mathbf{x}(s)\|_2 ds. \quad (6.25)$$

Notice that the integral below must be computed numerically. A possible simple choice is to use the first order Newton-Cotes formula (trapezoidal rule). This would yield to the following approximation of  $\hat{\tau}(t)$

$$\hat{\tau}(t) = \frac{r}{\delta t} \sup_{\mathbf{x} \in \mathcal{C}} \left\| \frac{\partial \hat{\mathbf{f}}(\mathbf{x}, t)}{\partial \mathbf{x}} \right\|_2 \int_{t-\delta t}^t \|\mathbf{x}(s)\|_2 ds \quad (6.26)$$

$$\approx \frac{r}{2} \sup_{\mathbf{x} \in \mathcal{C}} \left\| \frac{\partial \hat{\mathbf{f}}(\mathbf{x}, t)}{\partial \mathbf{x}} \right\|_2 (\|\mathbf{x}(t)\|_2 + \|\mathbf{x}(t-\delta t)\|_2). \quad (6.27)$$

It worths to be observed that with this numerical integration algorithm the estimated smoothness threshold does not explicitly depends on  $\delta t$ . Other empirical methods for computing the Lipschitz constant of multivariable functions are presented in Mladineo (1986); Wood and Zhang (1996). Notice that we do not have any *a priori* knowledge of  $\mathcal{C}$  and thus, in equation (6.27) an approximated flow set  $\hat{\mathcal{C}}$  should be employed.

**Remark 6.4.1.** The tuning of the multiplicative constant  $r$  should be addressed empirically. In fact, it has to be chosen considering a trade off between robustness (high  $r$  ensures that  $\hat{\tau}(t) \geq \tau(t) \forall t$ ) and accuracy (low  $r$  let  $\hat{\tau}$  stay below the peaks of  $D_{\delta t}\mathbf{x}(t)$  during jumps, i.e. Assumption 3 would be violated).

Thus, the final jump detection function becomes

$$\gamma(t) \triangleq \begin{cases} 0 & \frac{1}{\delta t} \|\mathbf{x}(t) - \mathbf{x}(t - \delta t)\|_2 \leq \frac{r}{2} \sup_{\mathbf{x} \in \hat{\mathcal{C}}} \left\| \frac{\partial \hat{\mathbf{f}}(\mathbf{x}, t)}{\partial \mathbf{x}} \right\|_2 (\|\mathbf{x}(t)\|_2 + \|\mathbf{x}(t - \delta t)\|_2) \\ 1 & \text{otherwise} \end{cases}. \quad (6.28)$$

### 6.4.2 Parameters Estimation

Let us assume to observe the system and measure the state  $\mathbf{x}$  with a sampling time  $\delta t$ . Suppose to collect  $N_f$  samples during the flows of the system. It holds:

$$\begin{bmatrix} \dot{\mathbf{x}}(t_1) \\ \dot{\mathbf{x}}(t_2) \\ \vdots \\ \dot{\mathbf{x}}(t_{N_f}) \end{bmatrix} = \begin{bmatrix} \Phi(\mathbf{x}(t_1)) \\ \Phi(\mathbf{x}(t_2)) \\ \vdots \\ \Phi(\mathbf{x}(t_{N_f})) \end{bmatrix} \boldsymbol{\alpha}. \quad (6.29)$$

Similarly, if  $N_j$  samples of the states are collected during jumps, i.e., if  $\gamma(t_i) = 1$  for all  $i = 1, \dots, N_j$ , yields

$$\begin{bmatrix} \mathbf{x}(t_1) \\ \mathbf{x}(t_2) \\ \vdots \\ \mathbf{x}(t_{N_j}) \end{bmatrix} = \begin{bmatrix} \Psi(\mathbf{x}(t_1 - \delta t)) \\ \Psi(\mathbf{x}(t_2 - \delta t)) \\ \vdots \\ \Psi(\mathbf{x}(t_{N_j} - \delta t)) \end{bmatrix} \boldsymbol{\beta}. \quad (6.30)$$

However, in practice, measurements are always affected by noise and, thus, relations (6.29) and (6.30) do not hold. In particular, let's assume that an additive noise,  $\tilde{\mathbf{x}}(t_i)$ , with zero-mean affects the system, i.e.,  $\mathbf{x}(t_i) = \bar{\mathbf{x}}(t_i) + \tilde{\mathbf{x}}(t_i)$ , where  $\bar{\mathbf{x}}(t_i)$  is the true value of the state variable.

Thanks to Assumption 6.2.1, the parameters in  $\boldsymbol{\alpha}$  and  $\boldsymbol{\beta}$  can be estimated by linear identification techniques. In fact, both equations, (6.29) and (6.30) belong to the error-in-variables (EIV) models:

$$\mathbf{y} \approx \mathbf{X}\mathbf{a}, \quad (6.31)$$

where  $\mathbf{y} = \bar{\mathbf{y}} + \tilde{\mathbf{y}}$  is an output's measurements vector and  $\mathbf{X} = \bar{\mathbf{X}} + \tilde{\mathbf{X}}$  is an observation matrix, both comprise of a noiseless part ( $\bar{\mathbf{y}}, \bar{\mathbf{X}}$ ), and a noisy part ( $\tilde{\mathbf{y}}, \tilde{\mathbf{X}}$ ). In this linear model, the vector of parameters  $\mathbf{a}$  could be estimated by mean of a standard linear estimator Ljung (1987). The choice of the proper estimation scheme should be done considering how the measurement noise is distributed on the possible state–nonlinearities of  $\Phi$  and  $\Psi$ .

The overall identification experiment is carried out as follows: at each sampling time, the jump detection function is computed. If the system is considered to be flowing, the estimated flow parameter  $\hat{\boldsymbol{\alpha}}$  is updated and the jump parameter  $\hat{\boldsymbol{\beta}}$  remains

unchanged. On the contrary, if a jump state is detected  $\gamma(t) = 1$ , the jump parameter  $\hat{\beta}$  will be updated and the flow parameters  $\hat{\alpha}$  will be unchanged.

Notice that, in order to update the flow parameters  $\hat{\alpha}$  according to the chosen linear estimation scheme, the knowledge of the derivative of the state,  $\dot{\mathbf{x}}(t)$ , is needed. Since we assume to be able of collecting only samples of the state, this quantity has to be computed numerically (Euler derivative, sliding mode, etc.). This cumbersome calculation can be avoided by considering that the linear relation holds even if it is integrated in an interval of time. In fact,

$$\dot{\mathbf{x}}(t) = \Phi(\mathbf{x}(t))\boldsymbol{\alpha} \quad (6.32)$$

$$\Leftrightarrow \underbrace{\mathbf{x}(t) - \mathbf{x}(t - \delta t)}_{\delta \mathbf{x}(t)} = \underbrace{\int_{t-\delta t}^t \Phi(\mathbf{x}(s)) ds}_{\tilde{\Phi}(t)} \boldsymbol{\alpha} \quad (6.33)$$

$$\Leftrightarrow \delta \mathbf{x}(t) = \tilde{\Phi}(t)\boldsymbol{\alpha}. \quad (6.34)$$

This property has been exploited in the identification experiments by employing the model (6.34). An overview of the procedure used to update the parameters at time  $t$  is presented in Algorithm 1.

#### 6.4.3 Reduced Order Identification

Suppose that some parameters in  $\boldsymbol{\alpha}$  are known before the identification experiment. In particular, without loss of generality, let us assume that all the  $m_l$  parameters of the first  $l$  components of  $\mathbf{f}$  are known. Thus,

$$\boldsymbol{\alpha} = (\boldsymbol{\alpha}_1, \boldsymbol{\alpha}_2), \quad (6.35)$$

---

#### Algorithm 1 Identification of the Hybrid System

---

- 1: **Input:**  $\hat{\alpha}(t - \delta t)$ ,  $\hat{\beta}(t - \delta t)$ ,  $\mathbf{x}(t)$ ,  $\mathbf{x}(t - \delta t)$
  - 2: Compute  $\hat{r}(t) = \frac{r}{2} \sup_{\mathbf{x} \in \mathcal{C}} \left\| \frac{\partial \hat{\mathbf{f}}(\mathbf{x}, t)}{\partial \mathbf{x}} \right\|_2 (\|\mathbf{x}(t)\|_2 + \|\mathbf{x}(t - \delta t)\|_2)$
  - 3: Compute  $\gamma(t)$
  - 4: **if**  $\gamma(t) = 0$  **then**
  - 5:      $\delta \mathbf{x}(t) = \mathbf{x}(t) - \mathbf{x}(t - \delta t)$ ,  $\tilde{\Phi}(t) = \int_{t-\delta t}^t \Phi(\mathbf{x}(s)) ds$
  - 6:     Update  $\hat{\alpha}(t)$  (Linear Estimator)
  - 7:      $\hat{\beta}(t) \leftarrow \hat{\beta}(t - \delta t)$
  - 8: **else**
  - 9:     Update  $\hat{\beta}(t)$  (Linear Estimator)
  - 10:     $\hat{\alpha}(t) \leftarrow \hat{\alpha}(t - \delta t)$
  - 11: **Output:**  $\hat{\alpha}(t)$ ,  $\hat{\beta}(t)$
-

where  $\boldsymbol{\alpha}_1 \in \mathbb{R}^{m_l}$  are the known parameters and  $\boldsymbol{\alpha}_2 \in \mathbb{R}^{m_f - m_l}$ . In this case,  $\Phi(\mathbf{x})$  can be partitioned as

$$\Phi(\mathbf{x}) = \begin{bmatrix} \Phi_1(\mathbf{x}) & \mathbb{O}_{l \times (m_f - m_l)} \\ \mathbb{O}_{(n-l) \times m_l} & \Phi_2(\mathbf{x}) \end{bmatrix}, \quad (6.36)$$

with  $\Phi_1(\mathbf{x}) \in \mathbb{R}^{l \times m_l}$  and  $\Phi_2(\mathbf{x}) \in \mathbb{R}^{(n-l) \times (m_f - m_l)}$ . Therefore, the identification experiment should be applied only to the subsystem

$$\dot{\mathbf{x}}_2 = \Phi_2(\mathbf{x})\boldsymbol{\alpha}_2. \quad (6.37)$$

This is justified in many physical systems described by a set of second order differential equations (see Example 6.4.2). Notice that the same situation might happen for a jump map. In this case,

$$\Psi(\mathbf{x}) = \begin{bmatrix} \Psi_1(\mathbf{x}) & \mathbb{O}_{l \times (m_j - m_l)} \\ \mathbb{O}_{(n-l) \times m_l} & \Psi_2(\mathbf{x}) \end{bmatrix}, \quad \boldsymbol{\beta} = (\boldsymbol{\beta}_1, \boldsymbol{\beta}_2) \quad (6.38)$$

and the model considered for the identification would be

$$\mathbf{x}_2^+ = \Psi_2(\mathbf{x})\boldsymbol{\beta}_2. \quad (6.39)$$

Similarly, if  $\Phi(\mathbf{x})$  can be partitioned as

$$\Phi(\mathbf{x}) = [\Phi_1(\mathbf{x}) \quad \Phi_2(\mathbf{x})] \quad (6.40)$$

and the first  $m_l$  parameters are known, the identification problem can be set up as

$$\dot{\mathbf{x}} - \Phi_1(\mathbf{x})\boldsymbol{\alpha}_1 = \Phi_2(\mathbf{x})\boldsymbol{\alpha}_2. \quad (6.41)$$

In the same way, for a jump, if

$$\Psi(\mathbf{x}) = [\Psi_1(\mathbf{x}) \quad \Psi_2(\mathbf{x})], \quad (6.42)$$

the linear model for the identification experiment would result to be

$$\mathbf{x}^+ - \Psi_1(\mathbf{x})\boldsymbol{\beta}_1 = \Psi_2(\mathbf{x})\boldsymbol{\beta}_2. \quad (6.43)$$

This approach is justified when, for some components of  $\mathbf{f}$  or  $\mathbf{g}$ , the parameters vector is partially known (see Example 6.4.3).

**Example 6.4.2.** Let the flow of the hybrid system be described by the following differential equation

$$\ddot{z} = a\dot{z} + b \sin(z). \quad (6.44)$$

Define  $\mathbf{x} = [x_1, x_2]^\top = [z, \dot{z}]^\top$ . The canonical first order state-space equation becomes

$$\dot{\mathbf{x}} = \begin{bmatrix} x_2 \\ ax_2 + b \sin(x_1) \end{bmatrix} = \begin{bmatrix} x_2 & 0 & 0 \\ 0 & x_2 & \sin(x_1) \end{bmatrix} \begin{bmatrix} 1 \\ a \\ b \end{bmatrix}. \quad (6.45)$$

*It is clear that we are interested only in the parameters  $a$  and  $b$ . Therefore it is convenient to consider only the subsystem*

$$\dot{x}_2 = [x_2 \quad \sin(x_1)] \begin{bmatrix} a \\ b \end{bmatrix}, \quad (6.46)$$

*in the identification experiment.*

**Example 6.4.3.** Let  $\mathbf{x} = (x_1, x_2)$  and consider the following jump map

$$\mathbf{x}^+ = \begin{bmatrix} x_1 + cx_2^2 \\ a\|x_2\|_2 + b\sin(x_1) \end{bmatrix} = \begin{bmatrix} x_1 & x_2^2 & 0 & 0 \\ 0 & 0 & \|x_2\|_2 & \sin(x_1) \end{bmatrix} \begin{bmatrix} 1 \\ c \\ a \\ b \end{bmatrix}. \quad (6.47)$$

*Then, during the Identification experiment it is worth considering only the linear relation*

$$\mathbf{x}^+ - \begin{bmatrix} x_1 \\ 0 \end{bmatrix} = \begin{bmatrix} x_2^2 & 0 & 0 \\ 0 & \|x_2\|_2 & \sin(x_1) \end{bmatrix} \begin{bmatrix} c \\ a \\ b \end{bmatrix}. \quad (6.48)$$

#### 6.4.4 Flow and Jump Sets Approximation

The method to approximate the flow and jump sets proposed in this work is developed from the following idea. Since it is possible to determine the "state" of the system, i.e. whether the system is flowing or it has jumped, it is possible to subdivide the samples of the state in two different sets, a set  $\Lambda$  containing the state's samples during flows and a set  $\Gamma$  containing the state's samples corresponding to jumps. Then, the approximated flow set  $\hat{\mathcal{C}}$  and jump set  $\hat{\mathcal{D}}$  are obtained by computing the convex hull of  $\Lambda$  and  $\Gamma$  respectively. The detailed procedure is reported in Algorithm 2.

**Remark 6.4.4.** In case  $\mathcal{C}$  and  $\mathcal{D}$  are assumed convex sets, the approximation results offer an accurate representations of them, consistent with the regions explored by the state of the system. Otherwise,  $\hat{\mathcal{C}}$  and  $\hat{\mathcal{D}}$  will be a redundant representation of the flow and jump sets. In this case, other techniques might be implemented for a better approximation, e.g. machine-learning-related methods. However, these further investigations fall out of the scope of this thesis and will be treated in future work.

**Algorithm 2** Approximation of the flow and jump sets

```

1: Input:  $\hat{\alpha}(t - \delta t), \mathbf{x}(t), \mathbf{x}(t - \delta t), \Lambda(t - \delta t), \Gamma(t - \delta t)$ 
2: Compute  $\hat{\tau}(t) = \frac{r}{2} \sup_{\mathbf{x} \in \hat{\mathcal{C}}} \left\| \frac{\partial \hat{\mathbf{f}}_t}{\partial \mathbf{x}} \right\| [\|\mathbf{x}(t)\| + \|\mathbf{x}(t - \delta t)\|]$ 
3: Compute  $\gamma(t)$ 
4: if  $\gamma(t) = 0$  then
5:    $\Lambda(t) \leftarrow \Lambda(t - \delta t) \cup \{\mathbf{x}(t)\}$ 
6:    $\Gamma(t) \leftarrow \Gamma(t - \delta t)$ 
7: else
8:    $\Lambda(t) \leftarrow \Lambda(t - \delta t) \cup \{\mathbf{x}(t)\} \setminus \{\mathbf{x}(t - \delta t)\}$ 
9:    $\Gamma(t) \leftarrow \Gamma(t - \delta t) \cup \{\mathbf{x}(t - \delta t)\}$ 
10:  $\hat{\mathcal{C}}(t) = \text{conv}(\Lambda(t))$ 
11:  $\hat{\mathcal{D}}(t) = \text{conv}(\Gamma(t))$ 
12: Output:  $\hat{\mathcal{C}}(t), \hat{\mathcal{D}}(t), \Lambda(t), \Gamma(t)$ 

```

## 6.5 Simulation Experiments

### 6.5.1 Case of Study: Impact Mass-Spring-Damper System

Let us consider an impact mass-spring-damper system like the one represented in Fig. 6.3 and let  $q$  be height from the ground of the mass. Assume the mass to be unitary and the rest position of the spring to be at the origin ( $q = 0$ ). The chosen system admits a hybrid port-Hamiltonian representation. In fact, we want to show that the developed identification procedure can be applied to the class of systems with which this Thesis is dealing.

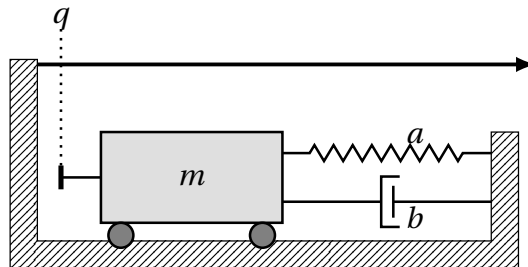


Fig. 6.3: Impact mass–spring–damper system:  $q$  is the distance of the cart from the wall,  $m$  is the mass of the cart,  $a$  is the spring stiffness and  $b$  the damping coefficient of the dashpot.

#### Model of the Flows

When the ball is not touching the floor, the system behaves as a simple damped linear oscillator. Let  $\mathbf{x} = [x_1, x_2]^\top = [q, \dot{q}]^\top$ . The flows of the system are described by

$$\dot{\mathbf{x}} = \begin{bmatrix} x_2 \\ -ax_1 - bx_2 \end{bmatrix} = \begin{bmatrix} x_2 & 0 & 0 \\ 0 & -x_1 & -x_2 \end{bmatrix} \begin{bmatrix} 1 \\ a \\ b \end{bmatrix}, \quad (6.49)$$

where  $a$  and  $b$  are the spring stiffness and the damping coefficient, respectively. The corresponding flow set flow set is

$$\mathcal{C} = \{\mathbf{x}: x_1 \geq 0\} \setminus \{\mathbf{x}: x_1 = 0, x_2 < 0\}. \quad (6.50)$$

#### Model of the Jumps

It is clear that during the collision between ball and the floor ( $x_1 = q = 0$ ) there is a discontinuity in the velocity. In this example, collisions are considered partially inelastic while the ball is modeled as a rigid body. The selected jump map to model the collisions is the following:

$$\mathbf{x}^+ = \begin{bmatrix} x_1 \\ -\lambda x_2 + \mu \end{bmatrix} = \begin{bmatrix} x_1 & 0 & 0 \\ 0 & -x_2 & 1 \end{bmatrix} \begin{bmatrix} 1 \\ \lambda \\ \mu \end{bmatrix}, \quad (6.51)$$

where  $\lambda$  is the restitution coefficient and  $\mu$  is introduced to consider possible unmodeled impact dynamics. The jump set is therefore,

$$\mathcal{D} = \{\mathbf{x}: x_1 = 0, x_2 \leq 0\}. \quad (6.52)$$

**Remark 6.5.1** (Hybrid port–Hamiltonian formulation). *The system indeed belongs to the class of impulsive port–Hamiltonian systems (3.3), defined in Chapter 3. Let  $p \triangleq \dot{q}$ . The hybrid port–Hamiltonian formulation of the impact mass–spring–damper system is*

$$\begin{cases} \begin{bmatrix} \dot{q} \\ \dot{p} \end{bmatrix} = \begin{bmatrix} 0 & 1 \\ -1 & -b \end{bmatrix} \begin{bmatrix} \nabla_q \mathcal{H}(q, p) \\ \nabla_p \mathcal{H}(q, p) \end{bmatrix} + \begin{bmatrix} 0 \\ 1 \end{bmatrix} u & (q, p) \in \mathcal{C} \\ \begin{bmatrix} q^+ \\ p^+ \end{bmatrix} = \begin{bmatrix} q \\ -\lambda p + \mu \end{bmatrix} & (q, p) \in \mathcal{D} \\ y = p \end{cases}, \quad (6.53)$$

with

$$\mathcal{H}(q, p) \triangleq \frac{1}{2} p^2 + \frac{a}{2} q^2. \quad (6.54)$$

Note that, if  $\mu \leq 0$ , the system is flow passive.

### Model Identification

In order to estimate the system's parameters, a reduced order identification has to be performed for both the flow and the jump as in (6.37) and (6.39). Let  $\boldsymbol{\alpha} = [\alpha_1, \alpha_2]^\top = [a, b]^\top$  and  $\boldsymbol{\beta} = [\beta_1, \beta_2]^\top = [\lambda, \mu]^\top$ . The reduced model for the flow is

$$\dot{\mathbf{x}}_2 = [-x_1 \quad -x_2] \begin{bmatrix} \alpha_1 \\ \alpha_2 \end{bmatrix} \quad (6.55)$$

and the one for the jump is

$$\dot{\mathbf{x}}_2^+ = [-x_2 \quad 1] \begin{bmatrix} \beta_1 \\ \beta_2 \end{bmatrix}. \quad (6.56)$$

The approximation of the smoothness bound can be derived by computing the supremum of the norm of the estimated flow map Jacobian. Hence, the estimated flow map in the reduced model will be

$$\hat{f}(\mathbf{x}, t) = -\hat{\alpha}_1(t)x_1(t) - \hat{\alpha}_2(t)x_2(t) = -\boldsymbol{\alpha}^\top \mathbf{x}. \quad (6.57)$$

Therefore,

$$\frac{\partial \hat{f}(\mathbf{x}, t)}{\partial \mathbf{x}} = -\hat{\boldsymbol{\alpha}}(t) \Rightarrow \sup_{\mathbf{x} \in \hat{\mathcal{C}}} \left\| \frac{\partial \hat{f}(\mathbf{x}, t)}{\partial \mathbf{x}} \right\|_2 = \|\hat{\boldsymbol{\alpha}}(t)\|_2. \quad (6.58)$$

### 6.5.2 Numerical Simulation

To validate the proposed identification method, numerical simulations have been performed. The simulation experiments have been carried out using Hybrid Equations (HyEQ) Toolbox Sanfelice et al. (2013) for the MATLAB environment. The parameters of the system have been chosen as  $a = 5$ ,  $b = 0.1$ ,  $\lambda = 0.99$ ,  $\mu = 0$ . The initial condition and the time span of the simulation have been set to  $\mathbf{x}(t_0) = [20, 0]^\top$  and 20 seconds, respectively. Furthermore, the sampling time  $\delta t$  has been chosen to be  $0.5 \cdot 10^{-3}$  s, the multiplicative constant  $r$  in the smoothness bound has been set to 220 and the estimated smoothness bound has been initialized to  $10^5$ .

Here, as both the flow and jump maps result linear in the state, the chosen estimation scheme is the *recursive least squares* (RLS) Ljung (1987). However, due to how noise would influence the system, i.e. it affects the observation matrix, alternative results might be achieved with a *recursive generalized total least squares* (Rhode et al. , 2014) or a *recursive Frisch scheme* (see [c1,c2]). The resulting time evolution of the system is represented in Fig. 6.4. It can be noticed that the behavior of the system is similar

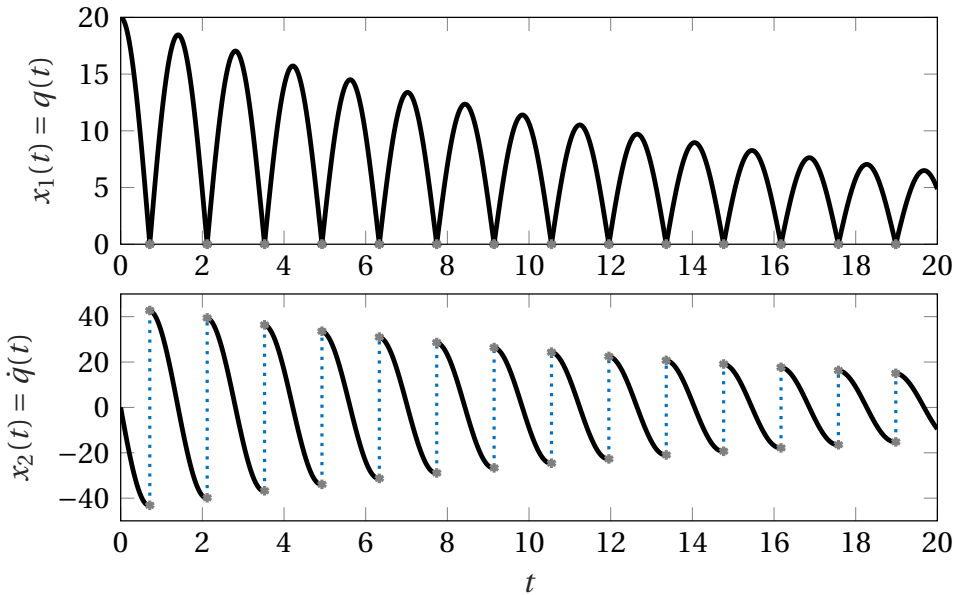


Fig. 6.4: Time evolution of the position and velocity of the system. The gray dots correspond to system's jumps while dotted blue lines highlight the change of state which creates discontinuities.

to the one of a bouncing ball under the effect of constant gravitational acceleration. However, in this case, the ball is pulled to the ground by the force of the spring.

Along the trajectory, the norm of the Euler time derivative  $D_{\delta t}\mathbf{x}(t)$  and the estimated smoothness bound  $\hat{\tau}(t)$ , have been computed. These quantities have been employed to evaluate the function  $\gamma(t)$  and thus, to identify the parameters  $\alpha$  and  $\beta$  through the RLS. Initially, to test the overall procedure in nominal conditions, no additive noise has been added to the measurements of the states. The trend of  $D_{\delta t}\mathbf{x}(t)$  during the

simulation, is shown in the upper part of Fig. 6.5. The figure also shows the comparison between the approximated  $\hat{\tau}$  and the true smoothness bound  $\tau$  (scaled by an arbitrary constant  $r$ ). The approximation error of the smoothness bound, defined as  $e_\tau(t) = \|\hat{\tau}(t) - r \cdot \tau(t)\|$ , it is plotted in the lower part of Fig. 6.5. It can be noticed that after just few iterations the estimated smoothness bound  $\hat{\tau}$  can accurately track the scaled nominal bound  $\tau$ . At the same time, as the estimation of the parameters becomes more accurate, the tracking error decreases. The performance of the system in the identification of the parameters has been evaluated by defining the absolute estimation errors  $e_{\alpha}(t) = \|\boldsymbol{\alpha} - \hat{\boldsymbol{\alpha}}(t)\|$  and  $e_{\beta}(t) = \|\boldsymbol{\beta} - \hat{\boldsymbol{\beta}}(t)\|$ . The time evolution of the components of  $\hat{\boldsymbol{\alpha}}$  and  $\hat{\boldsymbol{\beta}}$ , and the one of the estimation errors  $e_{\alpha}(t)$  and  $e_{\beta}(t)$ , are plotted in Fig. 6.6. As expected, in the nominal case, the estimation error decreases with the number of iterations. A zero-mean Gaussian noise with standard deviation  $\tilde{\sigma}_x = 0.25$  has successively been added to the state observations and the experiment repeated. The results are shown in Figs. 6.7 and 6.8. The tracking error of the smoothness quickly converges to a values oscillating around  $10^3$  which correspond to a mean relative error of about 2.5%, Fig. 6.7. This proves a certain level of robustness to noise in the approximation of  $\tau(t)$ . This result is also pictured in Fig. 6.8 where good estimates are achieved for both, the flow and the jump parameters. Besides, it must be mentioned that, in case of excessive noise, the approximation of the smoothness becomes less accurate and the difference of  $D_{\delta t}\mathbf{x}(t)$  during flows and jumps less prominent, making the detection of the jumps difficult. In fact, the system is sensitive to the choice of the multiplicative constant  $r$  and  $\delta t$ , which should be empirically made. To ensure a clear separation between the Euler derivatives and thus, increase the robustness to noise, a small value should be assigned to  $\delta t$ . Indeed, this would also help to enforce the validity of Assumption 3. A major drawback of the proposed approach is that the erroneous classification of some of the states as *flows* or *jumps* inevitably introduce errors in the estimation process. This might be due to a poor choice of the scalar  $r$  or, in the first iterations of the identification algorithm, to rough estimates of the flow parameters. However, the problem might be partially solved introducing a *forgetting* term in the estimation scheme Söderström (2018) allowing a quick recover of the estimates together with a method to retroactively re-classify the wrong sample. These further investigations are left for future work.

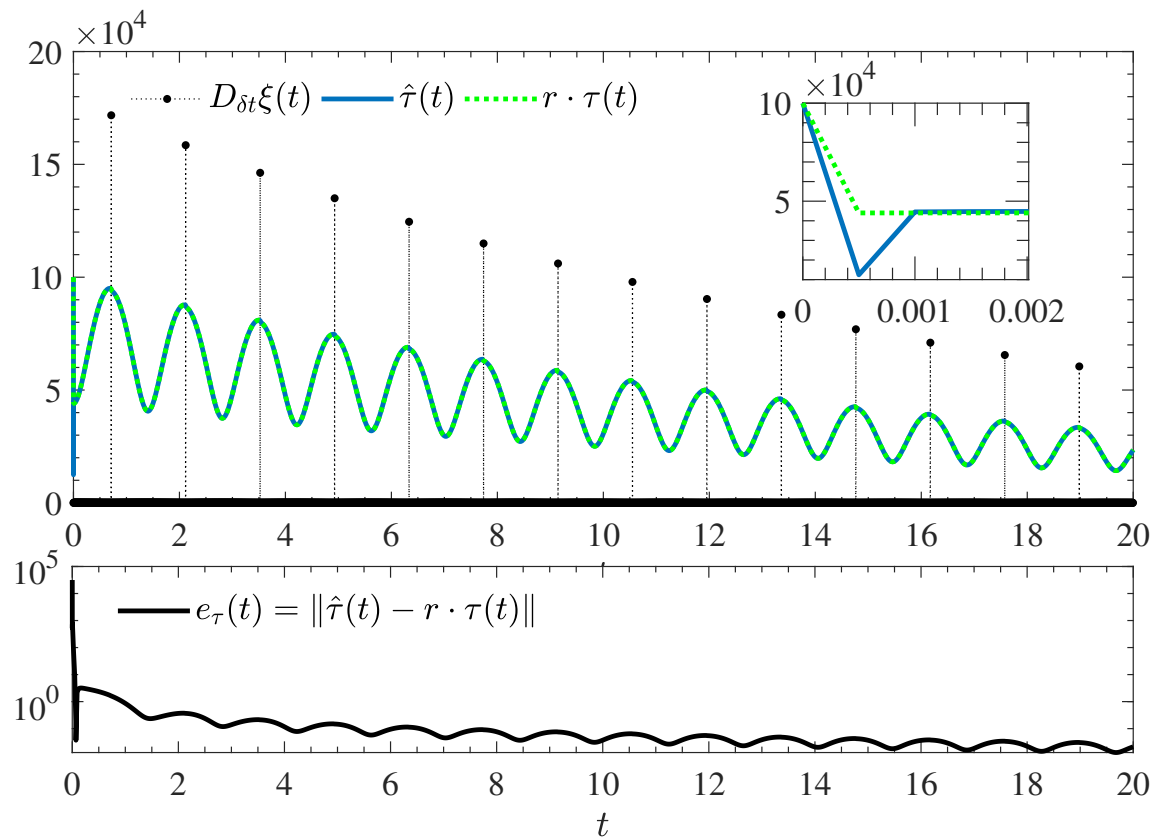


Fig. 6.5: Nominal experiment (no measurement noise). [Above] Norm of the Euler derivative  $D_{\delta t}\mathbf{x}(t)$ , (dotted black line and circle marker), estimated smoothness bound  $\hat{\tau}(t)$  (blue solid line) and nominal smoothness bound  $\tau(t)$  scaled by the arbitrary constant  $r$ . [Below] smoothness bound approximation error  $e_\tau(t)$  (log scale).

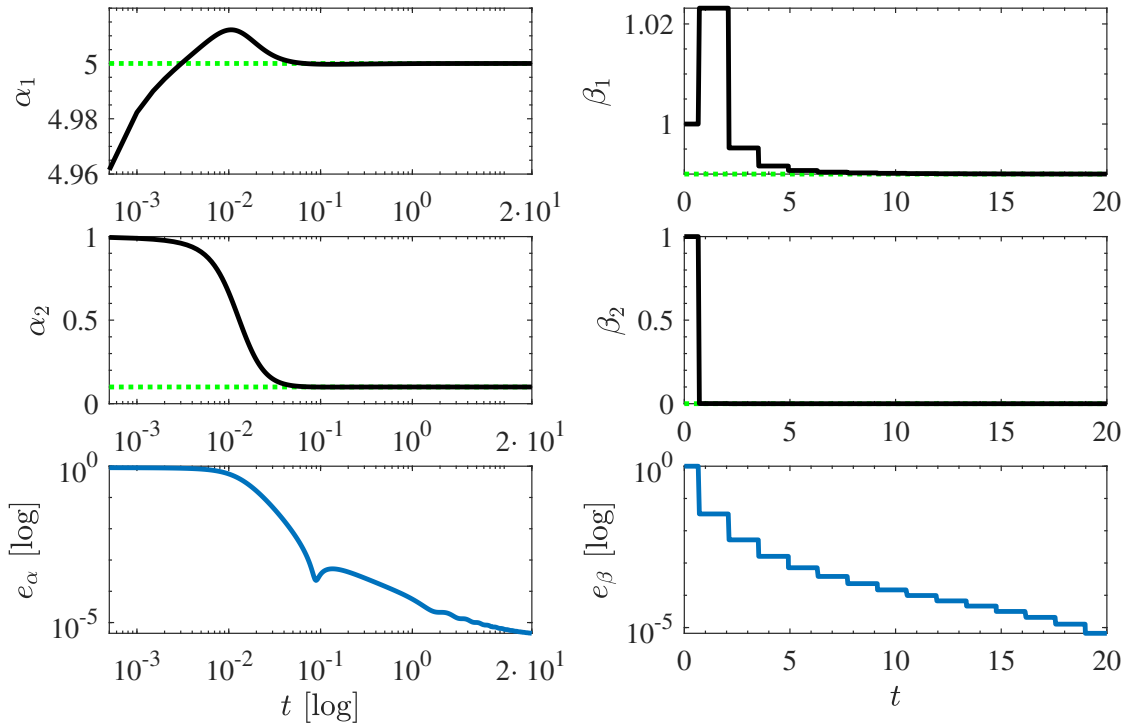


Fig. 6.6: Nominal experiment (no measurement noise): parameters estimation results. [Left] Estimates of the parameters in  $\boldsymbol{\alpha}$  and absolute estimation error  $e_{\boldsymbol{\alpha}}(t) = \|\boldsymbol{\alpha} - \hat{\boldsymbol{\alpha}}(t)\|$  (below). [Right] Estimates of the parameters in  $\boldsymbol{\beta}$  and absolute estimation error  $e_{\boldsymbol{\beta}}(t) = \|\boldsymbol{\beta} - \hat{\boldsymbol{\beta}}(t)\|$  (below).

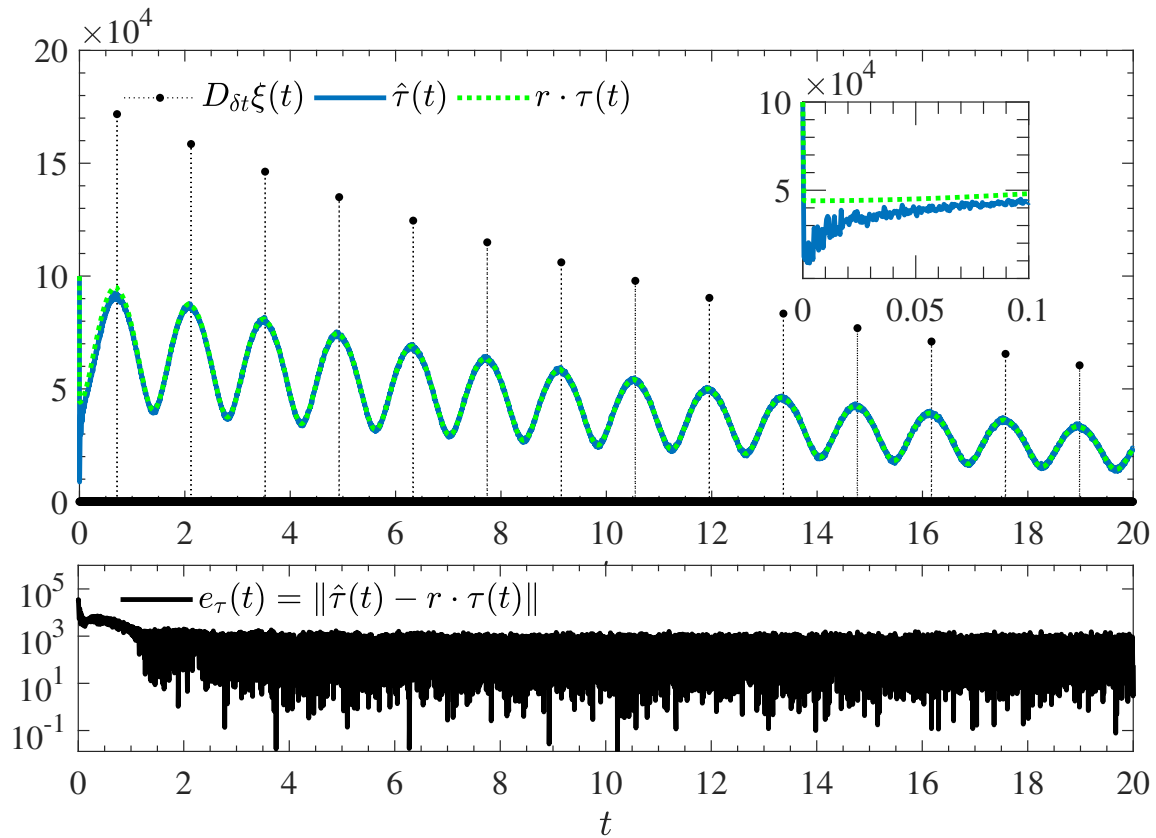


Fig. 6.7: Noisy experiment (measurement noise standard deviation  $\tilde{\sigma}_x=0.25$ ). [Above] Norm of the Euler derivative  $D_{\delta t}\xi(t)$ , (dotted black line and circle marker), estimated smoothness bound  $\hat{\tau}(t)$  (blue solid line) and nominal smoothness bound  $\tau(t)$  scaled by the arbitrary constant  $r$ . [Below] smoothness bound approximation error  $e_\tau(t)$  (log scale).

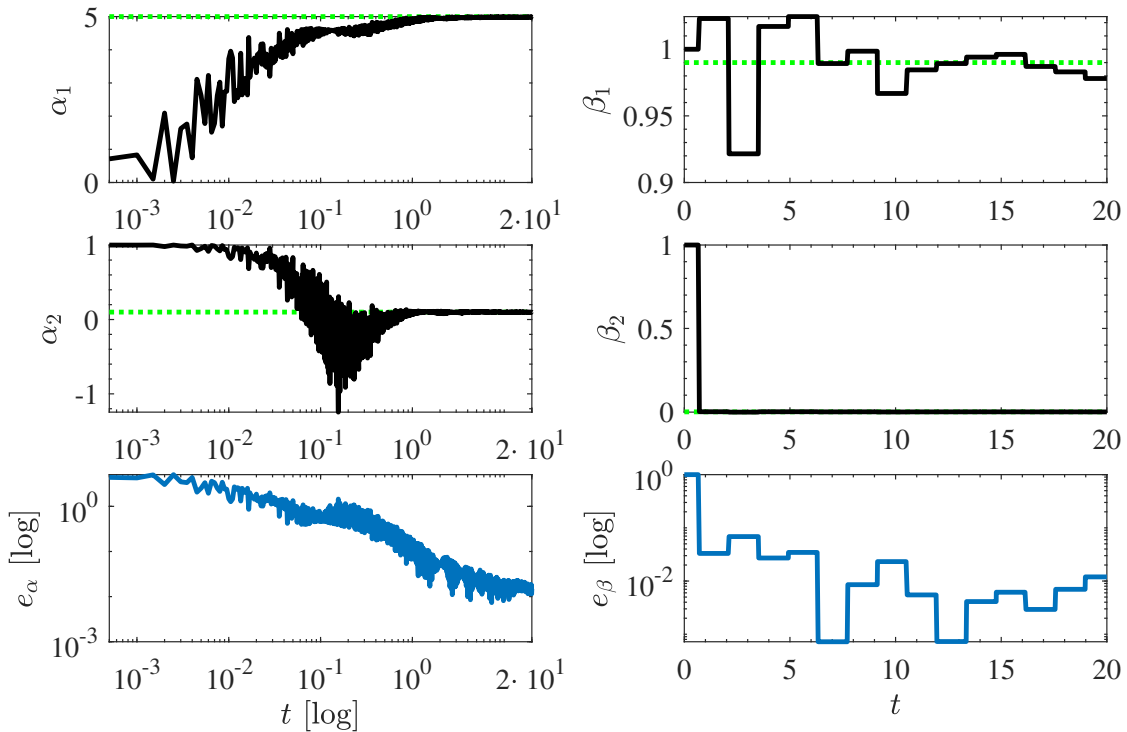


Fig. 6.8: Noisy experiment (measurement noise standard deviation  $\tilde{\sigma}_x=0.25$ ): parameters estimation results. [Left] Estimates of the parameters in  $\boldsymbol{\alpha}$  and absolute estimation error  $e_{\boldsymbol{\alpha}}(t) = \|\boldsymbol{\alpha} - \hat{\boldsymbol{\alpha}}(t)\|$  (below). [Right] Estimates of the parameters in  $\boldsymbol{\beta}$  and absolute estimation error  $e_{\boldsymbol{\beta}}(t) = \|\boldsymbol{\beta} - \hat{\boldsymbol{\beta}}(t)\|$  (below).

## 6.6 Summary

In this chapter, a new methodology for parameter identification of a class of hybrid dynamical systems, which evaluates the unknown parameters by employing a linear recursive estimator, has been proposed.

The developed procedure is able to identify the state of the system and explicitly determine the flowing and jumping states. The method has been applied to a system falling in the category of hybrid port–Hamiltonian systems.

## **Chapter 7**

# **Conclusion and Future Work**

---

7.1	Conclusion.....	120
7.2	Future Work .....	121

---

## 7.1 Conclusion

This thesis proposed a novel framework to deal with the challenging problem of controlling robots in highly dynamic tasks. The proposed solution has been developed by fashioning the theory of *port-Hamiltonian systems* in the context of *hybrid inclusions*. The originality of the presented work consists in the derivation of operative tools embedding physical intuitions into the mathematical formalism of *hybrid dynamical systems* and *nonsmooth mechanics*.

In particular, the achieved results can logically organized in four main parts according to four different research objectives:

1. First, at a theoretical level, the framework of *hybrid port-Hamiltonian systems* has been developed from first principles and the existing results present in the literature. Basic definitions have been provided, highlighting different aspects of the proposed model like passivity and autonomous stability;
2. Second, at a robotics level, the chaotic dynamics of the ubiquitous and challenging *ball-dribbling robot* have been tamed by introducing of a novel energy-based hybrid controller: the *iterative energy-shaping control*. The stabilization capabilities and robustness of the proposed method have been tested. Results showed the attractiveness and stability of the reference periodic orbit attractive in the closed-loop system;
3. Third, at a control systems level, the broad application spectrum of the proposed modeling framework has been shown in a less practical example. A novel hybrid control system has been developed in the context of passivity theory. With respect to the previous applications, here the hybrid dynamics are given by the controller and not by the physics of the system. Nevertheless, the closed-loop system has been proven to belong to the *hybrid port-Hamiltonian* framework;
4. Last but not least, at implementation level, a brief insight has been provided regarding the parameter estimation for hybrid systems. System identification is certainly one of the most overlook, yet fundamental and challenging practical problems. The identification of hybrid systems has been tackled by rigorous analytical methods with certain dose of heuristics and intuitions. To validate the proposed approach, simulations have been performed on an hybrid port-Hamiltonian model.

## 7.2 Future Work

The outcome of this thesis creates a base for further challenging researches. From a theoretical point of view, several issues, such as well-posedness, stabilizability, passivity-based control etc., are still opened. However, once the framework of hybrid port-Hamiltonian systems is extended with further mathematical tools, it will may serve as an active substrate for a new generation of modeling and control technique for highly dynamic tasks in robotics applications.

Nevertheless, the directions for future work are given, in practice, by the limitations present in the current status of this research. They can be summarized as follows:

1. Experimental tests with a physical system of both, the proposed controllers and the identification scheme, haven't been addressed yet. Besides, this step is necessary to prove the real capabilities of the developed theory, in particular for the ball-dribbling robot;
2. Only one-dimensional motion of the ball-dribbling robot has been considered. For practical robotics application it will be necessary to scale the controller to deal with higher dimensions (3D). This problem will be tackled by geometric modeling of port-Hamiltonian systems rather than working in coordinates: in three physical dimensions the equation of motion becomes over-complicated losing physical insights necessary for robust and reliable robot control design;
3. The only control design application for hybrid port-Hamiltonian systems was the one of the ball-dribbling robot. Although it is a very good prototype example in this context, other robotics application will be explored such as the hopping robot or dynamic interaction tasks (including human-robot interactions);
4. On a theoretical level, several issues must still be addressed for hybrid port-Hamiltonian systems. Those will certainly be considered in the future together with more applications in the field on control theory as the example presented in Chapter 5. Beyond control theory, a new promising application directions for hybrid port-Hamiltonian systems is optimization for deep learning (see [c4]).
5. The identification protocol developed in Chapter 6, is only designed to deal with a restricted class of hybrid systems. Machine learning techniques might be employed to extend the range of identifiable systems. For multi-modal (multiple jumps) hybrid systems deep learning methods can be used to classify state measurements and later perform a model-based identification.



# Acknowledgements

## Acknowledgements

---

Now that I am writing the last few words of this thesis, I would like to thank all the people who contributed, in different ways, to this big achievement.

First, I would like to thank my supervisor **Professor Hajime Asama** who made me part of his group and always guided me, teaching me how research works. His honest and sincere advice has been extremely important throughout all the path who lead me to this final result. Nevertheless, at a personal level, I want to express my outmost gratitude towards him to be my mentor and inspiration.

I would like to extend my sincere gratitude to the reviewers of my thesis, **Professor Hideki Kawakatsu** and **Lecturer Shunsuke Yoshimoto**. Their experience brought me insightful and keen suggestions which certainly helped in improving the quality of this thesis. Thank you very much, in advance.

Special thanks also to **Associate Professor Atsushi Yamashita** whose hardworking attitude and devotion to research gave me unvaluable teaching. Moreover, his timely, focused and objective advice always helped me taking the right direction at every turn.

Although words are probably not enough, I have to extend my deepest gratitude to **Project Assistant Professor Angela Faragasso** for supervising me throughout all my Master course. I thank her for her patience, sincerity and friendship.

In the same way, I would like to spend few words for **Dr. Federico Califano**, from the University of Twente. He has been my bachelor thesis supervisor in Bologna University and, since then, we became friends, starting a collaboration which certainly has been fundamental to the development of this thesis. His theoretical, yet insightful approach thought me a lot on how to output good research.

I would also like to extend my thanks to everyone at the Asama-Yamashita lab. In particular, to **Project Associate Professor Yusuke Tamura**, **Assistant Professor Qi An**, **Project Assistant Professor Shota Chikushi**, **Technical Specialist Dr. Hiroshi Yamakawa**, **Visiting Researcher Dr. Alessandro Moro**, **JSPS Post Doctoral Research Sarthak Pathak** and all the students who form the wonderful team of staff at the Asama and Yamashita laboratories, and all other lab members for their constant support and academic/non-academic discussions.

Thanks also to **Ms. Maki Ishida**, **Ms. Negumi Nakamura** and special thanks to **Hisae Narushima** for always helping me, and everyone at the laboratory, in all administrative matters.

Outside academia, I would like to thank all my family and friends who unconditionally supported me in every step of this path.

August 2019, **Stefano Massaroli**

---

# Bibliography

- [Agarwal et al. 2017] AGARWAL, E. ; McCOURT, M. J. ; ANTSAKLIS, P. J.: Dissipativity of finite and hybrid automata: An overview. In: *2017 25th Mediterranean Conference on Control and Automation (MED)*, 2017, Pag. 1176–1182
- [Aihara and Suzuki 2010] AIHARA, Kazuyuki ; SUZUKI, Hideyuki: Theory of hybrid dynamical systems and its applications to biological and medical systems. In: *Philosophical Transactions of the Royal Society of London A: Mathematical, Physical and Engineering Sciences* 368 (2010), Nr. 1930, Pag. 4893–4914
- [Arimoto 1984] ARIMOTO, Suguru: Stability and robustness of PID feedback control for robot manipulators of sensory capability. In: *Robotics Research: First International Symposium* MIT Press, Cambridge, Massachusetts, 1984, Pag. 783–799
- [Bätz et al. 2010] BÄTZ, G. ; METTIN, U. ; SCHMIDTS, A. ; SCHEINT, M. ; WOLLHERR, D. ; SHIRIAEV, A. S.: Ball dribbling with an underactuated continuous-time control phase: Theory and experiments. In: *Proceedings of the 2010 IEEE/RSJ International Conference on Intelligent Robots and Systems*, 2010, Pag. 2890–2895
- [Bemporad et al. 2001] BEMPORAD, A. ; ROLL, J. ; LJUNG, L.: Identification of hybrid systems via mixed-integer programming. In: *Proceedings of the 40th IEEE Conference on Decision and Control* Vol. 1, 2001, Pag. 786–792 vol.1
- [Bortolussi and Policriti 2008] BORTOLUSSI, Luca ; POLICRITI, Alberto: Hybrid Systems and Biology. In: BERNARDO, Marco (Hrsg.) ; DEGANO, Pierpaolo (Hrsg.) ; ZAVATTARO, Gianluigi (Hrsg.): *Formal Methods for Computational Systems Biology*. Berlin, Heidelberg : Springer Berlin Heidelberg, 2008, Pag. 424–448
- [Brogliato 1999] BROGLIATO, Bernard: *Nonsmooth mechanics*. Springer, 1999
- [Byrnes et al. 1991a] BYRNES, C. I. ; ISIDORI, A. ; WILLEMS, J. C.: Passivity, feedback equivalence, and the global stabilization of minimum phase nonlinear systems. In: *IEEE Transactions on Automatic Control* 36 (1991), Nov, Nr. 11, Pag. 1228–1240
- [Byrnes et al. 1991b] BYRNES, Christopher I. ; ISIDORI, Alberto ; WILLEMS, Jan C.: Passivity, feedback equivalence, and the global stabilization of minimum phase nonlinear systems. In: *IEEE Transactions on automatic control* 36 (1991), Nr. 11, Pag. 1228–1240
- [Donaire et al. 2017] DONAIRE, A. ; RUGGIERO, F. ; BUONOCORE, L. R. ; LIPPIELLO, V. ; SICILIANO, B.: Passivity-Based Control for a Rolling-Balancing System: The Nonprehensile Disk-on-Disk. In: *IEEE Transactions on Control Systems Technology* 25 (2017), Nov, Nr. 6, Pag. 2135–2142
- [Duindam et al. 2009] DUINDAM, Vincent ; MACCHELLI, Alessandro ; STRAMIGLIOLI, Stefano ; BRUYNINCKX, Herman: *Modeling and control of complex physical systems: the port-Hamiltonian approach*. Springer Science & Business Media, 2009
- [Efimov 2012] EFIMOV, Denis: Global lyapunov analysis of multistable nonlinear sys-

## Bibliography

---

- tems. In: *SIAM Journal on Control and Optimization* 50 (2012), Nr. 5, Pag. 3132–3154
- [Ferrari-Trecate et al. 2001] FERRARI-TRECATE, G. ; MUSELLI, M. ; LIBERATI, D. ; MORARI, M.: Identification of piecewise affine and hybrid systems. In: *Proceedings of the 2001 American Control Conference*. Vol. 5, 2001, Pag. 3521–3526 vol.5
- [Ficuciello et al. 2010] FICUCIELLO, F. ; CARLONI, R. ; VISSER, L. C. ; STRAMIGIOLI, S.: Port-hamiltonian modeling for soft-finger manipulation. In: *Proceedings of the 2010 IEEE/RSJ International Conference on Intelligent Robots and Systems*, 2010, Pag. 4281–4286
- [Goebel et al. 2009a] GOEBEL, R. ; SANFELICE, R. G. ; TEEL, A. R.: Hybrid dynamical systems. In: *IEEE Control Systems Magazine* 29 (2009), April, Nr. 2, Pag. 28–93
- [Goebel et al. 2009b] GOEBEL, Rafal ; SANFELICE, Ricardo G. ; TEEL, Andrew R.: Hybrid dynamical systems. In: *IEEE Control Systems* 29 (2009), Nr. 2, Pag. 28–93
- [Goebel et al. 2012] GOEBEL, Rafal ; SANFELICE, Ricardo G. ; TEEL, Andrew R.: *Hybrid Dynamical Systems: Modeling, Stability, and Robustness*. Princeton University Press, 2012
- [Haddad et al. 2006] HADDAD, Wassim M. ; CHELLABOINA, VijaySekhar ; NERSESOV, Sergey G.: Impulsive and hybrid dynamical systems. In: *Princeton Series in Applied Mathematics* (2006)
- [Haddad et al. 2003] HADDAD, Wassim M. ; NERSESOV, Sergey G. ; CHELLABOINA, VijaySekhar: Energy-based control for hybrid port-controlled Hamiltonian systems. In: *Automatica* 39 (2003), Nr. 8, Pag. 1425–1435
- [Haddadin et al. 2018] HADDADIN, Sami ; KRIEGER, Kai ; ALBU-SCHÄFFER, Alin ; LILGE, Torsten: Exploiting Elastic Energy Storage for “Blind” Cyclic Manipulation: Modeling, Stability Analysis, Control, and Experiments for Dribbling. In: *IEEE Transactions on Robotics* 34 (2018), Nr. 1, Pag. 91–112
- [Harib et al. 2018] HARIB, Omar ; HEREID, Ayonga ; AGRAWAL, Ayush ; GURRIET, Thomas ; FINET, Sylvain ; BOERIS, Guilhem ; DUBURCQ, Alexis ; MUNGAI, M E. ; MASSELIN, Mattieu ; AMES, Aaron D. et al. : Feedback control of an exoskeleton for paraplegics: Toward robustly stable, hands-free dynamic walking. In: *IEEE Control Systems Magazine* 38 (2018), Nr. 6, Pag. 61–87
- [Ishikawa et al. 2003] ISHIKAWA, M. ; NEKI, A. ; IMURA, J. ; HARA, S.: Energy preserving control of a hopping robot based on hybrid port-controlled Hamiltonian modeling. In: *Proceedings of the 2003 SICE Annual Conference* Vol. 3, 2003, Pag. 2611–2616
- [Juloski et al. 2005a] JULOSKI, Aleksandar L. ; HEEMELS, W. P. M. H. ; FERRARI-TRECATE, Giancarlo ; VIDAL, René ; PAOLETTI, Simone ; NIESSEN, J. H. G.: Comparison of Four Procedures for the Identification of Hybrid Systems. In: MORARI, Manfred (Hrsg.) ; THIELE, Lothar (Hrsg.): *Hybrid Systems: Computation and Control*, Springer Berlin Heidelberg, 2005, Pag. 354–369
- [Juloski et al. 2005b] JULOSKI, Aleksandar L. ; WEILAND, Siep ; HEEMELS, WPMH: A Bayesian approach to identification of hybrid systems. In: *IEEE Transactions on Automatic Control* 50 (2005), Nr. 10, Pag. 1520–1533
- [Khalil and Grizzle 2002] KHALIL, Hassan K. ; GRIZZLE, JW: *Nonlinear systems*. Vol. 3. Prentice hall Upper Saddle River, NJ, 2002
- [LaSalle 1960] LASALLE, Joseph: Some extensions of Liapunov’s second method. In: *IRE Transactions on circuit theory* 7 (1960), Nr. 4, Pag. 520–527

- [Ljung 1987] LJUNG, Lennart: *System identification: theory for the user.* Prentice-hall, 1987
- [Ljung 2010] LJUNG, Lennart: Perspectives on system identification. In: *Annual Reviews in Control* 34 (2010), Nr. 1, Pag. 1 – 12
- [Lv et al. 2018] Lv, Ge ; ZHU, Hanqi ; GREGG, Robert D.: On the design and control of highly backdrivable lower-limb exoskeletons: A discussion of past and ongoing work. In: *IEEE Control Systems Magazine* 38 (2018), Nr. 6, Pag. 88–113
- [Macchelli et al. 2009] MACCHELLI, A. ; MELCHIORRI, C. ; STRAMIGIOLI, Stefano: Port-Based Modeling and Simulation of Mechanical Systems With Rigid and Flexible Links. In: *IEEE Transactions on Robotics* 25 (2009), 10, Nr. 5, Pag. 1016–1029
- [Macchelli 2003] MACCHELLI, Alessandro: Port Hamiltonian systems. A unified approach for modeling and control finite and infinite dimensional physical systems. In: *PhD thesis. University of Bologna* (2003)
- [Macchelli and Melchiorri 2004] MACCHELLI, Alessandro ; MELCHIORRI, Claudio: Modeling and control of theIn fact, a Timoshenko beam. The distributed port Hamiltonian approach. In: *SIAM Journal on Control and Optimization* 43 (2004), Nr. 2, Pag. 743–767
- [Macchelli et al. 2004a] MACCHELLI, Alessandro ; SCHAFT, Arjan J. d. ; MELCHIORRI, Claudio: Port Hamiltonian Formulation of Infinite Dimensional Systems II. Boundary Control by Interconnection. In: *Atlantis* (2004)
- [Macchelli et al. 2004b] MACCHELLI, Alessandro ; VAN DER SCHAFT, Arjan ; MELCHIORRI, Claudio: Port Hamiltonian formulation of infinite dimensional systems I. Modeling. In: *Proceedings of the 43rd IEEE Conference on Decision and Control* Vol. 4 IEEE, 2004, Pag. 3762–3767
- [Maschke and Schaft 1992] MASCHKE, Bernard M. ; SCHAFT, Arjan J. Van D.: Port-Controlled Hamiltonian Systems: Modelling Origins and Systemtheoretic Properties. In: *2nd IFAC Symposium on Nonlinear Control Systems Design* 25 (1992), Nr. 13, Pag. 359 – 365
- [Maschke and van der Schaft 2001] MASCHKE, Bernhard ; SCHAFT, Arjan van d.: Hamiltonian representation of distributed parameter systems with boundary energy flow. In: *Nonlinear control in the year 2000 volume 2.* Springer, 2001, Pag. 137–142
- [Maschke and der Schaft 2000] MASCHKE, Bernhard M. ; SCHAFT, Arjan J. V.: Port Controlled Hamiltonian Representation of Distributed Parameter Systems. In: *Proceedings of the IFAC Workshop on Lagrangian and Hamiltonian Methods for Nonlinear Control* 33 (2000), Nr. 2, Pag. 27 – 37
- [Messai et al. 2006] MESSAI, N. ; ZAYTOON, J. ; RIERA, B.: Using neural networks for the identification of a class of hybrid dynamical systems. In: *Proceedings of the 2nd IFAC Conference on Analysis and Design of Hybrid Systems* 39 (2006), Nr. 5, Pag. 217 – 222
- [Messai et al. 2008] MESSAI, Nadhir ; RIERA, Bernard ; ZAYTOON, Janan: Identification of a class of hybrid dynamic systems with feed-forward neural networks: About the validity of the global model. In: *Nonlinear Analysis: Hybrid Systems* 2 (2008), Nr. 3, Pag. 773 – 785. – Special Issue Section: Analysis and Design of Hybrid Systems
- [Mladineo 1986] MLADINEO, Regina H.: An algorithm for finding the global maximum of a multimodal, multivariate function. In: *Mathematical Programming* 34 (1986), Nr. 2, Pag. 188–200

## Bibliography

---

- [Naldi and Sanfelice 2013] NALDI, Roberto ; SANFELICE, Ricardo G.: Passivity-based control for hybrid systems with applications to mechanical systems exhibiting impacts. In: *Automatica* 49 (2013), Nr. 5, Pag. 1104–1116
- [Ortega and Mareels 2000] ORTEGA, R. ; MAREELS, I.: Energy-balancing passivity-based control. In: *Proceedings of the 2000 American Control Conference. ACC* Vol. 2, 2000, Pag. 1265–1270 vol.2
- [Ortega and Mareels 2000] ORTEGA, R. ; MAREELS, I.: Energy-balancing passivity-based control. In: *Proceedings of the 2000 American Control Conference. ACC* ( Vol. 2, 2000, Pag. 1265–1270 vol.2
- [Ortega et al. 2008] ORTEGA, Romeo ; VAN DER SCHAFT, Arjan ; CASTANOS, Fernando ; ASTOLFI, Alessandro: Control by interconnection and standard passivity-based control of port-Hamiltonian systems. In: *IEEE Transactions on Automatic Control* 53 (2008), Nr. 11, Pag. 2527–2542
- [Ortega et al. 2001] ORTEGA, Romeo ; VAN DER SCHAFT, Arjan J. ; MAREELS, Iven ; MASCHKE, Bernhard: Putting energy back in control. In: *IEEE Control Systems* 21 (2001), Nr. 2, Pag. 18–33
- [Paoletti et al. 2007] PAOLETTI, Simone ; JULOSKI, Aleksandar L. ; FERRARI-TRECATE, Gi-ancarlo ; VIDAL, René: Identification of Hybrid Systems A Tutorial. In: *European Journal of Control* 13 (2007), Nr. 2, Pag. 242 – 260
- [Paynter 1961] PAYNTER, Henry: *Analysis and Design of Engineering Systems*. 1961
- [Pisano and Usai 2011] PISANO, Alessandro ; USAI, Elio: Sliding mode control: A survey with applications in math. In: *Mathematics and Computers in Simulation* 81 (2011), Nr. 5, Pag. 954–979
- [Pisarchik and Feudel 2014] PISARCHIK, Alexander N. ; FEUDEL, Ulrike: Control of multistability. In: *Physics Reports* 540 (2014), Nr. 4, Pag. 167 – 218. – Control of multistability
- [Rhode et al. 2014] RHODE, Stephan ; BLEIMUND, Felix ; GAUTERIN, Frank: Recursive Generalized Total Least Squares with Noise Covariance Estimation. In: *Proceedings of the 9th IFAC World Congress* 47 (2014), Nr. 3, Pag. 4637 – 4643
- [Rodríguez et al. 2001] RODRÍGUEZ, Hugo ; VAN DER SCHAFT, Arjan ; ORTEGA, Romeo: On stabilization of nonlinear distributed parameter port-controlled Hamiltonian systems via energy shaping. In: *Proceedings of the 40th IEEE Conference on Decision and Control* Vol. 1, 2001, Pag. 131–136
- [Ruggiero et al. 2018] RUGGIERO, F. ; PETIT, A. ; SERRA, D. ; SATICI, A. C. ; CACACE, J. ; DONAIRE, A. ; FICUCIELLO, F. ; BUONOCORE, L. R. ; FONTANELLI, G. A. ; LIPPIELLO, V. ; VILLANI, L. ; SICILIANO, B.: Nonprehensile Manipulation of Deformable Objects: Achievements and Perspectives from the Robotic Dynamic Manipulation Project. In: *IEEE Robotics Automation Magazine* 25 (2018), Sep., Nr. 3, Pag. 83–92
- [Sanfelice et al. 2013] SANFELICE, Ricardo ; COPP, David ; NANEZ, Pablo: A toolbox for simulation of hybrid systems in Matlab/Simulink: Hybrid Equations (HyEQ) Toolbox. In: *Proceedings of the 16th ACM international conference on Hybrid systems: computation and control*, 2013, Pag. 101–106
- [Sanfelice 2011] SANFELICE, Ricardo G.: Interconnections of hybrid systems: Some challenges and recent results. In: *Journal of Nonlinear Systems and Applications* 2 (2011), Nr. 1-2, Pag. 111–121

- [Sanfelice et al. 2007] SANFELICE, Ricardo G. ; TEEL, Andrew R. ; SEPULCHRE, Rodolphe: A hybrid systems approach to trajectory tracking control for juggling systems. In: *Proceedings of the 46th IEEE Conference on Decision and Control*, 2007, Pag. 5282–5287
- [Secchi et al. 2007] SECCHI, Cristian ; STRAMIGIOLI, Stefano ; FANTUZZI, Cesare: *Control of interactive robotic interfaces: A port-Hamiltonian approach*. Vol. 29. Springer Science & Business Media, 2007
- [Sepasi and Sadrnia 2008] SEPASI, S ; SADRNIA, MA: On-line identification of an electronic component placement process using a potential fuzzy clustering scheme. In: *Proceedings of the 2008 2nd International Conference on Electrical Engineering* IEEE, 2008, Pag. 1–6
- [Serra et al. 2019] SERRA, D. ; RUGGIERO, F. ; DONAIRE, A. ; BUONOCORE, L. R. ; LIPPIELLO, V. ; SICILIANO, B.: Control of Nonprehensile Planar Rolling Manipulation: A Passivity-Based Approach. In: *IEEE Transactions on Robotics* 35 (2019), April, Nr. 2, Pag. 317–329
- [Söderström 2018] SÖDERSTRÖM, Torsten: *Errors-in-variables methods in system identification*. Springer, 2018
- [Söderström 2019] SÖDERSTRÖM, Torsten: A user perspective on errors-in-variables methods in system identification. In: *Control Engineering Practice* 89 (2019), Pag. 56 – 69
- [Sontag 2008] SONTAG, Eduardo D.: Input to state stability: Basic concepts and results. In: *Nonlinear and optimal control theory*. Springer, 2008, Pag. 163–220
- [Spong et al. 2007] SPONG, M. W. ; HOLM, J. K. ; LEE, D.: Passivity-Based Control of Bipedal Locomotion. In: *IEEE Robotics Automation Magazine* 14 (2007), June, Nr. 2, Pag. 30–40
- [Stramigioli et al. 1999] STRAMIGIOLI, S. ; MELCHIORRI, C. ; ANDREOTTI, S.: A passivity-based control scheme for robotic grasping and manipulation. In: *Proceedings of the 38th IEEE Conference on Decision and Control* Vol. 3, 1999, Pag. 2951–2956 vol.3
- [Stronge 2018] STRONGE, William J.: *Impact mechanics*. Cambridge University Press, 2018
- [Tian et al. 2013] TIAN, X. ; KOESSLER, J. H. ; SANFELICE, R. G.: Juggling on a bouncing ball apparatus via hybrid control. In: *Proceedings of the 2013 IEEE/RSJ International Conference on Intelligent Robots and Systems*, 2013, Pag. 1848–1853
- [Valentin et al. 2006] VALENTIN, C ; MAGOS, M ; MASCHKE, B: Hybrid port-Hamiltonian systems: From parameterized incidence matrices to hybrid automata. In: *Nonlinear Analysis: Theory, Methods & Applications* 65 (2006), Nr. 6, Pag. 1106–1122
- [Valentin et al. 2007] VALENTIN, Claire ; MAGOS, Miguel ; MASCHKE, Bernhard: A port-Hamiltonian formulation of physical switching systems with varying constraints. In: *Automatica* 43 (2007), Nr. 7, Pag. 1125–1133
- [Van Der Schaft et al. 2014] VAN DER SCHAFT, Arjan ; JELTSEMA, Dimitri et al. : Port-Hamiltonian systems theory: An introductory overview. In: *Foundations and Trends in Systems and Control* 1 (2014), Nr. 2-3, Pag. 173–378
- [Van Der Schaft and Schumacher 2000] VAN DER SCHAFT, Arjan ; SCHUMACHER, Johannes M.: *An introduction to hybrid dynamical systems*. Vol. 251. Springer London, 2000
- [Vulpiani 2010] VULPIANI, Angelo: *Chaos: from simple models to complex systems*.

## Bibliography

---

- Vol. 17. World Scientific, 2010
- [Westervelt et al. 2018] WESTERVELT, Eric R. ; GRIZZLE, Jessy W. ; CHEVALLEREAU, Christine ; CHOI, Jun H. ; MORRIS, Benjamin: *Feedback control of dynamic bipedal robot locomotion*. CRC press, 2018
- [Wood and Zhang 1996] WOOD, G. R. ; ZHANG, B. P.: Estimation of the Lipschitz constant of a function. In: *Journal of Global Optimization* 8 (1996), Jan, Nr. 1, Pag. 91–103
- [Zhang and Liu 2016] ZHANG, Q. ; LIU, G.: Precise Control of Elastic Joint Robot Using an Interconnection and Damping Assignment Passivity-Based Approach. In: *IEEE/ASME Transactions on Mechatronics* 21 (2016), Dec, Nr. 6, Pag. 2728–2736

# **Research Publications**

## Peer Reviewed Journal Papers

- [j1] Jiaxu Wu, Hanwool Woo, Yusuke Tamura, Alessandro Moro, **Stefano Massaroli**, Atsushi Yamashita, and Hajime Asama. "Pedestrian trajectory prediction using BiRNN Encoder–Decoder Framework." *Advanced Robotics*, 2019.
- [j2] **Stefano Massaroli**, Federico Califano, Angela Faragasso, Atsushi Yamashita, and Hajime Asama: "Port–Hamiltonian approach to asymptotic stabilisation of Lotka–Volterra equations.", *Nature Communications*, 2019 (To be submitted).
- [j3] **Stefano Massaroli**, Federico Califano, Angela Faragasso, Atsushi Yamashita, and Hajime Asama: "Iterative energy shaping of a ball–dribbling robot.", *Mechatronics*, 2019 (To be submitted).

## Peer Reviewed Conference Papers

- [c1] **Stefano Massaroli**, Renato Miyagusuku, Federico Califano, Claudio Melchiorri, Atsushi Yamashita, and Hajime Asama: "Recursive algebraic Frisch scheme: a particle–based approach", *Proceedings of the 9th IFAC Symposium of Robust Control*, pp. 409–415, Florianopolis (Brazil), September 2018.
- [c2] **Stefano Massaroli**, Renato Miyagusuku, Federico Califano, Angela Faragasso, Atsushi Yamashita, and Hajime Asama: "A novel recursive linear estimator based on the Frisch scheme.", *Proceedings of the 12th Asian Control Conference*, pp. 1106–1011, Kitakyushu (Japan), June 2019.
- [c3] **Stefano Massaroli**, Federico Califano, Angela Faragasso, Atsushi Yamashita, and Hajime Asama. "Iterative energy shaping of a ball–dribbling robot." *Prooceedings of the 2019 IFAC Workshop on Robot Control*, Daejeon (Korea), September 2019. (Accepted)
- [c4] **Stefano Massaroli**, Michael Poli, Federico Califano, Angela Faragasso, Jinkyoo Park, Atsushi Yamashita, and Hajime Asama: "Port–Hamiltonian approach to neural network training." *Prooceedings of the 58th IEEE Control and Decision Conference*, Nice (France), December 2019. (Accepted)
- [c5] **Stefano Massaroli**, Federico Califano, Claudio Melchiorri, Atsushi Yamashita, and Hajime Asama: "A novel identification procedure for the dynamic parameters of robots based on the Frisch scheme." *Prooceedings of the 15th IFAC Workshop on Advanced Control and Diagnosis*, Bologna (Italy), November 2019. (Submitted)
- [c6] **Stefano Massaroli**, Federico Califano, Angela Faragasso, Mattia Risiglione, Atsushi Yamashita, and Hajime Asama. "Identification of a class of hybrid dynamical systems." *2020 IFAC World Congress*, Berlin (Germany), 2019. (To be submitted)
- [c7] **Stefano Massaroli**, Federico Califano, Angela Faragasso, Atsushi Yamashita, and Hajime Asama: "Multistable energy shaping of linear time–invariant systems with hybrid mode selector." *2020 IFAC World Congress*, Berlin (Germany), 2019. (To be submitted)

---

## Poster Presentations

- [p1] **Stefano Massaroli**, Atsushi Yamashita, and Hajime Asama: “Hybrid energy-based control of a ball-dribbling robot”, *2019 IEEE/RSJ International Conference on Intelligent Robots and Systems*, Macau (China), November 2019 (Accepted)

## Oral Presentations

- [o1] **Stefano Massaroli**, Atsushi Yamashita, and Hajime Asama: “Biologically inspired control of robots for highly dynamic tasks”, Proceedings of the Tsinghua University- the University of Tokyo Joint Symposium on Multi-discipline, pp. 95, Beijing, China, March 2018.

